Theoretical studies of single molecule biophysical systems and photochemical ensembles

Thesis by

Meher Kiran Prakash Ayalasomayajula

In partial fulfillment of the requirements

for the degree of

Doctor of Philosophy

California Institute of Technology

Pasadena, California

2007

(Defended 1 August 2007)

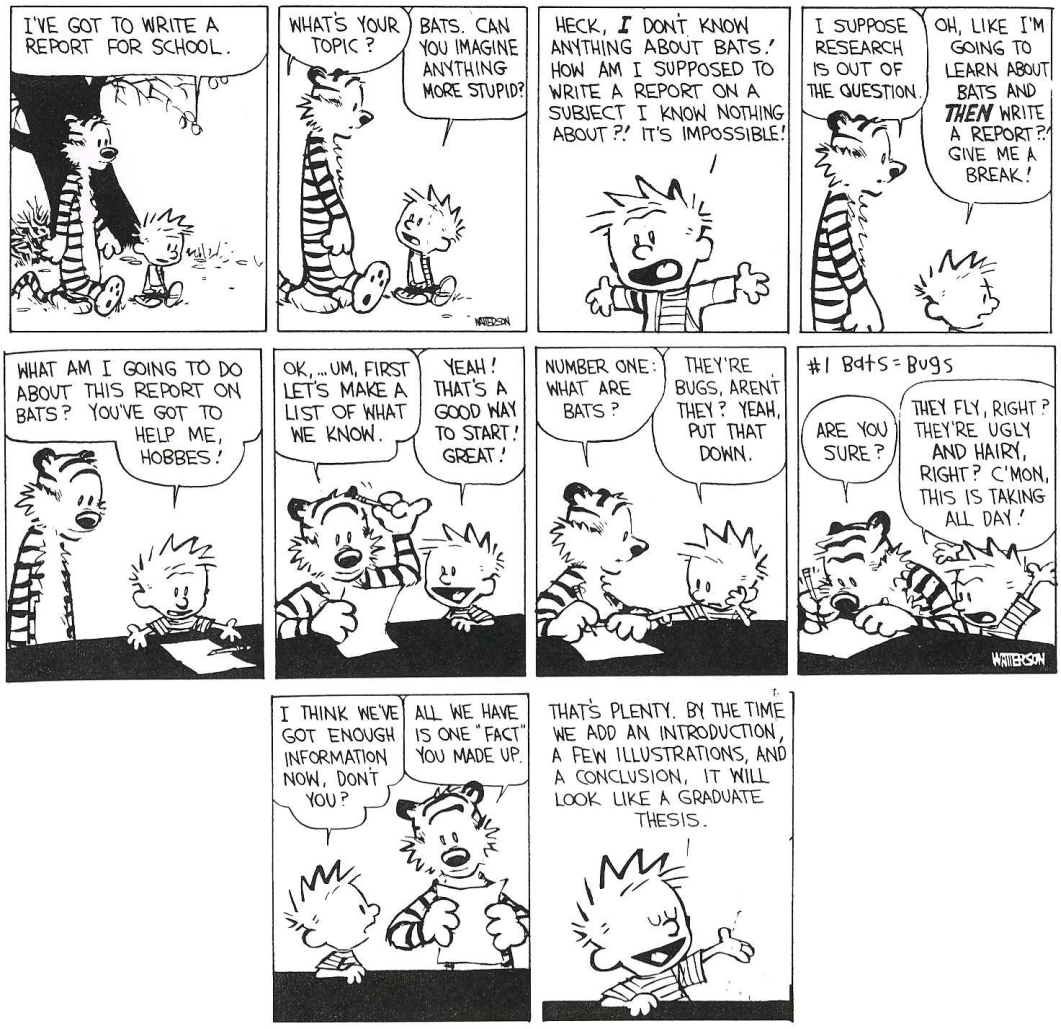

Acknowledgements

I take this opportunity to offer my heartfelt thanks to my research advisor, Professor Rudolph A. Marcus, Rudy! It was an extreme pleasure working with him for the past 3.5 years, seeing his grand vision, intense curiosity, boundless energy, and relentless effort to uncover the phenomena in nature, all wonderfully embedded in his trademark smiling personality with his great sense of humor. I have benefited greatly from the enormous amount of time he spent advising me - discussing everything from the toughest to the simplest of problems I encountered, over weekdays and weekends, without making me feel bad about my naivety in science.

One of the very valuable parts of my training with Rudy started in the summer of 2005 when I mentioned during our discussion that I browse a lot of current literature on different aspects of chemical physics and biophysics not directly related to our research, but was unable to ascertain the magnitude of the contributions of those works. Rudy very generously spent a lot of time placing some of the works in perspective to what has been understood and explaining what might be an important contribution in those problems. From those interactions I learnt a bit about how to think, and got an exposure to a wide range of problems with the enormous academic freedom he gave. Many thanks to you Rudy!

Thanks to my thesis committee - Profs. Bill Goddard, Bill Johnson, Rudy Marcus, and Rob Phillips for kindly agreeing to be on my committee and taking time from their busy schedules for the thesis defense. I benefited a great deal from their comments during my candidacy, and it is a pleasure to have them on my committee.

The members of the Marcus research group have been an extremely pleasant group to work with. I have benefited from the scientific discussions with everyone. The non-scientific interactions have been very notable and have a very significant place in my memories of Caltech! Many thanks to Evans for his interesting stories from the California Tech; Hollis for all the amusing narrations of her scripts and for very patiently teaching me how to be presentable and to be a morning person (I am still working on my definition of morning!); Jau for his advice on career, especially to work on 'protein something'; Nima for all the fun discussions in the office on a wide range of topics from quantum measurement to spirituality; Wei-Chen for the help with N_2O problem, the hikes I did with him and his inspiring appreciation of nature; Yousung for the discussions over green tea about the nerdy talk on *ab initio*, soccer and the pros and cons of becoming faculty in Korea and India; and Zhaoyan for the very refreshing talks on fashion. Special thanks to Nima and Yousung for mentoring me on the various career possibilities I have been considering for the past few months.

I really appreciate the help of Prof. Rob Phillips in allowing me to tranfer to the Applied Physics department. This opened a wide range of possibilities for me to explore. And many thanks to Prof. Michael Roukes for accepting me as a student in experimental research. The only experiments I have done are in his group and in that way, I am very thankful to him for enriching my experience in science. Many thanks to Henry and Hong for training me in experiments and instilling a sense of practicality in my mind. Roukes group members Ben, Blake, James, Jeff (epecially for introducing me to *Dilbert*), Phillip, Shwetank, and Sotiris were a fun bunch to hang out with!

I am extremely indebted to Master Yuanhua Yan, my Tai-Chi, Qi Gong instructor, who improved my health miraculously over a matter of few days through the healing arts he taught me, after suffering from various health ailments for 4 years. Sustained levels of mental and physical energy for my work over the past 2 years have been possible only because of this training. And many thanks to Walter Rodriguez for introducing me to the Master, and patiently trying to teach me the true meaning of the soft martial art practice, push hands.

Prof. Swaminathan Krishnan (Swami) deserves a special thanks for teaching me to ERR - Eat healthy, Regularly exercise, Read a paper abstract everyday! Thanks to all my roommates over the years - Prashant, Saurabh, Shwetank, Sriram, Vijay - for all the fun time I had. Special acknowledgements to my TV partners - Prashant and Vikram Gavini for the 'gult movies' (no, no, they are not cult movies, they are movies in my regional language, sometimes referred to as gult!), Vijay for the '70's show' we used to watch while enthusiastically singing the background score and Shwetank for the introductory segment of the 'Tonight show' filled with all sorts of useless information on politics and hollywood. Many thanks to Abhishek, Ajay, Deeku, Kaushik, Mandar, Puru, Shaunak, Sonali, Sowmya, Subash, Subhashini, Vaibhav, Vijay Natraj, Vikram Deshpande, and all the OASIS members, and to honorary OASIS members Alex, Amir the group I hung out with the most. Special thanks to Vikram Deshpande, and his mother Chhaya Deshpande for giving me the nice company, and more importantly great food while this thesis was being written. Special thanks to you from my mother as well!

This is a wonderful occassion to thank Profs. P. Ashwatha Narayana, M. S. Siva Kumar, Babu Vishwanath, A. Venkatesh, and friend Neeraj Jayaraman from IIT Madras. Were it not for their kind advice and monetary help, I would not have pursued graduate studies at the time I did.

And all of my friends from IIT especially - 4b, Bacchu, Buss, Daddy, Haddi, HP, Laddu, Nayak, Pros, with whom I met regularly and had an even regular conversation on the phone - this is the group that refuses to grow up (if that was ever an option for them!), excluding Daddy who had grown up too much! These folks made me feel I was not too far from India during the first year of grad school.

Thanks to all the staff at the Caltech health center - Alice, Divina, and Jeannie who took good care of me especially in the first 3 years of stay at Caltech. Those were the days I saw them more often than my roommates!

Thanks to Caltech security officer Paul Barton for reminding me very often that "it's another

day in paradise"!

Very special thanks to my family - father SriRamachandra Murthy, mother Gayathri, sisters Sudha and Madhuri for teaching me the importance of education, especially when I was showing signs of what looked like aversion to formal education as early as at 10 years age! I really appreciate their patience in this regard and thank especially my sisters for their sacrifices which made my education at IIT a reality.

Thanks to the problems and solutions that walked into my thesis, there are many others which refused to do so despite the hospitality I promised them over the years!

Abstract

The focus of the present thesis is on theoretical analysis to understand the experimental results from three quite different systems - enzymes, RNA hairpins and nitrous oxide (N_2O). Some experiments on single enzymes showed very unusual data: in separate experiments the fluctuations in catalysis rate ($\delta k(t)$) and fluorescence lifetime ($\delta\gamma^{-1}(t)$) of chromophore in single enzymes showed long-lasting autocorrelations, represented by a stretched exponential and power-law, respectively. With the aim of interpreting the origin of these fluctuations, we proposed a formulation based on fluctuations in electrostatic interaction energy ($\delta E(t)$) at the active site in the enzyme leading to the fluctuations in the various observables. We developed relations between the autocorrelation functions of $\delta E(t)$, $\delta k(t)$, spectral diffusion ($\delta\omega_0(t)$) and the radiative component of fluorescence lifetime ($\gamma_r^{-1}(t)$). It was pointed out that the relation between δk and $\delta\omega_0(t)$, seen experimentally and modeled theoretically by using the relation noted above, is a dynamic analog of the solvatochromism concept used in the catalysis of organic reactions by solvent. The estimation of fluctuations in electrostatic interactions on the milliseconds to seconds time scale by computational methods is not possible, which are typically limited to tens of nanoseconds. To calculate the autocorrelation of electrostatic interactions and to compare them with experiments, we used the frequency dependent dielectric response of proteins and related it to the autocorrelation of $\delta E(t)$. Based on this formulation, we find a good agreement between the single molecule data on the enzyme candida antarctica lipase B and the calculation using dielectric response data on the enzyme. In single molecule data from other enzymes for which $\epsilon(\omega)$ is not yet available, we have predictions based on a commonly observed functional form of $\epsilon(\omega)$ for

other proteins.

Single molecule experiments on RNA hairpins were used to test a nonequilibrium statistical physics result - Crooks' theorem. Crooks' theorem is about an exact equality relating the probability distributions of work done (W) on a system by varying an external parameter in the forward and reverse directions in a predetermined way. Usually in the single molecule experiments this predetermined variation is a constant rate (μ) of increase or decrease of the external force for all runs of the experiment. Our study focuses on the relevance of the RNA hairpin unfolding experiments to the theorem. The unfolding of the molecule leads to a drop in the externally controlled force on the molecule, a condition which is not suited to the existing derivations of Crooks' theorem. An alternative interpretation of the experimental unfolding and refolding data using a phenomenological force-dependent distortion of activation barriers is provided to gain insight into the data on the probability distribution of work done during unfolding, refolding corresponding to different rates of change of force. This interpretation shows that the crossing of the unfolding and refolding work distributions which happens at the same value of W for all μ is a necessary but not sufficient condition to verify the theorem.

The experimental data on UV photodissociation of the greenhouse gas N_2O and the associated isotope effects are important from the perspective of atmospheric interest. The calculations in the literature to model the photodissociation observations are of two kinds - some are computationally intensive quantum mechanical methods using wave packet propagation and the others are based on empirical calculations. The two different calculations we present, based on two different variants of the 'multidimensional reflection principle' maintain the simplicity of computation, while using the available *ab initio* data on the molecule for the potential energy surfaces and the transition dipole moments. In one of the calculations, the absorption cross section was broadened empirically to get agreement with the absorption data and the results were then used to make calculations of isotopologue fractionation. This broadening was also needed in a wave packet propagation calculation.

In a later calculation, without introducing the broadening factor, the results were compared only on one side of the absorption cross section, where the isotopic fractionation measurements are available. Using these two methods, the fractionation of heavier isotopologues of N_2O with respect to the most abundant isotopologue $^{14}N^{14}N^{16}O$ were calculated and compared with the experiments. A simple relation between the fractionations of $^{14}N^{14}N^{17}O$ and $^{14}N^{14}N^{18}O$ was observed in the results from our calculations. A perturbation theoretical result was used to derive this relationship, which is independent of the detailed calculations required for each of the isotopologues individually.

Contents

Chapter 1

Introduction

Several new pioneering chemical physics experiments were performed in the recent past and in the following paragraphs we discuss some of these which were directly an object of our theoretical study in the present thesis and also the various challenges these problems posed for theoretical modeling. A more specific introduction to each of the problems is given in the chapters which are written in a self-contained way.

Besides the new found interest in the systems mentioned below, some of these new experiments were possible with technological advances, the single enzyme experiments because of the novel methods of immobilizing and imaging single molecules; the single molecule force induced experiments because of the advances in single molecule manipulation using laser traps, and the isotopologue effects in nitrous oxide because of the ultrsensitive experimentation to probe isotope effects.

Part I - Fluctuations in single enzymes

Single molecule experiments have shown several new phenomena that are usually averaged and not observed in ensemble experiments. A few of these single molecule experiments include regular, non-stochastic oscillations of GFP between anionic and neutral chromophore states near denaturation compared to the usual stochastic behavior (1) and power-law dependence of the on and off periods compared to the usual exponential distribution in the

blinking behavior of single quantum dots (2). Among these single molecule experiments are the observations on single enzymes showing fluctuations in catalysis rate (3), spectral diffusion (4) and fluorescence lifetime fluctuate (5). Using novel experimental techniques it was demonstrated that these fluctuations in the enzymes show unusual autocorrelations represented by stretched exponential and power law for different observables.

The theoretical challenges these data posed were: 1. the observation of fluctuation behavior in single enzymes was unprecedented, so the limited experimental data available needed a first order model for interpretation 2. there was a constraint on the models, imposed by the experimental observation that the autocorrelation functions of catalysis rate k and the spectral frequency of fluorescence emission ω_0 show a similar decay in time and 3. the observed behavior was modeled in terms of fluctuations in the local electrostatic interactions constrained as in #2 above. The experimental time scale of milliseconds to seconds is not within the range of current real time computational capabilities which are limited to tens of nanoseconds. It was thus difficult to form an intuition on these processes by performing molecular dynamics simulations. So, the theoretical framework developed should allow a comparison with the experiments, without being restricted by the limitation imposed by computations.

These questions on fluctuations of the observables in single enzymes are explored in **Part I** of the thesis.

In **Chapter 2** we build a common framework of fluctuations in electrostatic interactions to describe three different experimental observations - catalysis rate fluctuations, spectral diffusion and fluorescence lifetime fluctuations, deriving a relation between the autocorrelation functions of these observables (6).

In **Chapter 3** we explore one possible method of calculating local fluctuations in electrostatic interaction energy using experimentally measurable frequency dependent dielectric

properties of the proteins. The calculations are compared with the stretched exponential and power law behavior of the autocorrelation of experimental observables, catalysis rate fluctuations and fluorescence lifetime fluctuations, respectively (7). Several experiments are proposed based on this model for interpreting the data.

Part II - Nonequilibrium fluctuations in single molecules

Single molecule manipulation using laser traps has become possible recently and these techniques have been used to study the stochastic trajectories in single RNA hairpins (8) and colloidal particles (9). Because of the ability to track these individual trajectories and the fluctuations, these experiments were used to test a theorem in nonequilibrium statistical physics - Crooks' theorem (10). Crooks' theorem focuses on the nonequilibrium fluctuations in a system, which lead to the deviations from the mean work done on (or by) the system. These deviations lead to a probability distribution of work done on (or by) the system which can be obtained by performing several experimental runs on the system. Crooks' theorem provides an exact equality for relating the probability of work done in the forward and reverse directions, that can be obtained by varying a parameter of the system externally in forward and reverse directions. The challenge single molecule experiments on RNA hairpins for Crooks' theorem pose is in understanding the subtleties in the experimental conditions and those in the derivation of the theorem. The theorem is derived for the condition that a parameter of the system (for the RNA hairpin case it is either externally applied force or the length) can be varied for different runs of the experiment in a predetermined way, where as in the unfolding experiments this condition is violated when the applied force drops upon unfolding.

The origin and consequences of this discrepancy between Crooks' theorem and the experimental conditions are studied in **Part II** of the thesis.

In **Chapter 4** the derivation is examined for an activated process, as in the unfolding

experiments. The subtleties in the proof are noted, one of which leads to an expression for the free-energy difference ΔG obtained from the theorem and the other of which points out where the condition of jump in external parameter will appear in the proof. In the presence of a jump the existing derivations for the nonequilibrium case are not valid. However, it is shown that the final equality of the theorem is recovered under quasiequilibrium conditions (11).

In **Chapter 5** an alternative interpretation of the data on the probability distribution of the work done during unfolding and refolding is given in terms of the distortion of the free-energy surface under applied force. A few insights gained into the experiments using this interpretation are outlined in this chapter (12).

Part III - UV photodissociation of N_2O

Several experiments on photodissociation necessiate theoretical models to predict isotopologue fractionation (13), the effect of isotopic substitutions in the molecules undergoing photodissociation. The theoretical challenges posed by this problem need: 1. a theory which can model the process accurately to account even for the fine differences in the isotopic susbtitutions into consideration 2. preferably the computations are not intensive and 3. simplification of existing calculations to capture the essence of it transparently, especially when the exact quantitative details of each of the isotopologues can be neglected and only the ratio of the two isotopic effects is important.

These questions on isotope effects in photodissociation are addressed in **Part III** of the thesis.

In **Chapters 6** and **7** we present two different methods of calculating the absorption cross section (14; 15) with a computationally inexpensive method using two variants of the multidimensional reflection principle, and using the potential energy surfaces (PES) and tran-

sition dipole moments from *ab initio* calculations. Theoretical calculations of UV photodissociation of N_2O involving wavepacket dynamics exist in the literature, and the calculations presented in this thesis are computationally easier compared to these wavepacket calculations. Our calculations were used to capture the isotopic dependence of absorption cross sections, and the isotopic enrichments calculated using these absorption cross sections are compared with those observed in the stratosphere and in the laboratory experiments (13).

In **Chapter 8** emphasizes a particular result from Chapters 6 and 7, which is that the ratio of the fractionations of isotopologues $^{14}N^{14}N^{17}O$ and $^{14}N^{14}N^{18}O$ follow a simple relationship, even though the calculation of each of these independently involves the detailed information on potential energy surfaces and transition dipole moments. This relationship is derived using a perturbation theoretical expansion (16).

Bibliography

[1] G. Baldini, F. Cannone, and G. Chirico, *Science, 309,* 1096 (2005)

[2] M. Nirmal, B. O. Dabbousi, M. G. Bawendi, J. J. Macklin, J. K. Trautman, T. D. Harris, and L. E. Brus, *Nature, 383,* 802 (1997)

[3] B. P. English, W. Min, A. M. van Oijen, K. T. Lee, G. Luo, H. Sun, B. J. Cherayil, S. C. Kou, and X. S. Xie, *Nat. Chem. Bio., 2,* 87 (2006)

[4] H. P. Lu, L. Xun, and X. S. Xie, *Science, 282,* 1877 (1998)

[5] H. Yang, G. B. Luo, P. Karnchanaphanurach, T. M. Louie, I. Rech, S. Cova, L. Y. Xun, and X. S. Xie, *Science, 302*, 262 (2003).

[6] M. K. Prakash, and R. A. Marcus, *submitted to Proc. Natl. Acad. Sci. USA* (2007a)

[7] M. K. Prakash, and R. A. Marcus, *in preparation* (2007b)

[8] D. Collin, F. Ritort, C. Jarzynski, S. B. Smith, I. Tinoco, Jr., and C. Bustamante, *Nature, 437*, 231 (2005)

[9] V. Blickle, T. Speck, L. Helden, U. Seifert, and C. Bechinger, *Phys. Rev. Lett., 96*, 070603 (2006)

[10] G. E. Crooks, *Phys. Rev. E, 61*, 2361 (2000)

[11] M. K. Prakash, *submitted to J. Chem. Phys.* (2007a)

[12] M. K. Prakash, *submitted to Biophys. J.* (2007b)

[13] P. von Hessberg, J. Kaiser, M. B. Enghoff, C. A. McLinden, S. L. Sorensen, T. Rockmann, and M. S. Johnson, *Atm. Chem. Phys., 4,* 1237 (2004).

[14] M. K. Prakash, J. D. Weibel, and R. A. Marcus, *J. Geophys. Res. Atmos., 110,* Art. No. D21315 (2005)

[15] W. C. Chen, M. K. Prakash, and R. A. Marcus, *in preparation* (2007)

[16] M. K. Prakash, and R. A. Marcus, *J. Chem. Phys., 123,* 174308 (2005)

Part I

Fluctuations in single enzymes

Chapter 2

Fluctuations in enzyme catalysis rate, spectral diffusion and radiative lifetimes. Interpretation in terms of electric field fluctuations

Time-dependent fluctuations in the catalysis rate ($\delta k(t)$) observed in single enzyme experiments were found in a particular study to have an autocorrelation function decaying on same time scale as that of spectral diffusion $\delta\omega_0(t)$. To interpret this similarity, the present analysis focuses on a factor in enzyme catalysis - the local electrostatic interaction energy (E) at the active site and its effect on the activation free energy barrier. We consider the slow fluctuations of the electrostatic interaction energy ($\delta E(t)$) as a contributor to $\delta k(t)$ and relate the latter to $\delta\omega_0(t)$. The resulting relation between $\delta k(t)$ and $\delta\omega_0(t)$ is a dynamic analog of the solvatochromism used in interpreting solvent effects on organic reaction rates. The effect of the postulated $\delta E(t)$ on fluctuations in the radiative *component ($\delta\gamma_r^{-1}(t)$) of the fluorescence decay of chromophores in proteins is also examined, and a relation between $\delta\gamma_r^{-1}(t)$ and $\delta\omega_0(t)$ is obtained. Experimental tests will detemine whether or not the correlation functions for $\delta k(t)$, $\delta\omega_0(t)$ and $\delta\gamma_r^{-1}$ are indeed similar for any enzyme. Measurements of dielectric dispersion, $\epsilon(\omega)$, for the enzyme discussed elsewhere will provide further insight into the correlation function for $\delta E(t)$. They will also determine whether fluctuations in the nonradiative component γ_{nr}^{-1} of the lifetime decay has a different origin, fluctuations in distance for example.*

I. Introduction

Single molecule experiments on proteins have revealed novel phenomena. They include experiments on the fluctuations in the rates of enzyme catalysis (1-3), on-off blinking behavior in proteins (4-6) and oscillations under a near-denatured condition of a green fluorescent protein (7). The on-off blinking behavior of proteins and the fluctuations in the enzyme catalysis rate in the experiments were interpreted in terms of fluctuations of the protein/enzyme between various conformational substates (2, 3). The rates of enzyme-catalyzed reactions themselves occur typically on the milliseconds to seconds time scale, and the millisecond dynamics of enzymes are believed to contribute to the 'functional dynamics' of the enzyme (8). Single molecule enzyme experiments on cholesterol oxidase revealed an autocorrelation function of the rate of catalysis that decayed on a time scale about the same as that for the decay of the autocorrelation function of the spectral diffusion of a chromophore in the same enzyme in the absence of the substrate (1), thus suggesting a common origin for the two fluctuations.

Significant insight into the functioning of enzymes has been achieved using computer simulations (9-11), using empirical valence bond (EVB) (9) and hybrid quantum mechanical/molecular mechanics (QM/MM) (10) methods among others. In these studies the catalysis is affected by several factors - electrostatic effects of the enzyme on the substrate (9), and coupling of protein fluctuations with motions of the substrate-coenzyme pair in the transition state [*e.g.,* ref. (8)]. Electrostatic effects have been seen to be significant in enzymatic catalysis (9, 12-25). Direct molecular dynamics simulations of protein dynamics are typically restricted to tens of nanoseconds and so a detailed dynamical analysis of the observed millisecond rate fluctuations via an integration of the equations of motion of the atoms is presently beyond the scope of such simulations. Simulations with bias potentials using methods such as accelerated molecular dynamics (26), which allow long time scale trajectories up to milliseconds, have not yet been performed to study the equilibrium conformational fluctuations in enzymes.

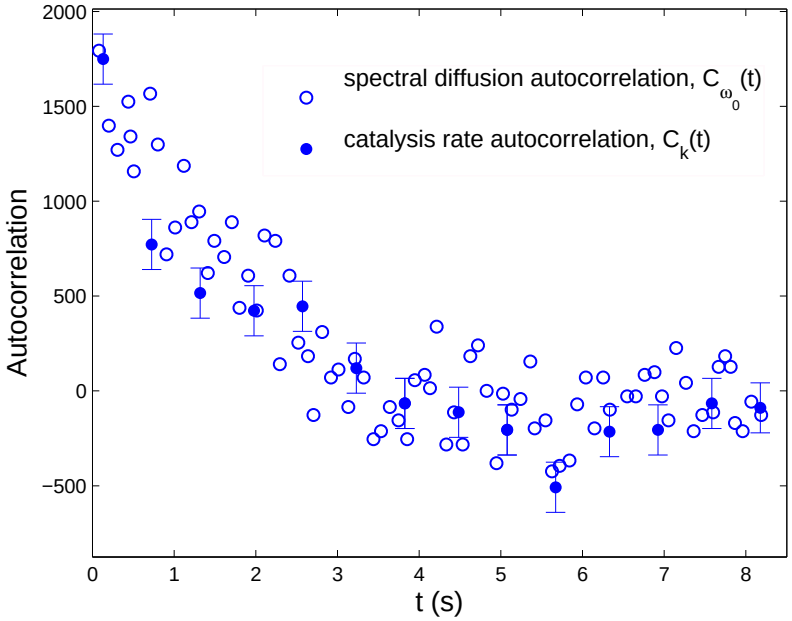

Figure 2.1: Comparison of the decay of autocorrelations of catalysis rate fluctuations ($C_k(t)$ in s^{-2}) and spectral diffusion ($C_{\omega_0}(t)$ in cm^{-2}) from Figs. 4A and 5C of Ref. 1. $C_k(t)$ is rescaled by a factor of 8750 cm^{-2}/s^{-2} to account for the difference in normalization factors for both of these autocorrelations. The abcissa for $C_k(t)$ is given in number of turnovers, converted to time units by using $\sim$ 600 ms/turnover (1). The value for $C_{\omega_0}(t)$ at t=0, 6000 cm^{-2}, possibly representing a decay component that is faster than the resolution of $C_k(t)$, is outside the range of the current plot.

Spectral diffusion of a chromophore has been interpreted as due to transitions of the molecule between different chromophore conformations (27) or in terms of the density fluctuations of the dielectric matrix leading to polarization fluctuations (28). Previous studies of a different nature have included the role of the electric field on time-dependent vibrational Stark shift at the heme site of myoglobin (29) and of the nitrile stretching mode in human aldose reductase (30), both in the picosecond regime. Considering the importance of electrostatics in enyzme catalysis (9, 12-25) and in spectral diffusion ($\delta\omega_0(t)$), we explore the possibility that $\delta k(t)$ and $\delta\omega_0(t)$ may be related to each other via the time-dependent fluctuations in the local electrostatic interaction energy, $\delta E(t)$.

The present work on correlation functions of different enzyme properties was prompted by

an experimental observation of the autocorrelation functions of catalysis rate of oxidation of cholesterol ($C_k(t)$) and the spectral diffusion ($C_{\omega_0}(t)$) for cholesterol oxidase (1). The two autocorrelation functions are compared in the present Fig. 2.1. The $C_{\omega_0}(t)$ in Fig 2. of ref. (1) has a fast initial decay, followed by a slow decay. The fast initial decay is attributed to the noise in the spectral means and/or fluctuations on a time scale faster than the experimental resolution (31). In the present Fig. 2.1 only the slow decay component is shown, by excluding the data point at $t = 0$. The result is seen to have the same functional form as the $C_k(t)$. To compare the time behavior of these two different physical measurements, the absolute value of $C_k(t)$ from ref. (1) was rescaled to match that of $C_{\omega_0}(t)$. The comparison in Fig. 2.1 highlights a similarity of the decay of the two autocorrelations with time. By examining the reduced autocorrelation functions, such as $\langle \delta\omega_0(t)\delta\omega_0(0)\rangle / \langle \delta\omega_0(0)^2\rangle$, the focus is on the time scale rather than on absolute values.

With a common theme of fluctuations in the local electrostatic interaction energy three different observables are examined - catalysis rate fluctuations ($\delta k(t)$), spectral diffusion ($\delta\omega_0(t)$) and fluctuations in the *radiative* component of fluorescence decay ($\delta\gamma_r^{-1}$). In the following analysis the $\delta k(t)$ and $\delta\omega_0(t)$ are first related to the fluctuations local electrostatic interaction energy ($\delta E(t)$) and then to each other. These fluctuations $\delta E(t)$ are used later to describe $\delta\gamma_r^{-1}$ by relating it to $\delta\omega_0$. Experimental tests are suggested for exploring the suggested relationships between the three quantities. A quantity not specifically treated but discussed later is the fluctuation in the *nonradiative* component γ_{nr}^{-1} of the lifetime decay of a fluorescing protein, which may have a different origin as studied by Xie and coworkers (32, 33). These two components of fluorescence decay, γ_r and γ_{nr}, can be distinguished by an experiment suggested later in the article to be performed in the total absence in the enzyme of any fluorescence quencher that is responsible for the nonradiative fluorescence decay γ_{nr} by electron transfer.

II. Enzyme fluctuations

A. Fluctuations in catalysis rate and in local electrostatic interaction energy

The autocorrelation function $C_E(t)$ of the fluctuations in local electrostatic interaction energy at the active site, $\delta E(t)$, can be defined as

$$C_E(t) = \frac{\langle \delta E(t) \delta E(0) \rangle}{\langle \delta E(0) \delta E(0) \rangle} \tag{2.1}$$

Experimentally the catalysis rate k is obtained by averaging the turnover times from several cycles of the enzyme (1), over which the enzyme is assumed to be in the same conformation. We assume that there is some slow protein coordinate $X(t)$ representing this conformation and the local electrostatic interaction energy at the active site E depends on this X, and since X varies with t we write the slowly fluctuating $E(X(t))$ as $E(t)$. Fluctuations in the catalysis rate ($\delta k(t)$) depend, among other factors, upon these slow fluctuations in the electrostatic energy ($\delta E(t)$) occuring on the time scale of the order of the reciprocal of the rate constant for the hydride (or other) transfer within the bound substrate and enzyme complex. We write $\delta k(\delta E(t))$ as $\delta k(t)$.

Fluctuations of k with time, $\delta k(t)$, around a mean value k_o, are related to the time-dependent fluctuations in E, $\delta E(t)$, around a mean value E_0. The relation can be regarded as occuring via a dependence of the activation free energy on $E(t)$ through the dipole moment difference ($\Delta \boldsymbol{\mu}_r$) of the transition state and the reactants. We assume for simplicity that fluctuations in X mainly affect those in E rather than those in $\Delta \boldsymbol{\mu}_r$. The approximate relationship can be written as

$$k(t) = A e^{-E_0/k_B T} e^{-\delta E(t)/k_B T} = k_0 \, e^{-\delta u(t)} \tag{2.2a}$$

where the notation

$$\delta u(t) = \delta E(t)/k_B T \tag{2.2b}$$

is used for convenience and A is a proportionality factor that can depend on other factors affecting the reaction rate. Assuming the fluctuations $\delta u(t)$ are Gaussian about a mean value $\langle \delta u \rangle = 0$, using a cumulant expansion (34) and neglecting the terms beyond the quadratic the following relation can be obtained

$$\langle k(t)k(0) \rangle = k_0^2 \langle e^{-\delta u(t)} e^{-\delta u(0)} \rangle = k_0^2 e^{\langle \delta u(t) \delta u(0) \rangle} \tag{2.3a}$$

and

$$\langle \delta k(t) \delta k(0) \rangle = \langle (k(t) - k_0)\,(k(0) - k_0) \rangle = k_0^2 \left[e^{\langle \delta u(t) \delta u(0) \rangle} - 1 \right] \tag{2.3b}$$

It was seen in ref. (1) that the ratio of the catalysis rate maximum to minimum was about a factor of 10. The root mean square fluctuation of k is much less, perhaps a factor of 2, as in Fig. 5C of ref. (3). These results mean that the catalysis rate fluctuates from the mean by a factor of about 3 ($\approx \sqrt{10}$), so in Eq. (2.2a), $\delta u(t)$ ranges from about -1.09 to 1.09, and the variance, $\langle \delta u(0)^2 \rangle$, is about 0.3. With this variance for δu, the following approximation can be made

$$\langle \delta k(t) \delta k(0) \rangle = k_0^2 \, \langle \delta u(t) \delta u(0) \rangle \tag{2.3c}$$

After normalization by division by the appropriate factors, $\langle \delta k(t) \delta k(0) \rangle$, $\langle \delta u(0) \delta u(0) \rangle$, the autocorrelation function $C_k(t)$ is approximated to that of $\delta u(t)$. We thus have

$$C_k(t) = \frac{\langle \delta k(t) \delta k(0) \rangle}{\langle \delta k(0) \delta k(0) \rangle} \approx C_u(t) \tag{2.4}$$

Using Eqs. (2.2b) and (2.4), we have

$$C_k(t) \approx C_E(t) \tag{2.5}$$

Thereby, the fluctuations in the catalysis rate of the enzyme are interpreted in terms of the fluctuations in the local electric field.

B. Spectral diffusion and fluctuations in electrostatic energy

The emission spectrum was obtained by collecting fluorescence emissions of photons for about 100 ms (1) at different time intervals. The spectral mean of broad emission spectrum is calculated by averaging over the spectrum. The spectral mean so obtained undergoes fluctuations, spectral diffusion (1). To relate the fluctuations in local electrostatic interaction energy to spectral diffusion in enzymes and so relate the latter to catalysis we note that to first-order in δE the change in emission frequency $\delta\omega_0$ of the chromophore is given as

$$\hbar\ \delta\omega_0 = -\delta E \tag{2.6}$$

In this case of spectral diffusion, the electrostatic interaction energy $\delta E(t)$ depends upon $\Delta\boldsymbol{\mu}$, the change in dipole moment of the chromophore upon electronic excitation. The autocorrelation function of the spectral diffusion is

$$C_{\omega_0}(t) = \frac{\langle \delta\omega_0(t)\delta\omega_0(0)\rangle}{\langle \delta\omega_0(0)^2\rangle} \tag{2.7a}$$

Using Eqs. (2.6) and (2.7a), we have

$$C_{\omega_0}(t) = C_E(t) \tag{2.7b}$$

where the equality between C_E and C_{ω_0} in Eq. (2.7b) follows from Eqs. (2.6) and **2.7a**. Comparing Eqs. (2.5) and (2.7b), we then have $C_k(t) = C_{\omega_0}(t)$.

C. Fluctuations in radiative component of the fluorescence decay rate

Fluorescence decay lifetime (γ^{-1}) was obtained experimentally by averaging the delay times between the excitation of the chromophore and emission of photons (32), and fluctuations in γ^{-1} were observed (32, 33). The fluorescence decay lifetime of a chromophore in the protein, γ^{-1}, depends upon the rate constants of radiative (γ_r) and nonradiative (γ_{nr}) components, with possible fluctuations in either or both of these quantities:

$$\gamma^{-1} = (\gamma_r + \gamma_{nr})^{-1} \tag{2.8}$$

Eq. (2.8) with a single exponential decay of fluorescence intensity was assumed in refs. (32, 33). The decay of fluorescence intensity of the chromophore on the nanosecond time scale could in principle be a multiexponential. However, in the current absence of detailed single molecule on a nanosecond time scale studies showing an evidence to the contrary (a point we discuss further below) a single exponential decay is assumed, as in refs. (32, 33).

We examine now a modeling of fluctuations in the *radiative* component of the fluorescence decay lifetime ($\delta\gamma_r^{-1}$) of a chromophore in the protein in terms of $\delta E(t)$. γ_r^{-1} and the spectral frequency (ω_0) are related by (28):

$$\gamma_r^{-1} \propto \frac{1}{\omega_0^3} \tag{2.9}$$

This relation was also observed experimentally in ref. (35), with a mostly linear relation between the $\delta\gamma_r$ and $\delta\omega_0$ over the observed range $\delta\omega_0$ of spectral diffusion.

The variations in the observables k, ω_0 and γ^{-1} can be discussed using either the standard deviation of their distribution or the variation between the maximum and minimum

of the observable (amplitude). In the following, we refer to the latter extreme variation (amplitudes) in all these observables, unless explicitly mentioned that it is the root mean square deviation. For a spectral diffusion between the extreme values of 550 nm and 580 nm for carbocyanine dye molecules in a polymeric matrix, a purely radiative decay coupled to the environmental fluctuations can explain the maximum fluctuations of lifetime $\approx \pm 0.5$ ns about a 2 ns fluorescence lifetime (35). In other experiments with chromophores embedded in polymeric matrix, a maximum variation in spectral diffusion between 650 nm and 670 nm for sulphorhodamine 101 (27) and fluorescence lifetime between 2 ns and 4 ns for the chromophore 1,10-dioctadecyl-3,3,30,30-tetramethylindodicarbocyanine (28) were observed. For the entire range of spectral diffusion between 520 nm and 535 nm observed in cholesterol oxidase-flavin adenine dinucleotide complex in ref. (1), a nearly linear relation between $\delta\gamma_r^{-1}$ and $\delta\omega_0$ is valid since $\delta\omega_0/\omega_0 = \pm 0.015$.

$$\gamma_r^{-1} + \delta\gamma_r^{-1} \sim (\omega_0 + \delta\omega_0)^{-3} \approx \frac{1}{\omega_0^3}(1 - 3\frac{\delta\omega_0}{\omega_0}) \tag{2.10}$$

From Eqs. (2.7b) and (2.10), the autocorrelation function of the radiative component of the lifetime is

$$C_{\gamma_r^{-1}}(t) = \frac{\langle \delta\gamma_r^{-1}(t)\delta\gamma_r^{-1}(0)\rangle}{\langle \delta\gamma_r^{-1}(0)\delta\gamma_r^{-1}(0)\rangle} = C_E(t) \tag{2.11}$$

We then have from Eqs. (2.5), (2.7b) and (2.11)

$$C_k(t) = C_{\omega_0}(t) = C_{\gamma_r^{-1}}(t) = C_E(t) \tag{2.12}$$

If other contributions to the radiationless transitions are minor, the autocorrelation of γ_r^{-1} can be obtained from single molecule experiments for mutated Tyr35 flavin reductase. This autocorrelation function of γ_r^{-1} does not appear to have been given explicitly in ref. (32). If for that system, the fluctuations in γ_r^{-1} prove to be negligible, then the fluctuations in γ^{-1}

in refs. (32, 33) are solely due to nonradiative fluorescence decay, γ_{nr}^{-1}. Fluctuations in γ_{nr}^{-1} have been treated in terms of fluctuations in donor-acceptor distance δr_{DA} for quenching of fluorescence by electron transfer (32, 33). Only if δr_{DA} and δE have a common origin, for example due to conformational fluctuations of the enzyme, could one then write $C_{\gamma^{-1}}(t) = C_{\gamma_r^{-1}}(t) = C_{\gamma_{nr}^{-1}}(t) = C_E(t)$ and hence $C_k(t) = C_{\omega_0}(t) = C_{\gamma^{-1}}(t)$.

III. Discussion

Different facets of enzyme catalysis have been examined previously (8, 9). For example, Warshel *et al.* (9) discussed the role of electrostatics at the active site in affecting the activation barrier for the reaction and Agarwal *et al.* (11) discussed statistical correlations of the dynamics of the different residues of the enzyme by mapping out the network of correlated motions using NMR. These discussions have not yet been applied to time-dependent fluctuations of the enzymatic catalysis rate observed in refs. (3) and (36), as noted earlier. Catalysis rate fluctuations have been interpreted qualitatively as due to conformational fluctuations of the enzyme, each rate corresponding to a different conformation (2, 3). Similarly spectral diffusion was attributed to different conformations of the enzyme (1).

The dynamics in proteins happens on multiple time scales from tens of femtoseconds to hundreds of seconds (37). Each motion in protein is associated with a typical time scale, for example, the vibrations are on the hundreds of femtoseconds and large motions such as domain movements in proteins are on the milliseconds time scales (37). The electric field fluctuations can arise from any or all of these different dynamics and so can last over the whole dynamic range of proteins from femtoseconds to seconds. The experimental techniques used in refs. (1, 3, 30, 31) focus on the slow dynamics on millisecond to second time scales. The dynamics faster than this are averaged over in the observations. One feature of formulating the fluctuations of observables, sometimes termed dynamic disorder (38), in terms of fluctuations in electrostatic interactions is seen from a method of computing the autocorrelation function, $C_E(t)$, discussed elsewhere (39), in terms of a measurable

frequency dependent dielectric dispersion ($\epsilon(\omega)$) of the protein. In that formalism, the dielectric constant varying in the frequency range of kHz to Hz provides an estimate of the electric field fluctuations on the desired milliseconds to seconds time scale.

The experimentally observed similarity in the time scale for decay of the autocorrelation function of catalysis rate fluctuations and the autocorrelation function of spectral diffusion seen in ref. (1) in the absence of the substrate also recalls the empirical relation (40) between organic reaction rates and electric field effects on spectra in different solvents. In the latter formalism, the solvatochromic shift of the spectral frequency of a dye in a solvent indicates the degree of polarity of the solvent and is empirically found to be proportional to the decrease in the activation free energy ($\Delta G^{\neq}$) for the reaction, expressed in terms of the logarithm of the rate constant. The present model with fluctuations is a dynamic analog of solvatochromism. Although the proportionality constant to $\Delta G^{\neq}$ will depend upon the chromophore and the polarity of transition state relative to the reactants, it can be ≈ 1 in an order of magnitude estimate (40). With this approximation the reduction in the activation free energy barrier for a reaction is equal to the shift in energy levels of a chromophore placed in the same environment, the enzyme in the present case.

The spectral frequency emitted by the chromophore in the enzyme may be different for every photon. Over a short time (milliseconds), the change in the frequency is due to the homogeneous broadening of the emission because of dynamics happening on time scales faster than nanoseconds. At times longer than a hundreds of milliseconds, as the slow conformational changes of the enzyme happen, the new enzyme environment leads to a new emission spectrum and the shift in the spectral mean is used to interpret the conformational dynamics. It should be noted that the width of the homogeneous broadening is much higher than the shift in the spectral mean (Figs. 5A, 5B of ref. (1)). So, broadening introduced in the emission my be interpreted only by studying the single molecules, since these small changes may not be noticeable in ensembles.

One can estimate the standard deviation of the fluctuations in enzymatic rate constant k from the standard deviation of the spectral diffusion. Using $k = k_0 exp(-\delta u)$, and $\langle k \rangle = k_0 exp(-2\langle \delta u^2 \rangle)$ from the cumulant expansion, we have

$$\sqrt{\frac{\langle k^2 \rangle - \langle k \rangle^2}{\langle k \rangle^2}} = \sqrt{2 \langle \delta u^2 \rangle} \tag{2.13}$$

The standard deviation of spectral diffusion in cholesterol oxidase as seen from Fig. 5C in ref. (1), after excluding the first data point which can be because of noise as noted earlier, is 46 cm^{-1} ($\approx$ 0.13 kcal.mol^{-1}). It corresponds to $\sqrt{\langle \delta u^2 \rangle} \approx 0.13\,\mathrm{kcal.mol^{-1}}/k_B T = 0.22$. This $\sqrt{\langle \delta u^2 \rangle}$ using Eq. (2.13) leads to a predicted fluctuation in k of a $\sqrt{2} \times 0.22 = 0.31$. The standard deviation of k in β- galactosidase from Fig. 5C of ref. (3) is roughly 60 s^{-1} from mean value of k, 170 s^{-1}. This gives a variation of 60 s^{-1}/170 s^{-1} which is approximately 0.35 and so is comparable to that predicted from spectral diffusion above.

Depending upon the specific properties of the chromophore and the polarity of the reaction, the fluctuations between the extreme values can vary by a factor different from this estimated value of 9. The simulations of human aldose reductase (hALR2) containing the inhibitor IDD743 show a distribution of electric fields, corresponding to various orientations of the side chains, ranging between extreme values separated by about 3 $k_B T/eA$ (= 7.7 MV/cm), 5 $k_B T/eA$ (= 12.9 MV/cm) for the wildtype and V47D enzymes (Fig. 3C of an article from Boxer's group (30)). In the introduction to this study (30), an electric field of 9 MV/cm was estimated to stabilize the transition state with a typical charge separation of 1 $\AA$ by 2.3 kcal/mol. Using this estimate of 1.8 kcal/mol, the catalysis rate can fluctuate by a factor of $exp(-1.8\mathrm{kcal.mol^{-1}}/k_B T) \approx 20$. The latter is approximately of the order of the observed fluctuation of a factor of 10 between the extreme values of k seen in Fig. 5 of English *et al.* (3) for β-galactosidase. So, the magnitude of fluctuations in electrostatic interaction energy in proteins are significant enough to be a possible origin of the obersved fluctuations in k. Had root mean square values been available, as they were in the previous paragraph, those quantities could also have been compared.

Fluctuations in γ_r^{-1} due to electric field fluctuations may be related in the model to catalysis rate fluctuations, $C_k(t) = C_{\gamma_r^{-1}}(t)$ in Eq. (2.12). The relation can be explored experimentally by comparing the two autocorrelation functions, analogous to the comparison of $C_k(t)$ and $C_{\omega_0}(t)$ pointed out in ref. (1). The experimental fluorescence lifetime autocorrelation function, $C_{\gamma^{-1}}(t)$, reported in the literature (32, 33), for flavin reductase and fluorescein-antifluorescein complex were interpreted, as noted earlier, in terms of the non-radiative lifetime fluctuations $\delta\gamma_{nr}^{-1}$ due to fluctuations in an electron donor - electron acceptor distance coordinate, r_{DA} (32). To relate γ_{nr}^{-1} fluctuations to $\delta k(t)$, one then uses information on how r_{DA} is related to k. The present fluctuation in γ_r^{-1} follows instead from the hypothesis of fluctuations in electrostatic interaction energy, which in turn can used to interpret the fluctuations in catalysis rate.

The ensemble data on the enzymes (Fig. 1 of ref (32)) shows a multiexponential decay of fluorescence intensity. This multiexponentiality can arise from the enzyme fluctuating between different conformations, each with a different single exponential decay. Alternatively the fluorescence decay can be multiexponential in each of these conformations. As we noted earlier that the data on the delay times for fluorescence emission thus far (32) do not distinguish between single and multiple exponential decay on a nanosecond time scale. Because of the very small intensity of the fluorescence, it was necessary to accumulate delay times for ≈ 1 ms in order to calculate the an approximate fluorescence lifetime. Despite the long binning time, the number of photons collected were not enough to distinguish a single exponential from a multiexponential on a nanosecond time scale.

Assuming a single exponential decay for each enzyme conformation as in Eq. (2.8), we have the fluctuations in the total radiative lifetime γ^{-1} as

$$\delta\gamma^{-1} = -\frac{1}{(\gamma_r + \gamma_{nr})^2}\,\delta\gamma_{nr} - \frac{1}{(\gamma_r + \gamma_{nr})^2}\,\delta\gamma_r = \phi_{nr}^2\,\delta\gamma_{nr}^{-1} + \phi_r^2\,\delta\gamma_r^{-1} \tag{2.14}$$

where ϕ_{nr} and ϕ_r are the quantum yields of nonradiative and radiative fluorescence decays,

respectively, $\gamma_{nr}/(\gamma_r+\gamma_{nr})$ and $\gamma_r/(\gamma_r+\gamma_{nr})$. In the single molecule experiments (32, 33) the multiexponentiality in the fluorescence decay was interpreted as being due to a distribution of conformations. In these experiments, the fluctuations in total fluorescence lifetime $\delta\gamma^{-1}$ were reported, rather than the individual components $\delta\gamma_r^{-1}$ and $\delta\gamma_{nr}^{-1}$.

To study the fluctuations in the purely radiative component in the enzyme environment from a single molecule experiment, the contribution of the nonradiative effect on the fluorescence decay must be reduced. Ensemble fluorescence decay on flavin reductase performed with and without Tyr35 responsible for fluorescence quenching by electron transfer is available (Fig. S3 of (32)). However, data on single molecule fluorescence lifetime fluctuations in the absence of a quencher are currently not available.

The radiative component we refer to is the radiative component of fluorescence decay of the chromophore in the enzyme environment. The single molecule fluctuations of fluorescence decay of a chromophore embedded in a gel in the absence of a quencher was studied (Fig. S5 of ref. (32)). There was no slow component in the decay in the autocorrelation function of that system. However, what would be particularly interesting is the measurement of the lifetime fluctuation autocorrelation function of the chromophore *in the enzyme* in the absence of a quencher: the slow motion (millisecond) in enzymes may not have a counterpart in gels.

When single molecule data without Tyr35 becomes available it will be possible to test Eq. (2.12) using spectral diffusion data for the same enzyme. If the experiments thus performed by eliminating quencher show an autocorrelation function ($C_{\gamma_r^{-1}}(t)$) similar to that with the quencher ($C_{\gamma^{-1}}(t)$) the result may indicate a common origin for the fluctuations $\delta\gamma_r^{-1}$ and $\delta\gamma_{nr}^{-1}$ in terms of protein conformations.

Molecular dynamics simulations were performed (41) on flavin reductase, an enzyme used in the single molecule experiments on fluctuations in γ^{-1} (32). The distribution of electron

transfer donor-acceptor distance fluctuations in these simulations ranging from femtoseconds to nanoseconds was found to be similar to that in the experiments. The next question in using these simulations to interpret the $\delta\gamma_{nr}^{-1}$ fluctuations is to see what molecular aspects of the motions of the protein are preserved between the experimentally observed time scales of milliseconds to seconds and the fast motions accessible to simulations.

The experimental autocorrelations from the observables $C_{\gamma^{-1}}(t)$, $C_k(t)$ and $C_{\omega_0}(t)$ from the enzymes antifluorescein (33), candida antarctica lipase B (2), β-galactosidase (3) and cholesterol oxidase (1) are compared in Fig. 2.2. In the top panel of Fig. 2.2, the experimental data were shifted in the log-log plot to make the comparison of the decay pattern of the autocorrelations easier. To compare the inherent timescales in different enzymes, the lower panel is shown without any shift in time. The experimental data on $C_{\omega_0}(t)$ and $C_k(t)$ from cholesterol oxidase (1) show the same normalized autocorrelation function, after eliminating the data point at $t = 0$ from the $C_{\omega_0}(t)$ data as noted earlier. The autocorrelation functions from different enzymes in the lower panel of Fig. 2.2 (no scaling in time) are different from one another. Whether the differences in Fig. 2.2 are due to differences in properties of the observables or to differences in enzymes remains to be determined by future experiments. It would be helpful to test the proposed relations between the C's to see whether different C's from the same enzyme fall on the same plot, and whether the differences in Fig. 2.2 are because of the different enzymes used in the experiments. One feature of the present formulation as given in Eq. (2.12), if it is borne out by further experiments, is that it may also serve as a guide in further theoretical analyses. It also reduces the number of necessary independent properties to be evaluated from the computational or other theoretical studies.

IV. Experiments suggested by the analysis

Several experimental measurements can serve to explore the consequences of the present equations and test equations such as Eq. (2.12). These tests involve quantitative comparisons of catalysis rate correlation $C_k(t)$ and spectral diffusion $C_{\omega_0}(t)$ similar to the study

in ref. (1) and new measurements to compare them with fluctuations in the radiative component of fluorescence decay $C_{\gamma_r^{-1}}(t)$.

1. A comparison of the autocorrelation function $C_{\omega_0}(t)$ and $C_k(t)$ can be made from experimental data and the validity of Eq. (2.12) tested, if possible over a time range longer than the one order of magnitude in ref. (1).

2. The two different measurements for a chromophore in an enzyme, $C_{\omega_0}(t)$ and $C_{\gamma_r^{-1}}(t)$, do not appear to have been made for the same enzyme in the absence of the quencher (so reducing the value of γ_{nr}). The measurements of these two autocorrelation functions provide a test of Eq. (2.12). Green fluorescent protein (GFP) is another possible candidate for the test. Recent experiments have shown a spectral diffusion in GFP (42). Since the fluorescence quantum yield of GFP is very high, about 0.8, it might be a useful system to study the fluctuations in γ_r^{-1} in a way less affected by the γ_{nr}^{-1} contributions.

3. The fluctuations in fluorescence lifetime γ^{-1} are attributed to γ_{nr}^{-1} through electron transfer (ET) (32). A comparison of $\delta\gamma_{nr}^{-1}$ and $\delta\gamma_r^{-1}$ for a given system can be obtained most clearly by performing the control experiments with the nonradiative pathways reduced. In flavin reductase, experiments show that Tyr35 is the primary quencher responsible for the electron transfer process (32). If the autocorrelation function measurements can be performed by mutating Tyr35, so as to eliminate the quenching by ET (and also removing less important quenchers), the fluctuations in γ_r^{-1} would become more evident and so the data can be used to test Eq. (2.12).

V. Conclusion

A mechanism involving local electrostatic interaction energy fluctuations was explored to interpret an experimentally observed similarity (1) of time scale for spectral diffusion and fluctuations in catalysis rate. A theoretical relation between the two quantities arises if both fluctuations reflect the fluctuations in local electrostatic interaction energy. It can be regarded as a dynamical analog of the solvatochromism used in the catalysis of organic reac-

tions by different solvents. The formalism was also extended to fluctuations of the radiative component γ_r^{-1} of the fluorescence decay lifetime, information on which can be obtained when nonradiative pathways such as quenching of fluorescence by electron transfer are reduced. The various tests may help provide a broader framework for relating fluctuations in physical quantities to each other and to enzyme kinetics.

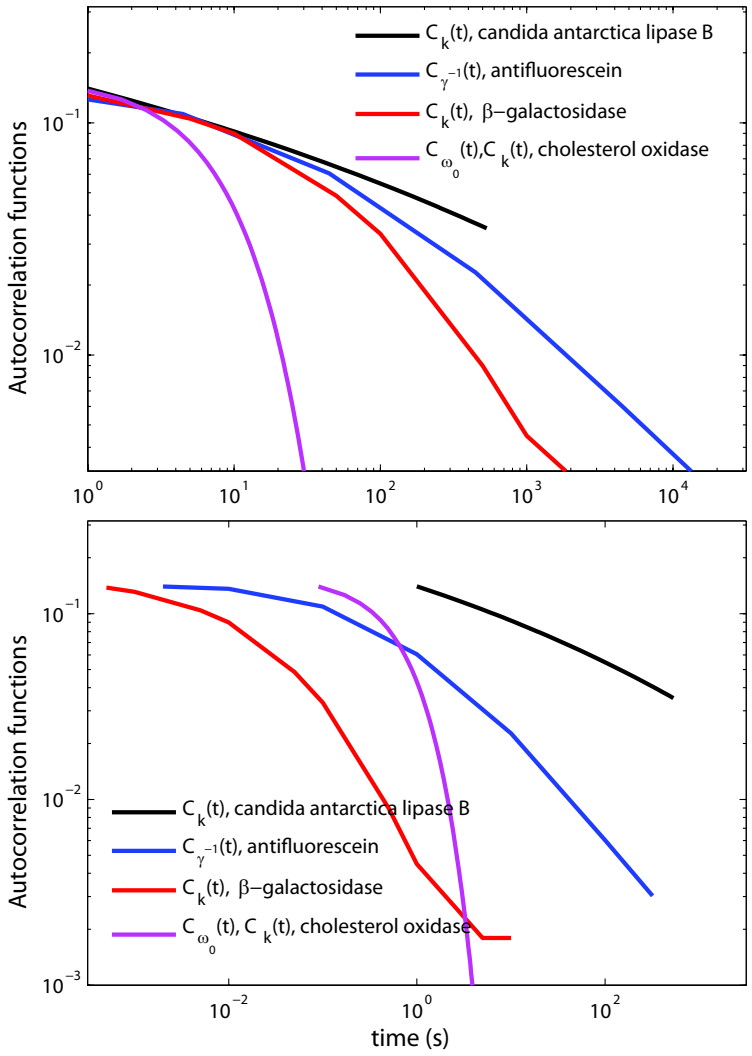

Figure 2.2: Comparison of the fits to experimental autocorrelation functions $C_{\gamma^{-1}}(t)$, $C_k(t)$ and $C_{\omega_0}(t)$ from three different enzymes. The autocorrelation functions were scaled to the same value at short time for comparison. In the top panel the autocorrelation functions were shifted horizontally in the log-log plot to make the comparison between them easier; the bottom panel is without this shift.

Bibliography

[1] H. P. Lu, L. Xun, and X. S. Xie, *Science, 282,* 1877 (1998)

[2] O. Flomenbom, K. Velonia, D. Loos, S. Masuo, M. Cotlet, Y. Engelborghs, J. Hofkens, A. E. Rowan, R. J. M. Nolte, M. Van der Auweraer, F. C. de Schryver, and J. Klafter, *Proc. Natl. Acad. Sci. USA, 102*, 2368 (2005)

[3] B. P. English, M. Min, A. M. van Oijen, K. T. Lee, G. Luo, H. Sun, B. J. Cherayil, S. C. Kou, and X. S. Xie, *Nat. Chem. Bio., 2,* 87 (2006)

[4] R. M. Dickson, A. B. Cubitt, R. Y. Tsien, and W. E. Moerner, *Nature, 388*, 355 (1997)

[5] S. Habuchi, R. Ando, P. Dedecker, W. Verheijen, H. Mizuno, A. Miyawaki, and J. Hofkens, *Proc. Natl. Acad. Sci. USA, 102*, 9511 (2005)

[6] M. F. Garcia-Parajo, G. M. J. Segers-Nolten, J. A. Veerman, J. Greve, and N. F. van Hulst, *Proc. Natl. Acad. Sci. USA, 97*, 7237 (2000)

[7] G. Baldini, F. Cannone, and G. Chirico, *Science, 309*, 1096 (2005)

[8] S. J. Benkovic, and S. Hammes-Schiffer, *Science, 301*, 1196 (2003)

[9] A. Warshel, P. K. Sharma, M. Kato, Y. Xiang, H. Liu, and M. H. M. Olsson, *Chem. Rev., 106*, 3210 (2006)

[10] J. Gao, and D. J. Truhlar *Ann. Rev. Phys. Chem., 53*, 467 (2002)

[11] P. K. Agarwal, S. R. Billeter, P. T. R. Rajagopalan, S. J. Benkovic, and S. Hammes-Schiffer, *Proc. Natl. Acad. Sci., 99,* 2794 (2002)

[12] A. Warshel, and M. Levitt, *J. Mol. Bio., 103*, 227 (1976)

[13] R. W. Pickersgill, P. W. Goodenough, I. G. Sumner, and M. E. Collins, *Biochem. J., 254*, 235 (1988)

[14] L. E. Dardenne, A. S. Werneck, M. D. Neto, and P. M. Bisch, *Proteins Struct. Funct. Genet., 52*, 236 (2003)

[15] K. F. Wong, J. B. Watney, and S. Hammes-Schiffer, *J. Phys. Chem. B, 108* 12231 (2004)

[16] J. Benach, J. -O. Winberg, J. -S. Svendsen, S. Atrian, R. Gonzalez-Duarte, and R. Ladenstein, *J. Mol. Biol. 345*, 579 (2005)

[17] K. E. Ranaghan, L. Ridder, B. Szefczyk, W. A. Sokalski, J. C. Hermann, and A. J. Mulholland, *Org. Biomol. Chem. 2*, 968 (2004)

[18] A. Warshel, *J. Biol. Chem., 273*, 27035 (1998)

[19] M. Garcia-Viloca, J. Gao, M. Karplus, and D. G. Truhlar, *Science, 303*, 186 (2004)

[20] A. Kienhofer, P. Kast, and D. Hilvert, *J. Am. Chem. Soc., 125* 3206 (2003)

[21] R. Wolfenden, and M. J. Snider, *Acc. Chem. Res., 34*, 938 (2001)

[22] S. Marti, J. Andres, V. Moliner, E. Silla, I. Tunon, and J. Bertran, *Theo. Chem. Acc., 105*, 207 (2001)

[23] M. Garcia-Viloca, D. G. Truhlar, and J. L. Gao, *J. Mol. Bio., 327*, 549 (2003)

[24] S. Bjelic, and J. Aqvist, *Biochem., 45*, 7709 (2006)

[25] J. Gao, S. Ma, D. T. Major, K. Nam, J. Pu, and D. G. Truhlar, *Chem. Rev., 106*, 3188 (2006)

[26] S. A. Adcock, and J. A. McCammon, *Chem. Rev., 106*, 1589 (2006)

[27] H. P. Lu, and X. S. Xie, *Nature, 385*, 143 (1997)

[28] R. A. L. Vallee, N. Tomczak, L. Kuipers, G. J. Vansco, and N. F. van Hulst, *Chem. Phys. Lett., 384*, 5 (2004)

[29] K. A. Merchant, W. G. Noid, R. Akiyama, I. J. Finkelstein, A. Goun, B. L. McClain, R. F. Loring, and M. D. Fayer, *J. Am. Chem. Soc., 125*, 13804 (2003)

[30] I. G. Suydam, C. D. Snow, V. S. Pande, and S. G. Boxer, *Science, 313*, 200 (2006)

[31] H. P. Lu, and X. S. Xie, *Nature, 385*, 143 (1997)

[32] H. Yang, G. B. Luo, P. Karnchanaphanurach, T. M. Louie, I. Rech, S. Cova, L. Y. Xun, and X. S. Xie, *Science, 302*, 262 (2003)

[33] W. Min, G. Luo, B. J. Cherayil, S. C. Kou, and X. S. Xie, *Phys. Rev. Lett., 94*, 198302 (2005)

[34] R. Kubo, M. Toda, and N. Hashitsume, *Statistical physics*, Springer-Verlag, New York (1991)

[35] J. J. Macklin, J. K. Trautman, T. D. Harris, and L. E. Brus, *Science, 272*, 255 (1996)

[36] L. Edman, Z. Fldes-Papp, S. Wennmalm, R. Rigler, *Chem. Phys., 247*, 11 (1999)

[37] J. A. McCammon, and S. C. Harvey, *Dynamics of proteins and nucleic acids*, Cambridge Univ Press, New York (1987)

[38] R. Zwanzig, *Acc. Chem. Res., 23* 148 (1990)

[39] M. K. Prakash, and R. A. Marcus, accepted to *J. Phys. Chem. B,* (2007)

[40] C. Reichardt, *S*olvents and solvent effects in organic chemistry, Wiley-VCH, New York (2003)

[41] G. Luo, I. Andricioaei, X. S. Xie, and M. Karplus, *J. Phys. Chem. B, 110*, 9363 (2006)

[42] C. Blum, A. J. Meixner, and V. Subramaniam, *Biophys. J., 87*, 4172 (2004)

Chapter 3

Dielectric dispersion interpretation of single enzyme dynamic disorder, spectral diffusion and radiative fluorescence lifetime

A formulation based on measurable dielectric dispersion of enzymes is developed to estimate fluctuations in electrostatic interaction energy on time scales as long as milliseconds to seconds at a local site in enzymes. Several single molecule experimental obsevations occur on this time scale, currently unreachable by real-time computational trajectory simulations. We compare the experimental results on the autocorrelation function of the fluctuations of catalysis rate with the calculations using the dielectric dispersion formulation. We also discuss the autocorrelation function of the fluorescence lifetime. We use a previously derived relation between these observables and the electric field fluctuations and calculate the latter using dielectric dispersion data for the proteins.

I. Introduction

Recent advances in single molecule spectroscopy allow the observation of real time trajectories of individual molecules. With these experimental techniques several novel observations were made on single proteins: on-off switching of fluorescence in proteins (1-3), oscillations of green fluorescent proteins between neutral and anionic conformations at a near-denatured

condition (4, 5), spectral diffusion of the chromophore in an enzyme (6), fluctuations of fluorescence lifetime in enzymes (7, 8), and the fluctuations in the rates of enzyme catalysis (6, 9-11). All of these observations have been regarded as reflecting the dynamics of the enzyme between different conformational substates on the milliseconds timescale. For example, several enzyme-catalyzed reactions occur typically on the timescale of milliseconds to seconds, and the millisecond conformational dynamics of enzymes is considered as an important contributor to the 'functional dynamics' of the enzyme (12). Fluctuations in catalysis rate observed in single enzymes were also interpreted as being due to fluctuations in the conformation of the enzyme (9, 10).

The ensemble experimental data on enzyme catalysis have often been studied with the aid of computer simulations e.g., Refs. (13-26). In these studies, electrostatic interactions play a key role in enzyme catalysis (13, 16-28). Earlier a relation between three different observables, catalysis rate fluctuations ($\delta k(t)$), spectral diffusion ($\delta\omega_0(t)$) and radiative fluorescence lifetime fluctuations ($\delta\gamma_r^{-1}(t)$), was derived on the basis of fluctuations of electrostatic interaction energy ($\delta E(t)$) (29). Computer simulations of protein dynamics in real time are currently limited to tens of nanoseconds. Accordingly a detailed dynamical analysis for the estimation of $\delta E(t)$ on the milliseconds timescale is not analyzable by current real-time trajectory computational methods, and resort to other methods must be made. As a step towards estimating the $\delta E(t)$, we model the autocorrelation function of $\delta E(t)$ by relating it to another experimental observable, the frequency-dependent dielectric response function $\epsilon(\omega)$ of the protein. The experimentally obtainable $\epsilon(\omega)$ makes possible the comparison of experimental and theoretical autocorrelation function of fluctuations in δk, $\delta\omega_0$ and $\delta\gamma_r^{-1}$ that are observables from single molecule experiments. This comparison of experiment and theoretically derived relations is the essence of the present chapter.

The chapter is organized as follows. Equations for the autocorrelation of δk, $\delta\omega_0$ and $\delta\gamma_r^{-1}$ are given in terms of those in $\delta E(t)$ in Section II, using results derived previously (29), and the autocorrelation function for $\delta E(t)$ is also given in terms of the dielectric dispersion of

the protein. The comparison of experimental and theoretical results is given in Section III and some general remarks on the treatment are given in Section IV, together with suggested further experiments.

II. Dielectric dispersion and fluctuations in electrostatic interaction

A. Relation among observables

In Chapter 2 on the observables in single molecule experiments (29), the fluctuations in the rate of catalysis of a substrate by the enzyme ($\delta k(t)$), spectral diffusion of the fluorescence emission ($\delta\omega_0(t)$) and the radiative part of the fluorescence lifetime ($\delta\gamma^{-1}(t)$) of a chromophore in the enzyme were treated as arising from the fluctuations of electrostatic interaction energy $\delta E(t)$ at the local site in the enzyme. Based on this assumption, a relation was derived for the autocorrelation functions of each of these quantities in terms of the autocorrelation function $C_E(t)$ of fluctuations in electrostatic interactions at that active site, $\delta E(t)$. The latter correlation function is defined by

$$C_E(t) = \frac{\langle \delta E(t)\delta E(0)\rangle}{\langle \delta E(0)^2\rangle} \,. \tag{3.1a}$$

For the autocorrelation of the catalysis rate fluctuations, $C_k(t)$, we had (29)

$$C_k(t) = \frac{\langle \delta k(t)\delta k(0)\rangle}{\langle \delta k(0)\delta k(0)\rangle} \approx C_E(t) \,, \tag{3.1b}$$

for the autocorrelation of the spectral diffusion, $C_{\omega_0}(t)$,

$$C_{\omega_0}(t) = \frac{\langle \delta\omega_0(t)\delta\omega_0(0)\rangle}{\langle \delta\omega_0(0)^2\rangle} \approx C_E(t) \,, \tag{3.1c}$$

and for the autocorrelation function of the radiative component of the fluorescence lifetime, $C_{\gamma^{-1}}(t)$

$$C_{\gamma_r^{-1}}(t) = \frac{\langle \delta\gamma_r^{-1}(t)\delta\gamma_r^{-1}(0)\rangle}{\langle \delta\gamma_r^{-1}(0)\delta\gamma_r^{-1}(0)\rangle} \approx C_E(t)\,. \tag{3.1d}$$

We consider next a way of evaluating $C_E(t)$ in terms of the overall dielectric dispersion $\epsilon(\omega)$ for the protein and then relate the experimental observables to the calculations based on these equations. While the protein itself is heterogeneous we use its averaged property in the form of $\epsilon(\omega)$ as a first approximation, and then compare predictions from the model with experiments.

B. Autocorrelation of $\delta E(t)$

Using Onsager regression hypothesis (32), the autocorrelation function of the fluctuations of electrostatic interaction energy $E(t)$ about the equilibrium is related to the decay of interaction energy in a nonequlibrium process following an initial excitation

$$\frac{\langle \delta E(t)\delta E(0)\rangle}{\langle \delta E(0)\delta E(0)\rangle} = \frac{E(t) - E(\infty)}{E(0) - E(\infty)}\,. \tag{3.2}$$

The interaction energy $E(t)$ can be calculated by approximating the enzyme as a homogeneous dielectric with a frequency dependent dielectric constant $\epsilon(\omega)$ and the reactants/chromophore as a dipole embedded in a spherical cavity of dielectric constant ϵ_c in the enzyme. Using Eq. (3.2), the autocorrelation function of the equilibrium fluctuations of E can be studied by considering a model nonequilibrium system formed by the creation of a dipole $\Delta\boldsymbol{\mu}(t) = \Delta\boldsymbol{\mu}\theta(t)$ in the cavity at $t = 0$, where $\theta(t)$ is the unit step function. $\Delta\mu$ is the dipole moment created by electronic excitation of the chromophore in the case of spectral diffusion and the dipole moment difference between the transition state and the reactants in enzymatic catalysis. In the case of single enzyme experiments on catalysis rate (10), the rate is obtained by averaging the turnover times for several cycles of the enzyme over which the enzyme is assumed to be in the same conformation. $\Delta\boldsymbol{\mu}$ of the reaction has

an electrostatic interaction with this conformation of the enzyme. On longer time periods there are changes in conformations, resulting in fluctuations in this energy difference and so in the rate constant for the enzymatic catalysis.

The time-dependent interaction energy $E(t)$ of dipole in a spherical cavity of radius r following an initial creation of the dipole is given in terms of the time-dependent reaction field $\mathbf{R}(t)$ due to the protein environment acting on the dipole $\Delta\boldsymbol{\mu}(t)$ and the response function $\mathbf{r}(t)$ as (33)

$$\mathbf{R}(t) = \int_{-\infty}^{t} \mathbf{r}(t-t') \cdot \Delta\boldsymbol{\mu}(t)\,. \tag{3.3}$$

The Fourier-Laplace transform, $\mathcal{L}$ defined as $\mathcal{L}\left(f(t)\right) = \int_0^\infty exp(-i\omega t) f(t) dt$, of the response function $\mathbf{r}(t)$ is given as

$$\mathbf{r}(\omega) = \frac{2}{r_0^3}\,\frac{\epsilon(\omega)-\epsilon_c}{2\epsilon(\omega)+\epsilon_c}\,. \tag{3.4}$$

The interaction energy defined as

$$E(t) = -\Delta\boldsymbol{\mu}(t) \cdot \mathbf{R}(t) \tag{3.5}$$

is obtained using the above relations as (33)

$$E(t) = \frac{4\Delta\mu^2}{\pi r_0^3}\,\mathcal{L}^{-1}\left[-\frac{1}{i\omega}\,\frac{\epsilon(\omega)-\epsilon_c}{2\epsilon(\omega)+\epsilon_c}\right]\,. \tag{3.6}$$

C. Dielectric dispersion of proteins

The continuum dielectric response of proteins has been modeled in the literature (35; 36) using the Havriliak-Negami behavior (34) with a and b in the range [0,1]:

$$\frac{\epsilon(\omega)-\epsilon_\infty}{\epsilon_s-\epsilon_\infty} = \frac{1}{\left[1+(i\omega t_0)^a\right]^b}\,. \tag{3.7}$$

This dielectric response becomes a Cole-Cole dispersion when $b = 1$ and a Cole-Davidson dispersion when $a = 1$.

Dielectric dispersion measurements of some proteins are available for a frequency range corresponding to the time scale of milliseconds to seconds (Hz - kHz) (34-36). Dielectric properties of proteins were also used to study protein denaturation (38). One interest in the dielectric relaxation measurements of proteins in the millisecond timescale has been in the possible relation to biological activity (37).

In the case of hemoglobin, a Cole-Cole behavior with $a = 0.7, b = 1$ in Eq. (3.7) was observed for $2\pi/\omega$ in the range of milliseconds to seconds (35). For hydrated lysozyme powder, the imaginary part of the dielectric response was found to behave as $\epsilon''(\omega) \sim 1/\omega^{\alpha}, \alpha$ varying from 0.3 to 0.7 when temperature was changed from 260 K to 280 K (37). This imaginary part $\epsilon''(\omega)$ can correspond to $a = 0.3-0.7, b = 1$ in Eq. (3.7). Other dielectric measurements in this time range yield a decreasing from 0.50 to 0.36 for candida antarctica lipase B and from 0.8 to 0.6 for lysozyme and $b = 0.3$ for both these enzymes (36) as the temperature is changed from approximately 195 K to 255 K. The parameter a in the above experiments saturates and becomes a constant value at temperatures higher than 243 K. Among glassy materials, Cole-Cole behavior $\epsilon''(\omega) = \omega^{-1/2}$, (which can correspond to $a = 0.5, b = 1$) in the milliseconds range is commonly observed (39).

III. Comparison with experiments

A. Catalysis rate fluctuations

As noted in Section II C, the dielectric dispersion behavior of candida antarctica lipase B shows $b = 0.3$ and a saturation in parameter a at 0.36 at temperatures higher than 243 K (36). The autocorrelation $C_k(t)$ in Eq. (3.1b) calculated with these parameters in Eq. (3.7), and using Eqs. (3.2) and (3.6) is compared in the present Fig. 3.1 with the experimental data of Ref. (8) (Fig. 4A there). Numerical inversion of the Laplace transform

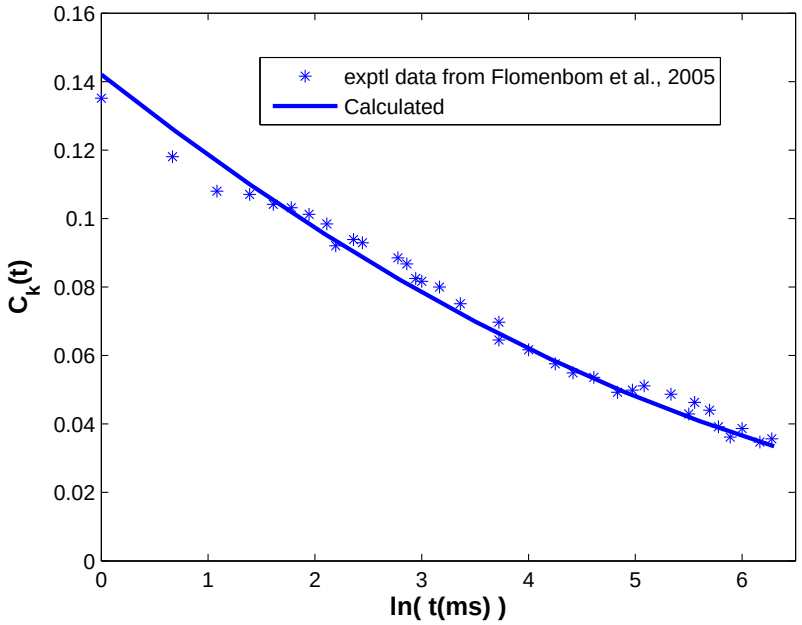

Figure 3.1: Comparison of $C_k(t)$ of the experimental data of candida antarctica lipase B from Fig. 4A of Ref. (9) with $C_k(t)$ calculated using the dielectric dispersion data on candida antarctica lipase B from Ref. (36)

was performed using the method in Ref. (41). In the calculation, ϵ_c of the cavity is assumed to be 2. The parameters $\epsilon_s, \epsilon_\infty$ and τ were not given in Ref. (36). We assume $\epsilon_s = 40$, $\epsilon_\infty = 4$, similar to the parameters observed experimentally for lysozyme (37). For those values of ϵ_s and ϵ_∞, a calculation using Eq. (3.2) with $\tau = 1$ s in Eq. (3.7) gives a good agreement with the $C_k(t)$ in Fig. 3.1 for the candida antarctica lipase B over the time range considered. With a different choice of $\epsilon_s, \epsilon_\infty$, the calculations can again be matched with the experiments by choosing an appropriate value for τ. The calculation of $C_k(t)$ is not very sensitive to a and $C_k(t)$ calculated using a in the range 0.25 to 0.4 fits the experimental data well. The experimental data on the autocorrelation function $C_k(t)$ for β-galactosidase (10) are compared with the calculated $C_k(t)$ using Eq. (3.2) in Fig. 3.2. The calculation was performed with $a = 0.6$ and $b = 1$ in Eq. (3.7), again assuming $\epsilon_0 = 40, \epsilon_\infty = 4$. The dielectric dispersion data on β-galactosidase are not presently available. However, the parameters a, b needed in Eq. (3.7) for the fit in Fig. 3.2 are close to those available for

hemoglobin (35) and lysozyme (37).

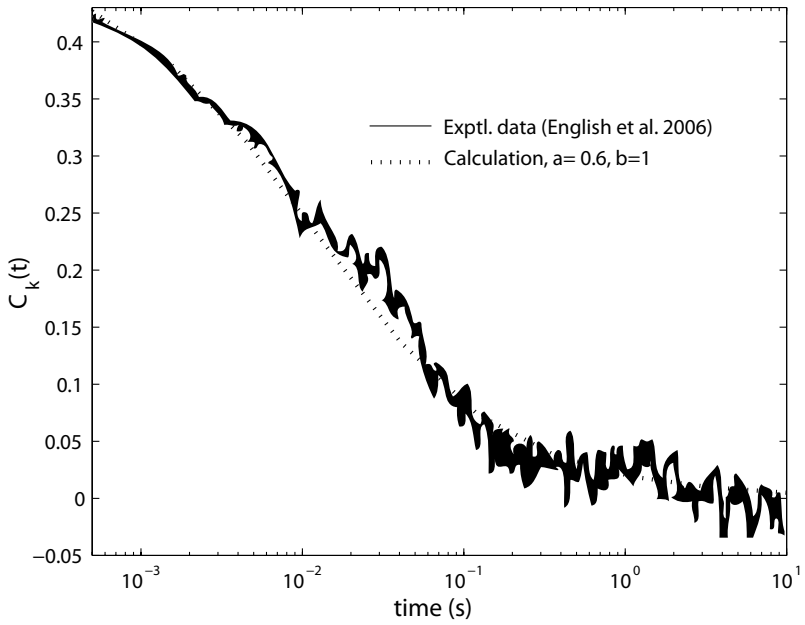

Figure 3.2: Comparison of experimental data from Ref. (10) and calculated correlation using Cole-Cole relation using $a = 0.60, b = 1$ in Eq. (3.7). The data points from Fig. S7 of *English et al.* [2006] were extracted using Adobe Illustrator

B. Fluctuations in fluorescence lifetime

The fluorescence lifetime of a chromophore in the protein, γ^{-1}, depends upon the rate constants of radiative (γ_r) and nonradiative (γ_{nr}) decays of fluorescence, with possible fluctuations in either or both of these:

$$\gamma^{-1} = (\gamma_{nr} + \gamma_r)^{-1} \ . \tag{3.8}$$

Regardless of the relative roles of fluctuations in γ_{nr} and γ_r they can have a common origin in fluctuations in conformation that lead to reorientations of polar groups and in the case of γ_{nr} fluctuations in donor-acceptor separation distance for electron transfer. With a common origin, the fluctuations in the radiative and nonradiative components can be represented by

the fluctuations in electrostatic interactions $\delta E(t)$, thereby yielding

$$C_{\gamma^{-1}}(t) = C_{\gamma_r^{-1}}(t) = C_E(t) \tag{3.9}$$

and the results of the previous section can be applied to the experimentally observed $C_{\gamma^{-1}}$ (7; 8).

To compare the calculated autocorrelation for $C_{\gamma^{-1}}(t)$ with the experimentally observed ones from Ref. (8), we use Eq. (3.1d) and $a = 0.5$ and $b = 1$ for the Cole-Cole exponents in Eq. (3.7). A comparison of the experimental data on antifluorescein from Ref. (8) with the calculated $C_{\gamma^{-1}}$ is shown in Fig. 3.3, using Eq. (3.9). To test the sensitivity of the calculated correlation to the value of a, numerical Laplace inversion was performed for the cases $b = 1$ and $a = 0.40$ to 0.65 in Eq. (3.7), and the results are shown in Fig. 3.3. The value of $a = 0.5$ and $b = 1$ gives the best agreement with the experiment on γ^{-1} fluctuations. From the discussion in Section II C, the assumption of a Cole-Cole exponent of $a = 0.5$ is not unreasonable, when the dielectric dispersion data on an enzyme are not available.

When $\epsilon_\infty = \epsilon_c$, an analytical relation can be derived from Eqs. (3.2) and (3.6) for the autocorrelation function $C_{\gamma^{-1}}(t)$ as

$$C_{\gamma^{-1}}(t) = exp(t/t_0)\ erfc(\sqrt{t/t_0}) \tag{3.10}$$

where *erfc* is the complementary error function, defined as $erfc(u) = (2/\sqrt{\pi}) \int_u^\infty exp(-v^2)dv$ and $t_0 = \tau(\epsilon_\infty + 1)^2/(\epsilon_0 + 1)^2$. Eq. (3.10) is functionally the same as the experimental fluorescence lifetime autocorrelation function reported in the literature (6, 7). A test is proposed later to help identify the relative importance of the radiative and nonradiative contributions to $\delta\gamma^{-1}$.

Since the Gaussian nature of protein fluctuations is assumed in studies of solvation of chromophores by protein dynamics (45) and is also seen in computer simulations (46), the

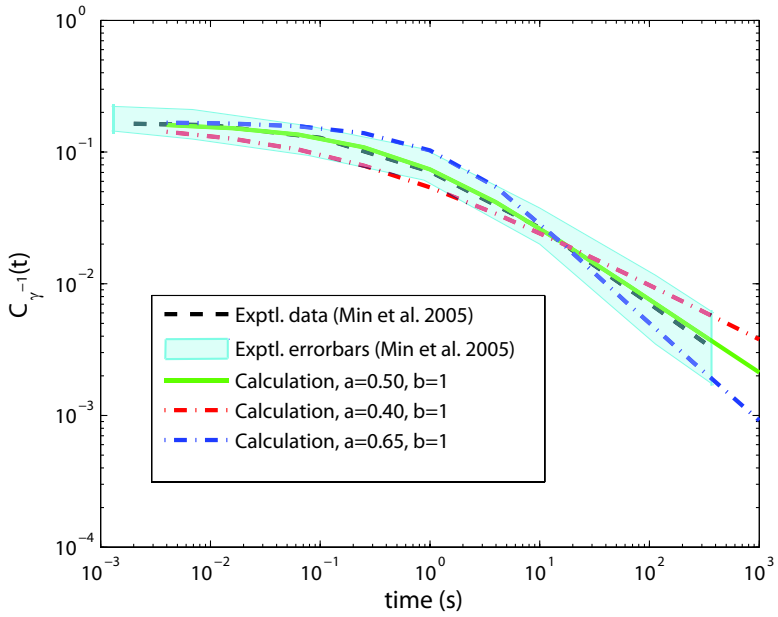

Figure 3.3: Comparison of the experimental data from Ref. (8) along with the errorbars and calculated correlation using Cole-Cole relation using $a = 0.40, 0.50, 0.65$ and $b = 1$ in Eq. (3.7). The normalized autocorrelation $C_{\gamma^{-1}}(t)$ was obtained by using Eq. (3) of Ref. (8) and $C_x(t)$ from Fig. 4 of Ref. (8)

higher-order correlations of lifetime fluctuations can be immediately calculated from the second order ones. They are obtained directly, for example, using Wick's theorem (47) and will be the same as the experimental observations. Results for the fourth order correlation for $a = 0.43, 0.5, 0.65$ are compared with the experimental data on flavin reductase from Ref. (48) in Fig. 3.4, to test the sensitivity of the calculation to the parameter a.

C. Memory kernel

The Cole-Cole relaxation has been mathematically cast into the formalism of continuous time random walk (CTRW), a diffusion with an associated memory kernel (32, 33). The difference between the usual random walk and CTRW is that in CTRW there is a distribution of times at which the random walker can take a step, unlike in conventional random walk where each step happens at a regular interval (50). This distribution of waiting times

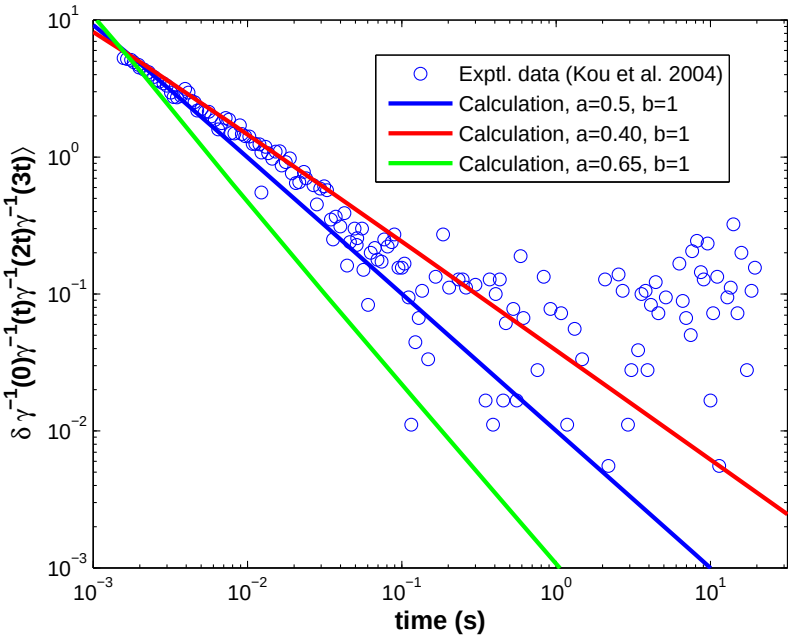

Figure 3.4: Comparison of fourth order correlation from the experimental data of Ref. (48) with the calculated correlation using Cole-Cole relation using $a = 0.40, 0.50, 0.65$ and $b = 1$ in Eq. (3.7) and Wick's theorem

leads to a lasting memory in the diffusive dynamics in CTRW (50). The Cole-Cole dielectric response ($0 < a < 1$, $b = 1$) has been modeled mathematically (50) as a problem of anomalous diffusion using the formalism of CTRW with a memory kernel of

$$K(t) \sim \frac{1}{t^{1-a}} \,. \tag{3.11}$$

For $a = 0.5$, this expression gives a memory kernel $K(t)$ of

$$K(t) \sim \frac{1}{\sqrt{t}} \,. \tag{3.12}$$

Thus, an alternative way of representing the Cole-Cole relaxation mathematically for the present problem, when $a = 0.5$ and $b = 1$, involves a diffusive dynamics of the protein structure with a memory kernel of $1/\sqrt{t}$. This memory kernel is the same as that assumed

in Ref. (8) to fit the correlation to the observed fluorescence lifetime autocorrelation data, attributed there to $\delta\gamma_{nr}^{-1}$. It has been shown (8) that this memory kernel approach provides a useful mathematical model for summarizing the data although the origin of the memory kernel remains to be addressed. Thus one feature in the γ^{-1} fluctuations modeled using dielectric dispersion is that the memory kernel can be obtained from the measurable $\epsilon(\omega)$.

IV. Discussion

A. General remarks

In the present chapter, a relation between the dynamic disorder (42), observed as catalysis rate fluctuations, to another experimental observable $\epsilon(\omega)$ is developed. This formulation is based on a role of electrostatic interactions in enzymatic catalysis (13, 16-28) and the relations derived previously relating various observables in single molecule experiments and fluctuations in electrostatic interaction energy (29). The possible origins of $\epsilon(\omega)$ in proteins and glasses have been discussed extensively in the literature (34-36, 38, 42), and are not the focus of the present article.

A relation between the autocorrelation function of fluorescence lifetime fluctuations and that of electron transfer donor-acceptor distance (x) fluctuations was derived in Eq. (3) of Ref. (8). For the range of parameters involved, it can be verified using a perturbation expansion that the autocorrelations of the fluorescence lifetime and that of x are the same after normalization. Because of this similarity, the functional form of the autocorrelation $C_x(t)$ shown in Ref. (8) is the same, to within a normalization constant, to that of $C_{\gamma^{-1}}(t)$, which in turn is equal to the present Eq. (3.10).

Other potential approaches interpreting the fluorescence lifetime autocorrelation function without invoking a memory kernel can be explored. In one of them a polymer dynamics model was used for the primary chain of the protein (35, 36). However, it was shown (52)

that the nanosecond timescale for the transition of $C_\gamma^{-1}(t)$ to $1/\sqrt{t}$ behavior in this model is not consistent with the experimental millisecond timescale.

B. Suggested experiments

1. Dielectric dispersion of proteins for which single molecule data on the fluctuations $\delta k(t)$, $\delta\gamma^{-1}(t)$ and $\delta\omega_0(t)$ are available, will be helpful in testing the present expressions. It would be helpful to have dielectric dispersion data on the milliseconds to seconds timescale for β-galactosidase and cholesterol oxidase enzymes on which $\delta k(t)$ were observed (6; 10) and flavin reductase on which $\delta\gamma^{-1}(t)$ were observed (7).

2. The fluorescence lifetime measurements can be performed by removing the quencher, for example Tyr35 in flavin reductase (7). Autocorrelation function measured in the absence of the quencher will be helpful in interpreting the relative contributions of the radiative and nonradiative components to $\delta\gamma^{-1}$. However, as noted earlier, if there is a common origin to both of these components, both $\delta\gamma_{nr}^{-1}$ and $\delta\gamma_r^{-1}$ can still be modeled using the present method.

V. Conclusion

The local fluctuations in the electrostatic interactions occuring in the milliseconds to seconds time scale in enzymes are modeled using the dielectric dispersion of the proteins. This model provides a formalism for interpreting the fluctuations in the observables on these timescales, which is presently not readily addressed using real time computational methods. Using the formulation presented earlier (29) relating various observables to the electrostatic interactions, both the stretched exponential behavior of the autocorrelation of catalysis rate and the power-law memory kernel in the fluorescence lifetime fluctuations can be modeled using a Cole-Cole dielectric behavior.

Bibliography

[1] R. M. Dickson, A. B. Cubitt, R. Y. Tsien, and W. E. Moerner, *Nature, 388*, 355 (1997)

[2] S. Habuchi, R. Ando, P. Dedecker, W. Verheijen, H. Mizuno, A. Miyawaki, and J. Hofkens, *Proc. Natl. Acad. Sci. USA, 102*, 9511 (2005)

[3] M. F. Garcia-Parajo, G. M. J. Segers-Nolten, J. A. Veerman, J. Greve, and N. F. van Hulst, *Proc. Natl. Acad. Sci. USA, 97*, 7237 (2000)

[4] G. Baldini, F. Cannone, and G. Chirico, *Science, 309*, 1096 (2005)

[5] G. Baldini, F. Cannone, G. Chirico, M. Collini, B. Campanini, S. Bettati, and A. Mozzarelli, *Biophys. J., 92*, 1724 (2007)

[6] H. P. Lu, L. Xun, and X. S. Xie, *Science, 282,* 1877 (1998)

[7] H. Yang, G. B. Luo, P. Karnchanaphanurach, T. M. Louie, I. Rech, S. Cova, L. Y. Xun, and X. S. Xie, *Science, 302*, 262 (2003)

[8] W. Min, G. Luo, B. J. Cherayil, S. C. Kou, and X. S. Xie, *Phys. Rev. Lett., 94*, 198302 (2005)

[9] O. Flomenbom, K. Velonia, D. Loos, S. Masuo, M. Cotlet, Y. Engelborghs, J. Hofkens, A. E. Rowan, R. J. M. Nolte, M. Van der Auweraer, F. C. de Schryver, and J. Klafter, *Proc. Natl. Acad. Sci. USA, 102*, 2368 (2005)

[10] B. P. English, M. Min, A. M. van Oijen, K. T. Lee, G. Luo, H. Sun, B. J. Cherayil, S. C. Kou, and X. S. Xie, *Nat. Chem. Bio., 2,* 87 (2006)

[11] L. Edman, Z. Fldes-Papp, S. Wennmalm, R. Rigler, *Chem. Phys., 247*, 11 (1999)

[12] S. J. Benkovic, and S. Hammes-Schiffer, *Science, 301*, 1196 (2003)

[13] A. Warshel, P. K. Sharma, M. Kato, Y. Xiang, H. Liu, and M. H. M. Olsson, *Chem. Rev., 106*, 3210 (2006)

[14] J. Gao, and D. J. Truhlar, *Ann. Rev. Phys. Chem., 53*, 467 (2002)

[15] P. K. Agarwal, S. R. Billeter, P. T. R. Rajagopalan, S. J. Benkovic, and S. Hammes-Schiffer, *Proc. Natl. Acad. Sci., 99,* 2794 (2002)

[16] A. Warshel, and M. Levitt, *J. Mol. Bio., 103*, 227 (1976)

[17] R. W. Pickersgill, P. W. Goodenough, I. G. Sumner, and M. E. Collins, *Biochem. J., 254*, 235 (1988)

[18] L. E. Dardenne, A. S. Werneck, M. D. Neto, and P. M. Bisch, *Proteins Struct. Funct. Genet., 52*, 236 (2003)

[19] K. F. Wong, J. B. Watney, and S. Hammes-Schiffer, *J. Phys. Chem. B, 108* 12231 (2004)

[20] J. Benach, J. -O. Winberg, J. -S. Svendsen, S. Atrian, R. Gonzalez-Duarte, and R. Ladenstein, *J. Mol. Biol., 345*, 579 (2005)

[21] K. E. Ranaghan, L. Ridder, B. Szefczyk, W. A. Sokalski, J. C. Hermann, and A. J. Mulholland, *Org. Biomol. Chem. 2*, 968 (2004)

[22] A. Warshel, *J. Biol. Chem., 273*, 27035 (1998)

[23] M. Garcia-Viloca, J. Gao, M. Karplus, and D. G. Truhlar, *Science, 303*, 186 (2004)

[24] S. Marti, J. Andres, V. Moliner, E. Silla, I. Tunon, and J. Bertran, *Theo. Chem. Acc., 105*, 207 (2001)

[25] M. Garcia-Viloca, D. G. Truhlar, and J. L. Gao, *J. Mol. Bio., 327*, 549 (2003)

[26] S. Bjelic, and J. Aqvist, *Biochem., 45*, 7709 (2006)

[27] A. Kienhofer, P. Kast, and D. Hilvert, *J. Am. Chem. Soc., 125* 3206 (2003)

[28] R. Wolfenden, and M. J. Snider, *Acc. Chem. Res., 34*, 938 (2001)

[29] M. K. Prakash, and R. A. Marcus, *Proc. Natl. Acad. Sci. USA* (submitted, 2007)

[30] H. P. Lu, and X. S. Xie, *Nature, 385*, 143 (1997)

[31] R. A. L. Vallee, N. Tomczak, L. Kuipers, G. J. Vansco, and N. F. van Hulst, *Chem. Phys. Lett., 384*, 5 (2004)

[32] D. Chandler, *Introduction to modern statistical mechanics*, Oxford University Press, New York (1987)

[33] C. P. Hsu, X. Y. Song, and R. A. Marcus, *J. Phys. Chem. B, 101*, 2546 (1997)

[34] S. Havriliak, and S. Negami, *Polymer, 8*, 161 (1967)

[35] H. Jansson, R. Bergman, and J. Swenson, *J. Phys. Chem. B, 109*, 24134 (2005)

[36] J. Mijovic, Y. Bian, R. A. Gross, and B. Chen, *Macromol., 38*, 10812 (2005)

[37] G. Careri, and G. Consolini, *Phys. Rev. E, 62*, 4454 (2000)

[38] K. M. Taylor, and D. W. van der Weide, *IEEE Trans. Microw. Theory Tech., 53*, 1576 (2005)

[39] J. C. Dyre, *Europhys. Lett., 71*, 646 (2005)

[40] C. Reichardt, *Solvents and solvent effects in organic chemistry*, Wiley-VCH, New York (2003)

[41] J. Abate, and P. P. Valko, *Int. J. Num. Meth. Eng., 60*, 979 (2004)
The Mathematica routine developed by Abate and Valko (2004) is available at http://library.wolfram.com/infocenter/MathSource/5026/

[42] R. Zwanzig, *Acc. Chem. Res., 23*, 148 (1990)

[43] C. P. Lindsey, and G. D. Patterson, *J. Chem. Phys., 73*, 3348 (1980)

[44] J. J. Macklin, J. K. Trautman, T. D. Harris, and L. E. Brus, *Science, 272*, 255 (1996)

[45] X. J. Jordanides, M. J. Lang, X. Y. Song, and G. R. Fleming, *J. Phys. Chem. B, 103*, 7995 (1999)

[46] T. Simonson, *Proc. Natl. Acad. Sci. USA, 99*, 6544 (2002)

[47] U. Frisch, and R. Bourret, *J. Math. Phys., 11*, 364 (1970)

[48] S. C. Kou, and X. S. Xie *Phys. Rev. Lett., 93*, 180603 (2004)

[49] K. Weron, and M. Kotulski, *Physica A, 232*, 180 (1996)

[50] W. T. Coffey, Yu. P. Kalmykov, and S. V. Titov, *J. Chem. Phys., 116*, 6422 (2002)

[51] P. Debnath, W. Min, X. S. Xie, and B. J. Cherayil, *J. Chem. Phys., 123*, 204903 (2005)

[52] J. Tang, and R. A. Marcus, *Phys. Rev. E, 73*, 022102 (2006)

Part II

Nonequilibrium fluctuations in single molecules

Chapter 4

Crooks' fluctuation theorem for an activated process: relevance to single molecule unfolding experiments

The applicability of Crooks' fluctuation theorem to systems with an activated process, especially with a coarse grained trajectory, is studied. The meaning of free-energy (ΔG) obtained in that context is also given. While noting the experimental conditions for single molecule mechanical unfolding experiments, it is shown that when the applied force drops upon unfolding, as it happens in the experiments, the existing derivations of Crooks' fluctuation theorem under nonequilibrium conditions are not applicable. It is, however, noted that the theorem is recovered for a quasiequilibrium case.

I. Introduction

When nonequilibrium work (W) is performed on a system, varying an external parameter (λ) of the system, the average work done, $\langle W \rangle$, is related to the free-energy difference (ΔG) between the initial and final states by an inequality

$$\langle W \rangle \geq \Delta G \,. \tag{4.1}$$

The nonequilibrium work theorem or Jarzynski's equality (1) focuses on a special way of averaging the nonequilibrium W leading to an exact equality

$$\langle e^{-\beta W} \rangle = e^{-\beta \Delta G} \,. \tag{4.2}$$

The fluctuation theorem by Crooks (2) is about a relation between the nonequilibrium probability distributions of work done on the system and by the system when λ is varied in forward ($\mathcal{F}$) and reverse ($\mathcal{R}$) directions in a predetermined way.

$$\frac{P_{\mathcal{F}}(W)}{P_{\mathcal{R}}(-W)} = e^{-\beta(\Delta G - W)} \tag{4.3}$$

In the simplest case λ could be increased at a constant rate for the forward process and decreased at the same constant rate during the reverse process. Crooks' theorem is a more general equality and Jarzynski's equality follows from this fluctuation theorem.

The interest in these theorems is two-fold: 1. from the perspective of nonequilibrium statistical physics to verify these exact equalities and 2. from the interest in performing nonequilibrium experiments and simulations on biological molecules to obtain the free-energy differences.

There was a debate on the correctness of these theorems (3,4): that a comparison of the rate of work being done and the rate of heat loss leading to equilibration was not explicit in the derivation given by Jarzynski (1); and that Crooks theorem (2) needed equilibration at intermediate steps and the use of detailed balance condition. The proof for Crooks' fluctuation theorem derived under certain conditions - markovian and instantaneous transition between the energy levels, in Refs. 5, 6 address the latter concern on the need for equilibration. Here, we specifically study the relevance of the derivations to the experimental system of unfolding single molecules. The present chapter does not focus on providing a new derivation, but re-examines the existing proofs for the subtleties of the assumptions. We point out that when the external parameter changes during unfolding, as in the single molecule

experiments, the existing derivations are not applicable. The need for the re-examination of the subtleties in the derivation comes from the fact that although Crooks' theorem is understood when the external parameter is varied in a predetermined way, there is presently no discussion on the consequences of the jump in force mentioned above. However, it will be shown that the theorem is still applicable under quasiequilibrium conditions.

The previous studies on these nonequilibrium theorems for specific systems have focused on the Crooks' theorem for: (i) a classical gas in a diathermal cylinder and (ii) a fluid under constant shear (2) and on Jarzynski's equality for: (i) a dilute classical gas system (7) (ii) an overdamped particle in a potential (8,9) and (iii) a Rouse polymer (10). These model systems do not have any activated process in them. We perform the analysis on a system with activated process to study the single molecule unfolding work distribution (11) experiments which were used to verify the fluctuation theorem (12).

II. Crooks' theorem for an activated process

The goal of the present section is to extend the derivation existing in the literature to the case of activated coarse grained trajectories and to extract the meaning of ΔG when Crooks' theorem is applicable. So we will only present the intermediate steps which are relevant to the present analysis. The proof in the present section goes through the route of fluctuation theorem for a Markovian system as given in Ref. 6. In the following we give specific references to some equations in Ref. 6 to complement our arguments. $P_{\mathcal{F}}(W)$, $P_{\mathcal{R}}(-W)$ denote the probability distributions of work (W) in forward ($\mathcal{F}$) and reverse ($\mathcal{R}$) processes respectively. Positive work is done on the system during the forward process and negative work is done by the system during the reverse trajectory. The system considered has a series of energy levels. The state of the system is defined as the occupied energy level (n_i). The gap between the energy levels changes with the external parameter (λ), which is varied according to a predetermined protocol for all the trajectories. The statistical mechanical definition of work W and heat Q are used (13): W is the change in energy of the occupied

level without any transitions between the different levels and Q is due to the transitions.

For a process with activation the trajectories involve occassional transitions between the macrostates, states 1 and 2 (which is the activation step), and more frequent transitions between the associated microstates. Some of the trajectories in that scenario may have a single transition between the two macrostates as shown below:

$$n_{(A)} = \overbrace{n_0 \to n_1 \to ... \to n_i}^{\text{State 1}} \xrightarrow{\text{activation}} \overbrace{n_{i+1} \to ... \to n_N}^{\text{State 2}} \ . \tag{4.4}$$

The above trajectory now includes activation as one of the steps. Also there will be other trajectories where no transitions to the second macrostate happen:

$$n_{(B)} = \overbrace{n_0 \to n_1 \to ... \to n_N}^{\text{State 1}} \ . \tag{4.5}$$

some other trajectories involving mulitple transitions between the two macrostates:

$$n_{(C)} = \overbrace{n_0 \to n_1 \to ... \to n_i}^{\text{State 1}} \xrightarrow{\text{activation}} \overbrace{n_{i+1} ... \to n_j}^{\text{State 2}} \xrightarrow{\text{activation}} \overbrace{n_{j+1} ... \to n_N}^{\text{State 1}} , \tag{4.6}$$

and several other possible combinations. We denote the generic stochastic trajectory corresponding to all the trajectories described above as:

$$n_{(\tau)} = n_0 \to n_1 \to n_2 \to ... \to n_N \tag{4.7}$$

similar to Eq. (53) of Ref. 6. The system is in an initial state (energy level) n_0 at time $\tau_0 = 0$, undergoes transitions at time τ_j from n_{j-1} to n_j, and ends in n_N at time $\tau_{N+1} = t$. As in Ref. 6, the considered trajectories have two parts to them: during the first part the external parameter λ is varied from λ_i to λ_f according to a predetermined protocol, and in the second part the system is allowed to equilibrate at the external parameter λ_f. The reverse trajectory $\left(n_{(\tilde{\tau})}\right)$ is defined as that passing through exactly the same states as in the forward one, but in a time-reversed way. The ratio of the probabilities of the forward

and reverse trajectories is given in Eqs. (68), (69) and (75) of Ref. 6:

$$\frac{P_{\mathcal{F}}(n_{(\tau)})}{P_{\mathcal{R}}(n_{(\tilde{\tau})})} = \frac{P_0(n_0)}{\tilde{P}_0(n_N)} \left[\frac{\prod_{j=1}^{N} \mathcal{W}(n_{j-1}, n_j; \lambda(\tau))}{\prod_{j=1}^{N} \mathcal{W}(n_j, n_{j-1}; \lambda(\tau))}\right] = \frac{P_0(n_0)}{\tilde{P}_0(n_N)} \left[\prod_{j=1}^{N} \frac{\mathcal{W}(n_{j-1}, n_j; \lambda(\tau))}{\mathcal{W}(n_j, n_{j-1}; \lambda(\tau))}\right] \tag{4.8}$$

where $P_0(n_0)$ and $\tilde{P}_0(n_N)$ denote the equilibrium probabilities of states n_0 and n_N at the beginning of the forward and reverse trajectories respectively. $\mathcal{W}$ is the probability of transition between the states at a λ corresponding to time τ. The standard relation of the ratio of the transition probabilities in the forward and reverse directions is (Eq. (48) of Ref. 6)

$$\frac{\mathcal{W}(n_{j-1}, n_j; \lambda(\tau))}{\mathcal{W}(n_j, n_{j-1}; \lambda(\tau))} = e^{-\beta(E_j - E_{j-1})} \tag{4.9}$$

where E_j is the energy of the state n_j. It should be noted that the above relation for transition probabilities is valid arbitrarily far from equilibrium, although the detailed balance condition involving the occupancy probabilities is an equilibrium condition.

Using the statistical physics definitions of W and Q during the trajectory, noted earlier, the heat lost during the jump from n_j to n_{j-1} is $\delta Q_j = E_j - E_{j-1}$. Using this condition in Eq. (4.9) it can be shown that

$$\frac{P_{\mathcal{F}}(n_{(\tau)})}{P_{\mathcal{R}}(n_{(\tilde{\tau})})} = \frac{P_0(n_0)}{\tilde{P}_0(n_N)} e^{-\beta Q} \tag{4.10}$$

where Q is the total heat loss over the forward trajectory composed of the heat lost over each of the transitions between the energy levels.

As λ is varied, the probabilities of occupancies of each of the microscopic states and the probability of transition between the macrostates change, but there is a non-zero probability of occupying both the macrostates at any value of λ. So $P_0(n_0)$ is given with respect to the

combined free-energy of both the macrostates 1 and 2.

$$P_0(n_0) = \frac{e^{-\beta E_{n_0}(\lambda_i)}}{\sum_1 e^{-\beta E(\lambda_i)} + \sum_2 e^{-\beta E(\lambda_i)}} = \frac{e^{-\beta E_{n_0}(\lambda_i)}}{e^{-\beta G_1(\lambda_i)} + e^{-\beta G_2(\lambda_i)}} = \frac{e^{-\beta E_{n_0}(\lambda_i)}}{e^{-\beta G(\lambda_i)}}$$
$$\tilde{P}_0(n_N) = \frac{e^{-\beta E_{n_N}(\lambda_f)}}{\sum_1 e^{-\beta E(\lambda_f)} + \sum_2 e^{-\beta E(\lambda_f)}} = \frac{e^{-\beta E_{n_N}(\lambda_f)}}{e^{-\beta G_1(\lambda_f)} + e^{-\beta G_2(\lambda_f)}} = \frac{e^{-\beta E_{n_N}(\lambda_f)}}{e^{-\beta G(\lambda_f)}} \tag{4.11}$$

where $\sum_1, \sum_2$ denote the sums over all microstates corresponding to the macrostates 1 and 2 respectively, and the following notation was used

$$e^{-\beta G(\lambda)} = e^{-\beta G_1(\lambda)} + e^{-\beta G_2(\lambda)} \,. \tag{4.12}$$

With a similar definition for $\tilde{P}_0(n_N)$ and further algebra as given in Section X of Ref. 6, it can be shown that

$$\frac{P_{\mathcal{F}}(n_{(\tau)})}{P_{\mathcal{R}}(n_{(\tilde{\tau})})} = e^{-\beta(\Delta G - W)} \tag{4.13}$$

where ΔG is the difference between the equilibrium free energies of the system at λ_f and λ_i

$$\Delta G = G(\lambda_f) - G(\lambda_i) \tag{4.14}$$

$G(\lambda)$ defined as in Eq. (4.12). Eq. (4.13) is the Crooks' theorem for activated process, where the ratio of the probabilities of the same trajectory in the forward and backward directions in terms of the work done during the nonequilibrium trajectory and the equilibrium ΔG given by

$$\Delta G = -k_B T \; ln \left[e^{-G_1(\lambda_f)/k_B T} + e^{-G_2(\lambda_f)/k_B T} \right] + k_B T \; ln \left[e^{-G_1(\lambda_i)/k_B T} + e^{-G_2(\lambda_i)/k_B T} \right] \tag{4.15}$$

Although the probabilities $P_{\mathcal{F}}(n_{(\tau)})$, $P_{\mathcal{R}}(n_{(\tilde{\tau})})$ change with the protocol for varying λ, the relation in Eq. (4.13) with their ratio is independent of the protocol. It should be noted

that $\mathcal{W}(n_{j-1}, n_j; \lambda(\tau))$ is required for calculating $P_{\mathcal{F}}(n_{(\tau)})$ and $P_{\mathcal{R}}(n_{(\tilde{\tau})})$ individually, but the ratio is independent of the actual functional form of $\mathcal{W}(n_{j-1}, n_j; \lambda(\tau))$.

III. Application to single molecule unfolding experiments

The differences in analyzing single molecule data will be described after the experimental conditions are described below. In the measured force-extension ($F - x$) curves of P5ab (14), there is a sudden drop in the force at about 14 pN indicating the folding $\rightarrow$ unfolding transition. This unfolding leads to an extension of $\sim$ 18 nm and the composite system of beads, handles and RNA hops from the folded to unfolded states. During the trajectory with a given force ramp rate, the only measurable feature is the hop between two macrostates - folded and unfolded and not the corresponding microstates. So until the point of transition, neither the work done nor the heat transfered is measurably different for different runs of the experiment. For example the curve at 1 pN/s can be exactly overlapped on the 10pN/s curve up to the point of transition (14). In some experiments on DNA unfolding, there were several intermediates for very long DNA, with each step ranging up to hundreds of base pairs (15, 16). When the number of base pairs in RNA/DNA is small, the unfolding happens in one step (17) without any intermediates. This is a cooperative transition which can be modeled by a two-state process.(18)

To make the Crooks' theorem and Jarzynski's equality applicable, a clear definition of the trajectories is needed, and the ratio of the forward and reverse trajectories can then be obtained following the analysis in the previous section. Because of the experimental observation, the system can be redefined as a two-state process with transitions between the folded and unfolded states, similar to Fig. 2C of Ref. 14. The validity of fluctuation theorem for a two-state system in an entirely different context was verified recently (19).

Also, it can be seen from Fig. 1 of Ref. 12 that the control parameter F drops during the unfolding. So, the equivalent of Eq. (4.9) for the single molecule unfolding trajectory with

unfolding/refolding is

$$\frac{\mathcal{W}(f,u;F_u)}{\mathcal{W}(u,f;F_f)} = \frac{\mathcal{W}(f,u;F_u)}{\mathcal{W}(u,f,F_u-\delta F)} \tag{4.16}$$

where δF is the drop in the force when the molecule unfolds and so the difference between the unfolding force F_u and refolding force F_f for the same trajectory. δF is experimentally seen to be a significant value of about 1.9 pN in Ref. 12. The same problem also appears in the proof given in Ref. (20) where

$$\frac{P(A\overset{\lambda}{\rightarrow}B)}{P(A\overset{\lambda}{\leftarrow}B)} = e^{-\beta(E_{B,\lambda}-E_{A,\lambda})} \tag{4.17}$$

was used to derive the final result. As pointed out earlier, λ, which is the applied force on a RNA hairpin, for $A \rightarrow B$ is different from the λ for $A \leftarrow B$, when A and B represent the folded and unfolded states. The analysis differs from that in Eq. (4.9) because corresponding to the same work done, the unfolding and refolding happen at forces separated by δF. In a nonequilibrium experiment, the ratio in Eq. (4.16) will be independent of the functional form of $\mathcal{W}$ only when both unfolding and refolding in a given trajectory happen at the same external parameter, i.e.,

$$\delta F \approx 0, \tag{4.18}$$

otherwise the functional form of $\mathcal{W}$ is needed for the evaluating the ratio in Eq. (4.16). In the framework of the existing proofs to the Crooks' theorem (Refs. 2, 5 and 6), this is an assumption and so these derivations are not suited for the nonequilibrium single molecule unfolding/refolding trajectories with a finite δF.

However, when the experiments are performed under quasi-equilibrium conditions, the functional form of $\mathcal{W}$ is known. The probabilty of unfolding or refolding at a force F and $F-\delta F$ respectively will depend upon the activation barriers to unfolding and refolding as

$e^{-\Delta G_u(F)/k_BT}$ and $e^{-\Delta G_f(F-\delta F)/k_BT}$. The ratio of these two transition probabilities yields

$$\frac{\mathcal{W}\left(f,u;F_u\right)}{\mathcal{W}\left(u,f,F_u-\delta F\right)} = e^{-(\Delta G_u(F)-)\Delta G_f(F-\delta F)/k_BT} = e^{-\delta Q/k_BT} \tag{4.19}$$

where δQ is the heat lost in the step involving an activation. Using Eq. (4.19), Crooks' theorem can be recovered under quasi-equilibrium condition following steps similar to those following Eq. (4.9).

IV. Discussion

The result in Eq. (4.8) was previously derived in the literature (6). The current work focuses on the subtleties in the two parts in this equation. The first is on the meaning of $P_0(n_0)/\tilde{P}_0(n_N)$ for the activated process, which gives rise to the equation for the ΔG in Eq. (4.15). If Eq. (4.15) is applied under quasi-equilibrium conditions to single molecule experiments performed such that the molecule is extremely likely to be in the unfolded (folded) state at the minimum (maximum) force applied on the system, the ΔG obtained by applying Crooks' theorem is given by using Eq. (4.15) as

$$\Delta G = G_u(F = F_m) - G_f(F = 0) \tag{4.20}$$

where $G_u(F = F_m)$ is the free-energy of unfolded state at the maximum force F_m applied on the molecule and G_f is defined similarly. However, when the experimental conditions are such that both the states are likely with comparable probabilities at the maximum and minimum applied forces, then the complete expression in Eq. (4.15) should be used. This could be the case when λ is varied to study the free-energy difference between two allosteric forms of an enzyme, with comparable probabilities of occupancy.

The second part was on the ratio $\mathcal{W}(n_{j-1}, n_j; \lambda(\tau))/\,\mathcal{W}(n_j, n_{j-1}; \lambda(\tau))$ in Eq. (4.8), when the molecule undergoes unfolding. Because of the drop in the force upon unfolding, for the same trajectory, the external parameter values are different for the forward and reverse

trajectories. The condition relating the transition probabilities between forward and reverse directions at the same λ to the energy difference between the states (Eq. (4.9)) is then not applicable. However as noted earlier, under quasi-equilibrium conditions, the functional forms of $\mathcal{W}(f, u, F)$ and $\mathcal{W}(u, f, F - \delta F)$ can be obtained in terms of activation barriers and Crooks' theorem can be derived under the quasi-equilibrium conditions.

V. Conclusions

Crooks' theorem as applicable to coarse-grained activated process with two state trajectories in single molecules was analyzed. It is shown that one of the experimental conditions that the force drops significantly as the molecule undergoes folding to unfolding transition makes the existing derivations for the identity inapplicable under nonequilibrium conditions. It was also shown that the equality in Crooks' theorem can be recovered under quasi-equilibrium conditions.

Bibliography

[1] C. Jarzynski, *Phys. Rev. Lett., 78*, 2690 (1997)

[2] G. E. Crooks, *Phys. Rev. E, 60*, 2721 (1999)

[3] E. G. D. Cohen, and D. Mauzerall, *J. Stat. Mech.,* P07006 (2004)

[4] C. Jarzynski, *J. Stat. Mech.,* P09005 (2004)

[5] U. Seifert, *Phys. Rev. Lett., 95*, 040602 (2005)

[6] M. Esposito, and S. Mukamel, *Phys. Rev. E, 73*, 046129 (2006)

[7] G. E. Crooks, and C. Jarzynski, cond-mat/0603116 (2006).

[8] T. Hatano, and S. Sasa, *Phys. Rev. Lett., 86*, 3463 (2001)

[9] V. Blickle, T. Speck, L. Helden, U. Seifert, and C. Bechinger, *Phys. Rev. Lett., 96*, 070603 (2006)

[10] A. Dhar, *Phys. Rev. E, 71*, 036126 (2005)

[11] J. Liphardt, S. Dumont, S. B. Smith, I. Tinoco Jr., and C. Bustamante, *Science, 296,* 1832 (2002)

[12] D. Collin, F. Ritort, C. Jarzynski, S. B. Smith, I. Tinoco and C. Bustamante, *Nature, 437* 231 (2005)

[13] J. Kestin, and J. R. Dorfman, *A course in statistical thermodynamics*, Academic Press, New York (1971)

[14] J. Liphardt, B. Onoa, S. B. Smith, I. Tinoco Jr., and C. Bustamante, *Science, 292*, 733 (2001)

[15] U. Bockelmann, B. Essevaz-Roulet, and F. Heslot, *Phys. Rev. Lett., 79*, 4489 (1997)

[16] C. Danilowicz, V. W. Coljee, C. Bouzigues, D. K. Lubensky, D. R. Nelson, and M. Prentiss, *Proc. Natl. Acad. Sci. USA,, 100*, 1694 (2003)

[17] M. T. Woodside, W. M. Behnke-Parks, K. Larizadeh, K. Travers, D. Herschlag, and S. M. Block, *Proc. Natl. Acad. Sci. USA, 103*, 6190 (2006)

[18] C. Hyeon, and D. Thirumalai, *Proc. Natl. Acad. Sci. USA, 102*, 6789 (2005)

[19] S. Schuler, T. Speck, C. Tietz, J. Wrachtrup, and U. Seifert, *Phys. Rev. Lett., 94*, 180602 (2005)

[20] G. E. Crooks, *J. Stat. Phys., 90,* 1481 (1998)

Chapter 5

Single molecule unfolding experiments: generalized Bell's formula and Crooks' theorem

The use of Bell's escape rate to model the single molecule mechanical unfolding experiments and to verify Crooks' theorem for such a model are explored. Bell's analysis models the distortion of free-energy surface of a molecule under an applied force. Using Bell's analysis for modeling unfolding and refolding force distributions, the difference between satisfying Crooks' theorem for the ratios of the forward and backward probability distributions and having a common intersection point for the two distributions is highlighted. The former is important to extract a meaningful free-energy (ΔG) from the measurements.

I. Introduction

With the recent advances in experimental techniques, several single molecule experiments have become possible. Such experiments include mechanical unfolding of RNA (1;2), proteins (3,4) and simultaneous measurements of force and velocity of optical beads (5). There are also theoretical studies related to such single molecule experiments (6,7). A few experiments used overdamped optical beads (5,8) and the unfolding of single molecules (9, 10) to verify Jarzynski's equality (11) and Crooks' fluctuation theorem (12). Jarzynski's equality and Crooks' theorem, described briefly in the introduction to Chapter 4, can be used to

extract free-energy difference (ΔG) between two equilibrium states (folded and unfolded for example) of the system using the work performed in nonequilibrium experiments. The indistinguishability of the force-extension trajectories of the single RNA and the handles system for various pulling rates up to the unfolding point (1) is noted; this encourages application of Bell's escape rate analysis to the unfolding/refolding force distribution. In this chapter, we explore the possibility of using Bell's escape rate analysis to gain insight into the use of experiments used to verify Crooks' theorem for single molecule unfolding experiments. The externally controlled parameter in these experiments, force, undergoes a jump as the molecule unfolds. This jump in the external parameter is not one of the conditions in the derivation of the Crook's theorem and so it motivates the present study on an alternative interpretation of the experiments.

II. Unfolding force and work distributions

A critical unfolding force of $\sim 13 - 14$ pN is experimentally observed (1,2,13) obtained for basepairs of different lengths with up to hundreds of base pairs being broken simultaneously (13,14). This critical force suggests that the activation barrier involved in the cooperative folded to unfolded transition is probably due to the block caused by a few base pairs. G-C rich areas usually form such bottlenecks in DNA (13,15). Similarly for the refolding transition, the activation is probably the nucleation of a few basepairs, which is followed by a zipping of the rest of the base pairs (2).

In the RNA P5ab mechanical unfolding experiments, multiple transitions between the folded and the unfolded states (recrossings) were seen within the experimental sensitivity of 20 Hz - 20 kHz at slow velocities (1,9). Since the recrossings were not explicitly discussed in the data of Collin et al. (10) or Manosas et al. (16), we will consider only the trajectories that do not have any recrossings. The probability of such a trajectory with no recrossings is essentially given by the probability for the first folded to unfolded transition (or unfolded to folded in the reverse trajectory).

This unfolding transition can be modeled as an escape over an activation barrier where the applied force distorts the barrier to change the escape rate $\nu_u(t)$ from the folded to unfolded states (17). The probability of having the unfolding at time t during the forward trajectory is:

$$P_u(t) = \nu_u(t) \left[exp\left(- \int_0^t \nu_u(\tau) d\tau \right) \right] \tag{5.1}$$

where the term in the square brackets is the survival probability in the folded state up to time t and $\nu_u(t)$ is the probability of escape from the folded to unfolded states at time t. The probability for the activated refolding process can be written similarly. From Fig. 1 of Ref. (10), it can be seen that the area under the $F - x$ curve (the work done) is linearly dependent on the unfolding force. And the work distribution can be computed using unfolding force distribution.

As noted earlier, the escape from folded to unfolded states happens because of the distortion of the free-energy surface and the reduction of the activation barrier with the applied force F (17). An exact computation of ΔG_u (or ΔG_f) dependence on F will require a knowledge of the energy landscape of the RNA and we do not discuss it here. So, the dependence of ΔG_u (or ΔG_f) on F will be treated phenomenologically to gain insight into the applicability of the fluctuation theorem to the unfolding experiments. The effect of having a linear and nonlinear dependence of the activation free energies for unfolding (ΔG_u) and refolding processes (ΔG_f), on F are considered.

Linear $\Delta G_u(F)$ and $\Delta G_f(F)$

A common assumption is that the effective activation free-energy changes linearly with the applied force (18):

$$\Delta G_u(F) = \Delta G_u(0) - F\Delta x \tag{5.2}$$

where Δx is usually interpreted as the difference in the position between the equilibrium value and the transition state (1;17). Substituting Eq. (5.2) in Eq. (5.1), the probability distribution of the unfolding force is given in terms of the frequency of escape at time t given by $\nu_u(t) = \nu_0\ exp\,(-\mu t \Delta x/k_B T)$ and the force ramp rate $\mu = F/t$ as (17):

$$P_u(F) = \frac{1}{\mu}\nu_0 e^{\frac{F\Delta x}{k_B T}}\ e^{-\frac{1}{\mu}\int_0^F \nu_0 e^{\frac{F\Delta x}{k_B T}} dF} \tag{5.3a}$$

$$P_u(F) = \nu_0 e^{\frac{F\Delta x}{k_B T} - ln(\mu)}\ e^{-\frac{\nu_0 k_B T}{\Delta x} e^{-ln(\mu)}\left(e^{\frac{F\Delta x}{k_B T}} - 1\right)} \tag{5.3b}$$

Eq. (5.3b) is obtained performing the integrations in Eq. (5.3a) and by using the identity $1/\mu = exp\,(-ln(\mu))$. As can be clearly seen from Eq. (5.3b), the probability distribution gets shifted without any change in the variance of the distribution as the force ramp rate μ changes. This can also be guessed based on Eq. (14) of (17) which gives an expression for the variance of the distribution in terms of the rate. However it was seen experimentally that the distribution of W widens with increasing μ (*c.f.* Fig. 2 of Ref. (10).

The work distribution for unfolding and refolding calculated using $P_u(F)$, $P_f(F)$ and the relation between F and W

$$W = 23\,k_B T + 4.76\,(k_B T/pN)\,F \tag{5.4}$$

obtained from Fig. 1 of Ref. (10) is shown in the present Fig. 5.1. It should be noted that although the variance of the calculated distribution does not change with μ as it does in the experiments, the crossing of the unfolding and refolding work distributions happens at the same W irrespective of μ. We will comment on this behavior later. Thus the linear dependence of the unfolding barrier on F is inadequate to model the experimental probability distributions. As shown in Fig. 5.2, the *log* of the ratio of the forward and reverse distributions has a slope of 1.8 in a plot against W. If Crooks' theorem is applicable

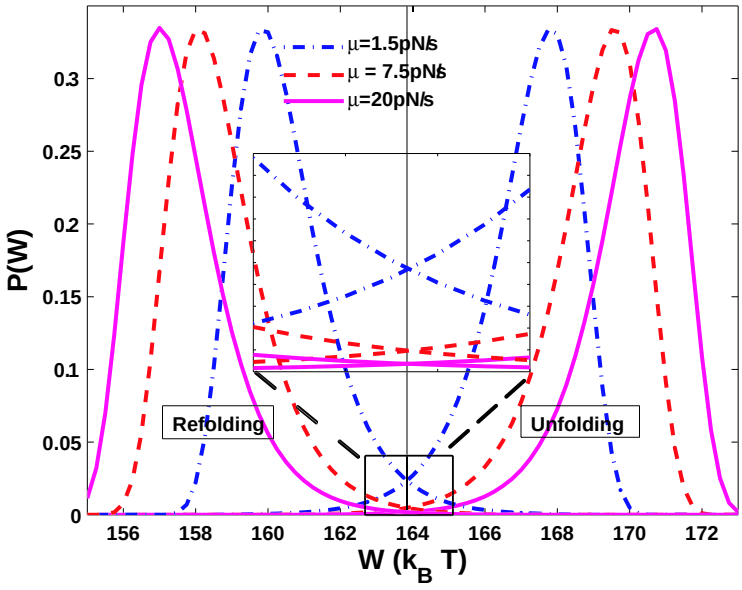

Figure 5.1: Probability distribution of work using the unfolding force distribution from Eq. 5.3b. The inset is a zoom of the curves highlighting that the crossing of the forward and reverse trajectories happens at the same point irrespective of μ

to the model we considered, the slope would be 1.

Nonlinear $\Delta G_u(F)$

As the linear $\Delta G_u(F)$ did not yield the correct behavior, we consider other models for ΔG_u which were used to account for the change in the variance of the distributions with μ (6,18). Essentially the broadening of the distribution at higher μ's is because of the nonlinear $\Delta G_u(F)$. One of the reasons for the the nonlinear dependence of of ΔG_u on F is that although the free-energy landscape changes linearly with the applied force and also the positions of the minima and maxima themselves change (19). The logarithm of the average lifetime in each of the states as a function of applied force as measured by (2) and the logarithm of the equilibrium constant as a function of the applied force as measured by (1) are almost linear, however the nonlinearity needed in the present analysis can be within the errorbars of the experiments.

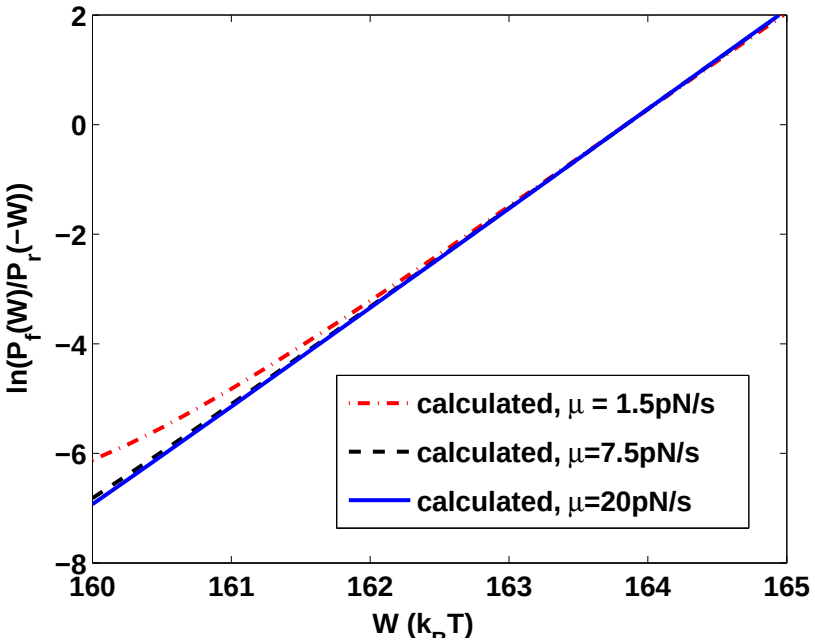

Figure 5.2: $ln(P_u(W)/P_f(-W))$ vs. W to check the validity of Crooks theorem for the model used. The slope of the above plot is ≈ 1.8

A phenomenological functional form is used for the activation free-energy for unfolding

$$\Delta G_u(F) = a - bF + cF^2 \, . \tag{5.5}$$

By performing the integration as in Eq. (5.3a) but with a nonlinear $\Delta G_u(F)$ from Eq. (5.5), the unfolding force distribution is given as:

$$P_u(F) = \frac{1}{\mu} e^{-a+bF-cF^2} \; e^{-\left[\frac{1}{2\mu}\sqrt{\frac{\pi}{c}}\, e^{-a+\frac{b^2}{4c}}\left(erf[\frac{b}{2\sqrt{c}}]-erf[\frac{b-2cF}{2\sqrt{c}}]\right)\right]} \tag{5.6}$$

where *erf* is the error function. The work distribution obtained using this unfolding force distribution was fitted to the distributions measured in Ref. (10) for all three force ramp rates. A comparison of the calculated unfolding distributions with experimental observations is given in Fig. 5.3. We used $a = 67\ k_BT$, $b = 5.7\, k_BT/pN$ and $c = 0.11\, k_BT/pN^2$ for the barrier to unfolding were used in the calculations.

It should be noted that the fit is not to each of the distributions at different force-ramp rates independently, but a common ΔG_u which gives all the distributions simultaneously depending upon the ramp rates. With data at more ramp rates (μ) than the presently available one at three μ's (1), possibly the ΔG_u can be extracted with minimal errors in the parameters in Eq. **5.5**.

For the refolding trajectories, a second order nonlinearity was not sufficient to fit all the three distributions, so we used

$$\Delta G_f(F) = a' - b'(F_m - F) + c'(F_m - F)^2 + d'(F_m - F)^3 + e'(F_m - F)^4 \tag{5.7}$$

and the integrations were performed numerically to obtain the distribution. Here F_m is the maximum force applied to the molecule in the experiment. The calculations were performed with parameters $a' = 84.1\ k_BT, b' = 6.9\ k_BT/pN, c' = 0.126\ k_BT/pN^2, d' = 2.94 \times 10^{-5}\ k_BT/pN^3, e' = 7 \times 10^{-6}\ k_BT/pN^4$ and the experimental parameter $F_m = 23\,pN$ and were compared with experiments in Fig. 5.3.

III. Crooks' theorem for the model

In Ref. (10), the $P_u(W)$ and $P_f(-W)$ curves cross at the same W irrespective of the μ. It was shown (10) that if Crooks' theorem is obeyed, the crossing points are expected to be the same as ΔG

$$\frac{P_u(W)}{P_f(-W)} = e^{-\beta(\Delta G - W)} = 1$$

$$\text{and so} \qquad W = \Delta G \tag{5.8}$$

However the converse need not be true. The work distributions for unfolding and refolding, $P_u(W)$ and $P_f(-W)$, in our model may intersect at a common W for different μ's, but may not satisfy Crooks' theorem as illustrated in Fig. 5.2.

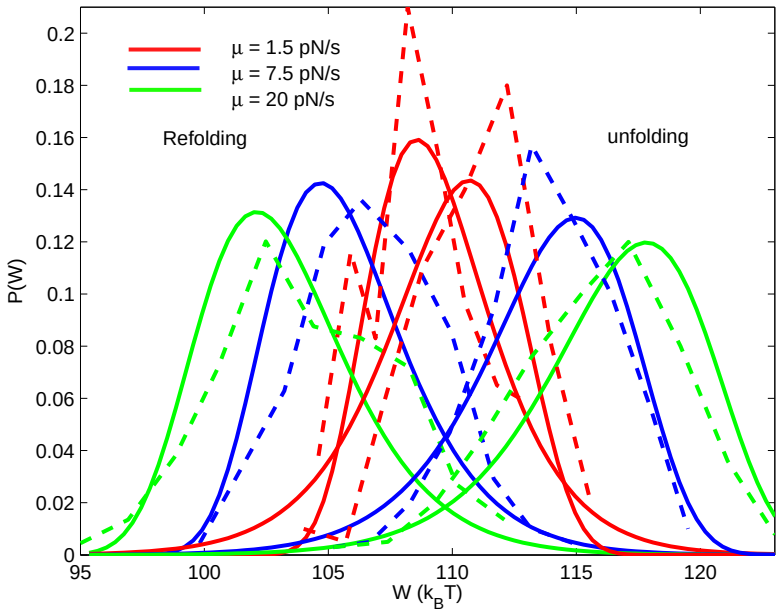

Figure 5.3: Calculated unfolding and refolding work distributions compared with the experiments. Solid lines are from the calculations and the dashed lines from Ref. (6)

According to Eqs. (5.1) and (5.6) for the unfolding distribution, the first part ($\nu_u(t)$) contributes to the rising part of $P_u(F)$ and the second - survival probability - to the decay of $P_u(F)$. As long as the crossing of the two distributions happens with in the region where survival probability is nearly equal to 1, the probability of intersection is seen to be independent of μ. So, the crossing happens at F defined by

$$\nu_u(F) = \nu_f(F) \;\Rightarrow\; \Delta G_u(F) = \Delta G_f(F)\,. \tag{5.9}$$

The common crossing point corresponds to the force at which the effective barrier in the forward direction equals that in the reverse direction and so is independent of the rate μ which only governs the survival probability. However it can be verified numerically that the more the character of the survival probability part of $P_u(F)$ is seen i.e., the intersection point close to the peaks of the distributions, the more the crossing point differs for various

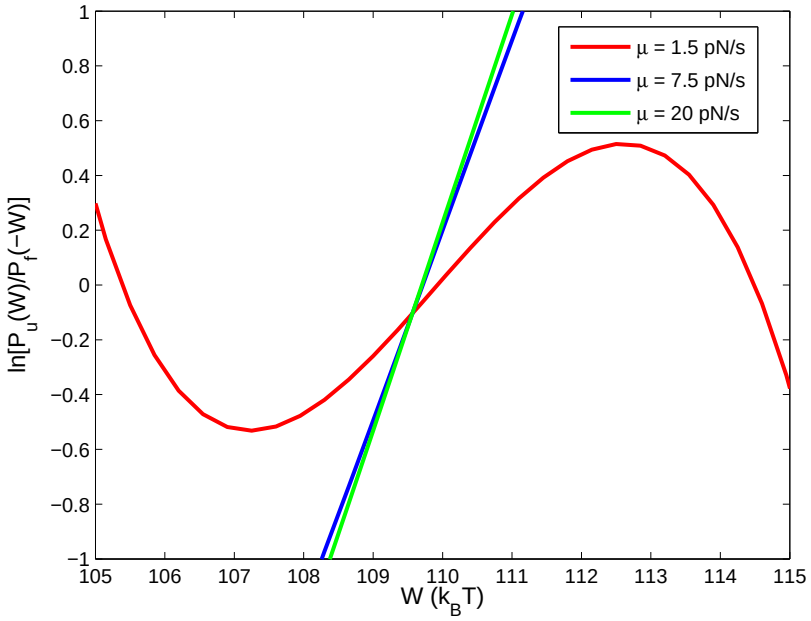

Figure 5.4: Calculated unfolding and refolding work distributions compared with the experiments. Solid lines are from the calculations and the dashed lines from Ref. (6)

μ. Similarly the following ratio of forward and reverse probabilities can also be evaluated.

$$ln\left(\frac{P_u(F)}{P_f(F)}\right) = -\Delta G_u(F) + \Delta G_f(F)\,. \tag{5.10}$$

This means that the slope of $ln\,(P_u(W)/P_f(-W))$ vs. W in the present model will depend upon the system dependent parameters such as $a, a', b, b', ...$ in Eqs. (5.5) and (5.7) and the relationship between unfolding force F and the work done W. Although we find in Fig. 5.4 a slope of 0.75, close to 1, for $\mu = 7.5\ pN/s, 20\ pN/s$, it is a pure coincidence for our model. For $\mu = 1.5\ pN/s$ the slope differs a lot from unity and the plot itself deviates significantly from linearity. This shows that to be sure that the result obtained from the intersection of $P_u(W)$ and $P_f(-W)$ is actually the free-energy difference (ΔG) between the unfolded state at $F = F_m$ and the folded state at $F = 0$, one needs to verify the Crooks' theorem for the ratios of trajectories besides just the common intersection point for various μ's.

IV. Unfolding experiments vs. fluctuation theorem

The model system in the previous sections thus shows the importance of recognizing the following features in single molecule unfolding experiments for verifying Crooks theorem and using it to extract ΔG: 1. intersection of the forward and reverse probability distributions happens at a common value of W for various μ's 2. the range of W over which the plot of $ln\,(P_u(W)/P_f(-W))$ vs. W is linear and 3. the verification of the slope of $ln(P_u(W)/P_f(-W))$ vs. W to be 1 in this linear range to test the Crooks' theorem.

V. Conclusions

We analyzed single molecule unfolding/refolding experimental data using Bell's escape rate formalism with a phenomenological activation barrier that depends (i) linearly and (ii) nonlinearly on the applied force F. Using the Bell's escape rate analysis we note that the crossing of forward and backward probability trajectories at the same W for various μ's is different from obeying Crooks' theorem, and that the latter is needed to estimate ΔG.

Bibliography

[1] J. Liphardt, B. Onoa, S. B. Smith, I. Tinoco Jr., and C. Bustamante, *Science, 292*, 733 (2001)

[2] M. T. Woodside, W. M. Behnke-Parks, K. Larizadeh, K. Travers, D. Herschlag, and S. M. Block, *Proc. Nat. Acad. Sci. USA, 103*, 6190 (2006)

[3] M. Rief, M. Gautel, F. Oesterhelt, J. M. Fernandez and H. E. Gaub, *Science, 276*, 1109 (1997)

[4] M. S. Kellermayer, S. B. Smith, H. L. Granzier, and C. Bustamante, *Science, 276*, 1112 (1997)

[5] V. Blickle, T. Speck, L. Helden, U. Seifert, and C. Bechinger, *Phys. Rev. Lett., 96* 070603 (2006)

[6] G. Hummer, and A. Szabo, *Biophys. J., 85*, 5 (2003)

[7] C. Hyeon, and D. Thirumalai, *Biophys. J., 90*, 3410 (2006)

[8] E. H. Trepagnier, C. Jarzynski, F. Ritort, G. E. Crooks, C. J. Bustamante and J. Liphardt, *Proc. Nat. Acad. Sci., 101*, 15038 (2004)

[9] J. Liphardt, S. Dumont, S. B. Smith, I. Tinoco Jr., and C. Bustamante, *Science, 296,* 1832 (2002)

[10] D. Collin, F. Ritort, C. Jarzynski, S. B. Smith, I. Tinoco, and C. Bustamante, *Nature, 437*, 231 (2005)

[11] C. Jarzynski, *Phys. Rev. Lett., 78*, 2690 (1997)

[12] G. E. Crooks, *Phys. Rev. E, 60*, 2721 (1999)

[13] U. Bockelmann, B. Essevaz-Roulet, and F. Heslot, *Phys. Rev. Lett., 79*, 4489 (1997)

[14] C. Danilowicz, V. W. Coljee, C. Bouzigues, D. K. Lubensky, D. R. Nelson, and M. Prentiss, *Proc. Nat. Acad. Sci. USA, 100*, 1694 (2003)

[15] J. F. Marko, and S. Cocco, *Phys. World , 16*, 37 (2003)

[16] M. Manosas, D. Collin, and F. Ritort, *Phys. Rev. Lett., 96*, 218301 (2006)

[17] E. Evans, and K. Ritchie, *Biophys. J., 72* 1541 (1997)

[18] G. I. Bell, *Science, 200*, 618 (1978)

[19] O. K. Dudko, G. Hummer, and A. Szabo, *Phys. Rev. Lett., 96*, 108101 (2006)

[20] P. -C. Li, and D. E. Makarov, *J. Chem. Phys., 119*, 9260 (2003)

Part III

UV photodissociation of N_2O

Chapter 6

Isotopomer fractionation in the UV photolysis of N_2O: comparison of theory and experiment. I

In the photodissociation of N_2O, absorption cross sections differ with isotopic substitution, leading to a wavelength-dependent fractionation of the various isotopomers. Several models ranging from shifts by zero-point energy differences to propagation of wave packets on the excited electronic state potential energy surface have been proposed to explain the observed fractionations. We present time-independent fractionation calculations for the absorption cross section of N_2O using multidimensional reflection principle and the ab initio *potential energy surface for N_2O. An empirical broadening was used in the calculated cross-section to match with the experiments. Using this absorption cross section calculation, the fractionation of isotopologues 447 (notation for $^{14}N^{14}N^{17}O$), 448, 456, 546 and 556 were calculated and compared with the experiments. Besides largely agreeing with the experimental data, these calculations have the advantage of not being computationally intensive. The present computations also provide data for the slope of a three-isotope plot of the fractionation of 447/446 relative to 448/446, using the fractionations at different wavelengths. The resulting slope is compared with a perturbation theoretical expression for direct photodissociation given in Chapter 7.*

I. Introduction

Nitrous oxide (N_2O) is an efficient greenhouse gas and a source of singlet oxygen. Even though its concentration in the atmosphere is about three orders of magnitude less than that of CO_2, it gains its importance because its per-molecule global warming potential is about $200 - 300$ times that of CO_2 (1). Isotopomer fractionation measurements are important in determining sources and sinks of atmospheric gases (2; 3). The sources and sinks and the isotopic behaviour of N_2O has been the subject of many studies (3; 4; 5), due to the atmospheric importance of N_2O. In the atmosphere there are two main pathways for removal of N_2O, photolysis and photo-oxidation by $O(^1D)$:

$$N_2O + \hbar\omega \rightarrow N_2(^1\Sigma^+) + O(^1D) \tag{6.1}$$

$$N_2O + O(^1D) \rightarrow N_2 + O_2 \text{ or } 2NO\,. \tag{6.2}$$

Although a photo-dissociation can also yield triplet oxygen $O(^3P)$, this reaction has a negligible quantum yield (6), compared to the quantum yield of Reaction (6.1) that is nearly unity (6; 7). The quantum yield of the triplet formation was recently measured (8) to be about 0.5%. Reactions (6.1) and (6.2) form the principal means of N_2O dissociation in the stratosphere, with contributions of about 90% and 10% respectively (9). The absorption in N_2O is peaked at around 182 nm and is dominated by a singlet-singlet transition (10). The transition dipole moment for the particular transition is zero when the molecule is linear and so the transition is electronic-dipole-forbidden. The transition, however, becomes allowed when the molecule deviates from linearity.

Selwyn and Johnston (11) measured the ultraviolet absorption cross sections of various isotopomers of N_2O over the wavelength range 172 to 197 nm and between 150 K and 500 K. In the analysis of their data, they concluded that the temperature dependence of the

absorption spectrum is due to the thermal activation of the bending mode. Further, no rotational structure was observed in their measurements. Several authors have performed laboratory experiments to study the relative absorption cross-sections/photolysis rates of various isotopomers (12; 13; 14). Atmospheric observations have been made to obtain the relative abundances of various isotopomers of N_2O (4; 15; 16). Prasad (17) proposed the possibility of new atmospheric sources of N_2O to account for the isotopomer fractionations. Yung and Miller (18) explained the lack of isotopomer enrichment in N_2O at 185 nm (12) by introducing a model for isotopomer fractionation that varied with absorption wavelength. In their model, isotopomer fractionation was calculated based on changes in the wavelength-dependent isotopomer optical absorption cross section due to differences in the zero-point energy (ZPE) of the isotopomers. While this model could provide only qualitative agreement with the experimental results, it motivated many wavelength dependent fractionation measurements (13; 14; 19; 20).

After this 1997 advance, efforts were made to bring the model into closer agreement with experimental measurements, and a time-dependent quantum mechanical calculation was made (21) based on *ab initio* potential energy surfaces obtained in Ref. (10) and using a propagated wave packet. The inclusion of the details of the potential energy and dipole moment surfaces into the analysis was a significant improvement. The results of their insightful work do not provide a full explanation of the experimental results (compare Figs. 6.2-6.4 given later). One possibility, as indicated in the normalization constant used for the ground vibrational state in their Eq. (10) and confirmed by private communication [Johnson, private communication, April 2005], was that the two-dimensional (2-D) nature of the bending vibration was treated as a bending in a plane for calculating bending mode wavefunctions, then treating the 2-D aspect only by a degeneracy factor. The 2-D bending vibrational wavefunctions differ from those for a single bending vibration in a plane. Using the present calculational method, the effect of using a single bending mode method as a substitute for the 2-D one is given later in Section IV.

In the experiments of Kaiser et al. (20), a depletion of some heavier isotopomers at 185 nm was recorded for the first time, while Johnson et al. (21) predict enrichment or near-zero fractionation. Blake et al. (22) achieved good results for the fractionation of 448 by adding a new feature to the ZPE model: the zero-point energy of the isotopomer affects not only the position of the absorption cross-section but also the width. They fitted the absorption spectrum to a Gaussian form to extract the parameters for the most abundant isotopomer, 446. Liang et al. (23), continued in a similar direction but they assumed, instead, that the ZPE contribution was from the two stretching modes rather than from all the modes, presumably because it yielded good results even for 546.

However, the actual experiment-based physics of the dissociation show that the two stretching modes play a very different role from each other, and the bending modes also play a very important role. Hanisco and Kummel (24) showed that the photodissociation of N_2O yields vibrationally cold (about 98% of dissociated N_2 is in the $\nu'' = 0$ state) and rotationally hot ($J = 74$) molecular nitrogen. Upon excitation to the higher electronic state, the N-O stretching mode becomes a repulsion and leads to a dissociation, while the N-N is not significantly excited. So, treating the two stretching modes on the same basis and excluding the bending is at odds with these observations.

Von Hessberg et al. (14) have published high precision cross-section measurements of 456, 546 and 556, over a wavelength range 181 nm-218 nm at 233 K and 283 K. The fractionation values computed from these cross-section measurements form an extensive set of data that can help in understanding the atmospheric measurements. Nanbu and Johnson (25) have removed a restriction present in the earlier *ab initio* calculations by calculating the full three-coordinate potential energy surface and using it for the cross-section and isotopomer fractionation computations. The wavefunctions used in this chapter for forming the wavepacket are the 2-D bending ones [Johnson, private communication, April 2005].

In the present chapter, a time-independent multidimensional reflection principle is used

for the calculation of the absorption cross sections of the N_2O isotopomers and thereby the fractionations of the heavy isotopomers relative to the 446. This method, described in section II, focuses on the envelope of the absorption cross-section rather than on the weak superimposed structure. We use the experimental force constant data to calculate the normal mode frequencies of the N_2O molecules in their initial vibrational state and hence calculate the wavefunctions. We use the *ab initio* potential energy surfaces calculated in Ref. (26). These potential energy surfaces depend on two coordinates, like the ones in Ref. (10). Experimentally, the N-N bond distance changes by only 3% during dissociation and was assumed constant in these two coordinate potential energy surface calculations. Nanbu and Johnson (25) have relaxed this restriction of keeping the N-N bond fixed. However, their potential energy surface data have not been published as yet and we have used the latest surfaces published in Ref. (26).

The article is organized as follows: the theory is presented in Section II, the detailed procedure for the present calculations in Section III, the results are presented and discussed in Section IV and conclusions are drawn in Section V.

II. Theory

Photodissociation is classified as either indirect (or predissociation) or direct. In the latter, the parent molecule dissociates immediately upon excitation to the upper electronic state. In indirect photofragmentation a potential barrier hinders direct fragmentation of the excited complex and the wavepacket spends a finite lifetime in the local potential energy well before dissociating. Direct dissociation is characterized by a diffuse, almost structureless absorption spectrum. A comparison among the absorption cross-sections of bands corresponding to direct, nearly-direct and indirect dissociations can be found in Fig. 1.6 of Ref. (27). In the case of N_2O, the broad envelope, with a superimposed weak structure, indicates that the dissociation proceeds primarily in a direct way. We are interested in the envelope of the absorption cross section, and calculate the energies absorbed in a vertical transition

from electronic ground to excited state. This procedure automatically includes the contribution due to the partial absorption cross sections corresponding to various quantum states of dissociating molecule. The formal theory for this behavior for multidimensional systems is due to Heller (28) and an early version is described in Ref. (27). It is summarized here, together with a more accurate version given in (29).

A. Absorption cross section

The molecular quantum states are given in terms of all electronic ($\mathbf{X}$) and nuclear ($\mathbf{R}$) coordinates. We consider the transition of the molecule from the initial molecular quantum state $\mathbf{I}$, with energy E_I, to a final quantum state $\mathbf{F}$, with energy E_F. The absorption cross section, $\sigma_{FI}(\omega)$, for an allowed transition is given in terms of the electric dipole operator $\mathbf{d}$ of the molecule as in Eq. (6.3), an example of Fermi's Golden rule.

$$\sigma_{FI}(\omega) = \frac{\pi}{\hbar\epsilon_0 c}\,\omega\,\delta(\omega_{F,I}-\omega)\,\left|\langle\mathbf{F}|\,\mathbf{e}.\mathbf{d}\,|\mathbf{I}\rangle\right|^2 \tag{6.3}$$

where $\omega_{F,I} = (E_F - E_I)/\hbar$ is the corresponding 'transition frequency', $\mathbf{e}$ is a unit vector in the direction of the polarization of the electric field and $|\langle\mathbf{F}|\,\mathbf{e}.\mathbf{d}\,|\mathbf{I}\rangle|$ is the matrix element for the transition from the initial to the final states. Eq. (6.3) is applicable equally to bound-bound, bound-free and free-free transitions and is the key equation for the time-independent photodissociation for spin-allowed, dipole allowed transitions.

To compute the absorption cross section in the present case, the Born-Oppenheimer approximation is introduced, separating the molecular wavefunction into a nuclear part $\Psi(\mathbf{R})$ and an electronic part $\Phi(\mathbf{X};\mathbf{R})$. The electronic wavefunction will be indexed by i,f and the nuclear wavefunction by ν,ν', respectively, corresponding to the initial and final states. The absorption cross section $\sigma_{i\nu}(\omega)$ for transition from the initial electronic and vibrational

(vibronic) state (i,ν), to the possibly degenerate final vibronic states (f,ν') is given as:

$$\begin{aligned}\sigma_{i\nu}(\omega) &= \frac{\pi}{\hbar\epsilon_0 c}\sum_{\nu'}\omega\ \delta(\omega_{f\nu',i\nu}-\omega)\ |\langle\Psi_{\nu'}|\langle\Phi_f|\mathbf{e}.\mathbf{d}|\Phi_i\rangle|\Psi_\nu\rangle|^2 \\ &= \frac{\pi}{\hbar\epsilon_0 c}\sum_{\nu'}\omega\ \delta(\omega_{f\nu',i\nu}-\omega)\ |\langle\Psi_{\nu'}|\mathbf{e}.\boldsymbol{\mu}_{fi}|\Psi_\nu\rangle|^2 \end{aligned} \tag{6.4}$$

where $\boldsymbol{\mu}_{fi} = \langle\Phi_f|\mathbf{d}|\Phi_i\rangle$ is the transition dipole moment, $\omega_{f\nu',i\nu} = (E_{f\nu'} - E_{i\nu})/\hbar$ and the sum is over the nuclear vibrational states ν' in the given final electronic state f. When the initial state ν is degenerate, one sums $\sigma_{i\nu}$ over the degenerate states ν.

The above expression for the absorption cross section is in the time-independent form, and its calculation requires a knowledge of the nuclear wavefunctions in the upper electronic state. The calculation of the wavefunctions in the excited electronic state would normally be complicated, unlike that of the ground electronic state vibrational wavefunctions which can be found easily using a harmonic oscillator approximation for the vibrational potential energy. To circumvent this problem, we use a Franck-Condon type approximation, which is more easily seen in the time-dependent form (29; 30). Using the details sketched in Appendix A, one obtains the expression for the absorption cross section as:

$$\sigma_{i\nu} = \frac{\pi\omega}{3\hbar\epsilon_0 c}\int |\Psi_\nu(\mathbf{R})|^2\,|\mu_{fi}(\mathbf{R})|^2\delta\left(\omega - (V_f(\mathbf{R}) - \frac{1}{2}E_{i\nu})/\hbar\right)d\mathbf{R} \tag{6.5}$$

where μ_{fi} is the magnitude of the vector $\boldsymbol{\mu}_{fi}$, $V_f(\mathbf{R})$ is the potential energy of the excited state, $E_{i\nu}$ is the average vibrational energy in the ground electronic state, and $\frac{1}{2}\,E_{i\nu}$ is the average potential energy for the case of a harmonic oscillator.

In this final form for the absorption cross-section only the excited state potential surface, transition dipole moment surface, and the probability density in the ground electronic state are needed to calculate the absorption cross section. The wavefunctions in the excited electronic state are not needed. A reflection principle for the one-vibration coordinate case was used by Winans and Steuckelberg (31) and is also given in Herzberg (32). It was

generalized in Ref. (28) for the multidimensional case. However, in that expression, at the vibrational turning point the kinetic energy in the direction of steepest descent as well as normal to it was taken to be zero. This approximation was corrected later by Lee et al. (29) and our Eq. (6.5) is this corrected form of multi-dimensional reflection principle. In the present case the **R** in Eq. (6.5) denotes the internal coordinates for the asymmetric stretching vibration and the doubly degenerate bending vibration.

According to Eq. (6.5), the absorption at any frequency, ω, is proportional to the probability that the initial state is at a **R** for which the vertical transition, given by the delta function in Eq. (6.5), is equal to the potential energy of the electronically excited state at **R** minus an average potential energy $\frac{1}{2}E_{i\nu}$, in the lower electronic vibrational state. Eq. (6.5) is implemented in section 4 to calculate the absorption cross section from each vibrational level in the ground electronic state and then the total absorption cross-section $\sigma(\omega)$ by using the thermal population as a weight.

B. Enrichment

Different isotopomers have the same potential energy function but differ in their normal mode frequencies and normal coordinates, and hence have different widths of the electronic ground-state wavefunctions. As such, they have different absorption cross sections $\sigma_{i\nu}(\omega)$, resulting in a wavelength dependent fractionation of isotopomers. Once the absorption cross sections for various isotopomers are calculated, the fractionation of the different isotopomers relative to the most common isotopomer can be found. The photodissociation rate $J(\omega)$ of a single molecule is given in terms of an absorption cross section $\sigma_{total}(\omega)$ calculated from $\sigma_{i\nu}$'s (Eq. (6.9)) as

$$J(\omega) = \sigma_{total}(\omega)\ I(\omega)\ \phi(\omega) \tag{6.6}$$

where $I(\omega)$ is the photon flux and $\phi(\omega)$ is the quantum yield at energy, $\hbar\omega$. The fractionation $\epsilon(\omega)$ of one isotopomer relative to another due to a one-step photolysis reaction can be

defined as the ratio of photodissociation rates,

$$\epsilon(\omega) = \frac{J'(\omega)}{J(\omega)} - 1 = \frac{\sigma'_{total}(\omega)\phi'(\omega)}{\sigma_{total}(\omega)\phi(\omega)} - 1 = \frac{\sigma'_{total}(\omega)}{\sigma_{total}(\omega)} - 1 \tag{6.7}$$

where the last equality ($\phi'(\omega) = \phi(\omega) = 1$) holds when the upper state is purely dissociative with no singlet-triplet intersystem crossing in the dissociative state (Triplet-singlet spin-forbidden transitions are enhanced by nuclear spin-electron spin coupling ('hyperfine interactions') when one of the nuclei has a non-zero nuclear spin).

III. Procedure

The isotope effects enter into the calculation only through the ground electronic state vibrational wavefunctions and the energy $E_{i\nu}$. The potential energy surfaces and dipole moment function expressed in mass-independent internal coordinates are independent of isotopic substitution. The results of the potential energy and dipole moment surface calculations by Daud et al. (26) are given in terms of mass-dependent Jacobi coordinates and for the present use, they had to be re-expressed in terms of the internal coordinates (Appendix B).

In its electronic ground state N_2O is a linear triatomic molecule and hence has four normal modes of vibration, the symmetric and asymmetric stretching modes and a doubly degenerate bending mode. As usual the wavefunctions for the ground electronic state are written in terms of the normal mode coordinates for these vibrations, and the total vibrational wavefunction is the product of the individual wavefunctions for each of the modes. In the normal coordinates the harmonic oscillator wavefunctions (for the asymmetric stretching and each of the two degenerate bending modes) are given in terms of the well-known Hermite polynomials (33). The vibrational ground state wavefunction for the asymmetric stretching mode is given, for example, as $\left(\alpha^2/\pi\right)^{1/4} exp\left(-\alpha^2 r^2/2\right)$, where α is a constant depending on normal mode frequencies, discussed in Appendix B and conversion factors from internal to normal coordinates, as discussed in Appendix C. Since the potential energy is dependent

only upon the magnitude of a bending angle θ and not upon the angle ϕ about the linear axis, the wavefunctions for the two degenerate bending modes can be combined so that the integrand in the Eq. (6.5) depends on wavefunctions as a function of θ and not of the azimuthal angle ϕ. The corresponding wavefunctions for such a case are given in terms of Laguerre polynomials (54; 33). For convenience, the first three wavefunctions for the degenerate bending vibrations are given in Table A in Appendix D.

Once the total wavefunction is found in terms of the normal coordinates, using the relationship between the internal and normal coordinates, also given in Appendix B, the wavefunctions are converted into functions of internal coordinates. The procedure and data needed for this transformation are given there.

For our calculations, the electronically excited state potential is approximated in the vicinity of the most probable initial spatial region by $V = V_e - V_1(r_{NO}) - V_2(\theta)$, where V_e is the difference of the potential energy of the excited electronic state from the average potential energy of ground electronic state, at the electronic ground state equilibrium position and (r_{NO}, θ) denote the deviations from the equilibrium internal coordinates (r_{NO}^{eq}, $\theta^{eq} = 0$) in the lower electronic state. $V_1(r_{NO})$ and $V_2(\theta)$ are the changes in potential energy as a function of the displacements r_{NO} and θ. In evaluating the $\sigma_{i\nu}$ given by Eq. (6.5), $\mathbf{R} = (r_{NO}, \theta)$ would thus be the relevant nuclear coordinates. The volume element for angles is $\sin\theta d\theta d\phi$. Given that the potential energy, dipole-moment surfaces and $|\Psi_\nu|^2$ are independent of ϕ, the integration over ϕ yields 2π. Using the delta function in Eq. (6.5), an integration is first performed over the coordinate r_{NO}. This step results in the replacing of r_{NO} in the integrand by r_{NO}^s, where r_{NO}^s is the function of θ obtained by solving the equation $\frac{1}{2}E_{i\nu} + \hbar\omega = V_e - V_1(r_{NO}) - V_2(\theta)$, a cubic in r_{NO}. One obtains

$$\sigma_{i\nu}(\omega) = \frac{\pi\omega}{3\hbar\epsilon_0 c}\, 2\pi \int \frac{-1}{(\partial V_1(r_{NO})/\partial r_{NO})_{r_{NO}^s}} \left|\Psi_\nu(r_{NO}^s, \theta)\right|^2 \left|\mu_{fi}(r_{NO}^s, \theta)\right|^2 \sin\theta d\theta \quad (6.8)$$

where the first term in the integrand appears because the argument of the δ-function is not

the integration variable r_{NO}, but a function of it. The integration over the coordinate θ was then performed numerically using *Mathematica*.

The absorption cross section was thus obtained as a continuous function of ω because the transition from any vibrational state in the ground electronic state occurs to a continuum of states in the excited electronic state. If the transition were instead to a single state, the absorption cross section would be a line spectrum rather than a continuum. For r_{NN}, it was observed (24), as noted earlier, that 98% of the dissociated N-N is formed in ground vibrational state. So, for the purpose of this work, we can assume that the transition is to the N-N ground vibrational state in the excited electronic state. The only effect of including this ground-vibrational mode of N-N in the calculations is to shift the absorption cross section by the difference in zero-point energy of N-N in ground and excited electronic states. We need the excited state potential surface along N-N coordinate to compute the N-N frequency, and not for obtaining a 'reflection principle' method based on that surface. To this end, we used Ref. (34) since this information was not reported in a later publication of Nanbu and Johnson (25). Within the wavelengths of interest, the calculations differ from those based on a fixed N-N coordinate by a maximum of about 10 per mil for 556 and 5 per mil for the other isotopomers.

Selwyn and Johnston (11) discuss the importance of the bending mode. In the analysis of their data they concluded that the temperature dependence of the absorption cross-section is due to the excitation of the bending mode. To explore this point we used the contributions to the absorption cross section calculated from the ground, first and second excited bending vibrational states denoted by [000], [010] and [020]. The stretching modes in this designation are in the vibrational ground state. The total absorption cross section is given by the formula:

$$\sigma_{total}(T) = \frac{\sigma_{[000]} + \left(\sigma_{[01^{+1}0]} + \sigma_{[01^{-1}0]}\right) e^{\frac{-\hbar\omega_2}{k_B T}} + \left(\sigma_{[02^{+2}0]} + \sigma_{[02^{0}0]} + \sigma_{[02^{-2}0]}\right) e^{\frac{-2\hbar\omega_2}{k_B T}}}{1 + 2e^{\frac{-\hbar\omega_2}{k_B T}} + 3e^{\frac{-2\hbar\omega_2}{k_B T}}} \quad (6.9)$$

Isotopomer	ν_1	ν_2	ν_3
446	1284.903[a]	588.768[b]	2223.757[d]
	1297.4	593.3	2280.5
447	1264.704[a]	586.362[c]	2220.074[d]
	1274.8	590.8	2276.8
448	1246.885[a]	584.225[c]	2216.711[d]
	1254.3	588.6	2273.7
456	1280.354[a]	575.434[b]	2177.657[d]
	1295.6	579.7	2231.4
546	1269.892[a]	585.312[b]	2201.605[d]
	1280.4	589.7	2257.8
556	1265.334[a]	571.894[c]	2154.726[d]
	1279.0	576.1	2207.9

Table 6.1: Normal mode frequencies of the isotopomers in cm^{-1}: lower rows - this work, upper rows - experimental values.[a][*Toth*, 1986]; [b][*Jolma et al.*, 1983]; [c][*Amiot*, 1976]; [d][*Toth*, 1987]

where $\omega_2 = 2\pi\nu_2$, with ν_2, as given in Table 6.1, being the frequency of the bending mode, where the notation such as $[0n^{+l}0]$ is used for the degenerate or nearly degenerate states of [0n0], distinguished by a vibrational quantum number l that varies from $-n$ to n in increments of ± 2 (54). The coefficients 1, 2, 3 in the denominator account for the degeneracy of the states [000], [010] and [020], respectively in the thermal population. Although the energy of [100] mode is less than that of [020] mode, in our calculations, the contribution of [100] to the absorption cross section is less than 1% of the total absorption cross-section at the same wavelength and we calculated that the difference it makes to fractionation calculations is less than 1 per mil. The reason for this low contribution is, besides the low thermal population of this non-degenerate mode, the low transition dipole moment, because the bending vibration is not in an the excited state in that thermal excitation. In the results presented in the next section, these small contributions from [100] state are omitted.

Selwyn and Johnston (11) attributed the weak structure in the absorption cross section to an effect of the bending vibrational state in the excited electronic state, although the origin of the weak structure is uncertain (26; 25). Our approximation, which smoothes over the weak structure, should not however be confused with the neglect of bending vibrations. The result obtained in the present study is a mean absorption cross section, on which the weak structure will be superimposed if the time evolution were indeed performed for long times instead of using the short-time approximation in Appendix A.

IV. Results and discussion

The normal mode frequencies for each of the isotopomers were obtained using the method described in Appendix B and are given in Table 6.1. The method of calculating the parameter α, as it appears in the N-O stretching wavefunction in section 3 and β, as it appears in the bending wavefunctions given in Table A in Appendix D, is also given in the Appendix C. α^2 and β^2 are defined there and their values for the various isotopomers are also given. These values were introduced into the wavefunctions for the further calculation.

Using these values the calculated absorption cross section for 446 at 297 K is compared in Fig. 6.1 with the experimental absorption cross sections from Ref. (35) at 299 K, Ref. (14) at 283 K, and with the spectra calculated numerically from wave packet propagation in Ref. (21) at 300 K and in Ref. (25) at 283 K. During these calculations (36), the calculated absorption cross section was inadvertently broadened by the use of a scaling factor 1.57 for the potential energy difference between the ground and the excited electronic states. The absorption cross section will be narrower than the one shown in Fig. 6.2 without this factor. A broadening was also needed in the wavepacket calculations (26). Although the broadening factor is empirical, the merit of the rest of the calculations lies in the ability to predict the isotopologue fractionations (Figs. 6.2-6.4) once this broadening is assumed for $^{14}N^{14}N^{1O}O$. Our peak value in the absorption and its position that we obtained are 1.53×10^{-19} cm^2 and $53,600$ cm^{-1}, as compared to the measured values of about 1.4×10^{-19} cm^2 and $55,000$

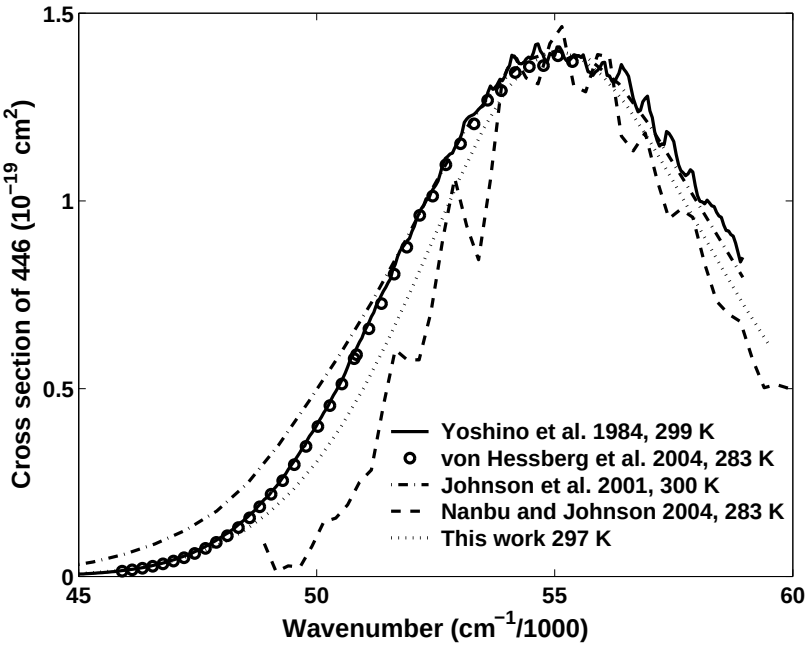

Figure 6.1: Absorption cross section of 446, peaks shifted and peak height rescaled for all the three calculations

cm^{-1}. In Fig. 6.1, the peak was rescaled by a factor of 0.91 and shifted to the right by about $1,400$ cm^{-1} to make the comparison of the shape with the experimental measurement clearer. The shift arises from a small error in the difference between the energy of the ground and excited state electronic energies obtained from *ab initio* calculations. The total absorption cross sections for the 447, 448, 456 and 546 at 297 K were calculated similarly and the same shift in peak position, as for 446, was applied to all of these isotopomers. The peak position of the absorption cross-sections of *Johnson et al.* (21) and of *Nanbu and Johnson* (25) are lower than that of the measured cross-section by 1000 cm^{-1} and 1300 cm^{-1}. In Fig. 6.1 alone, the peak obtained by Johnson et al. (21) and Nanbu and Johnson (25) was shifted by these amounts and rescaled to facilitate the comparison. The results of the calculation are presented as a function of wavenumber rather than wavelength, since then any application of a peak shift does not distort the shape of the plot. According to Ref. (34), the force constant for the N-N stretching in the excited electronic state is about 2.3 times less than that in the ground electronic state. When this value is used, we get the

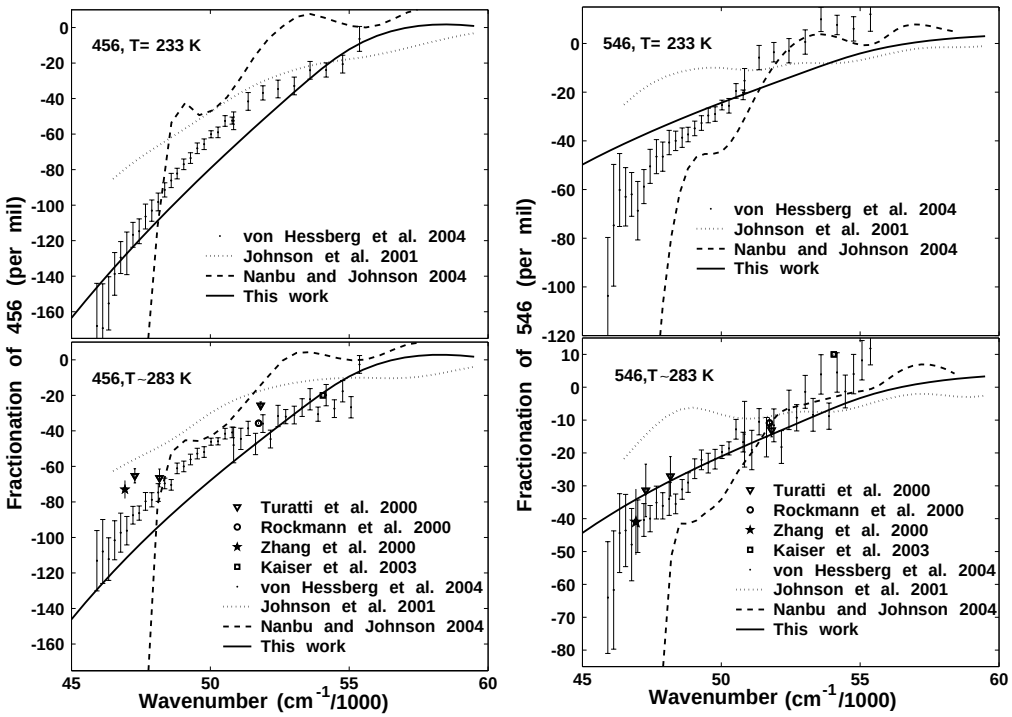

Figure 6.2: Fractionation of 456, 546 at 233 K and 283 K

zero-point energy corresponding to N-N stretching in the excited electronic state to be less than that in the ground state by approximately $0.17\nu_3$ for a given isotopomer. This zero-point energy difference (ΔZPE) reduces the vertical transition energy by $0.17\nu_3$ and was used in the absorption cross-section calculations. Since we are adjusting the position of the peak of 446, it is the difference in the ΔZPE's of different isotopomers, and not the absolute value of ΔZPE, that effects the fractionation calculations. When a more accurate local ZPE of N_2 in the excited N_2O electronic state becomes available, the calculated spectra can be shifted by the difference from the value used here.

A. Wavelength dependent fractionation

The fractionations for the isotopomers relative to the most abundant isotopomer 446, calculated as described in the previous section, are given in the Figs. 6.2-6.6. Because of the weak structure it is possible that there could be substantial fluctuations in the local frac-

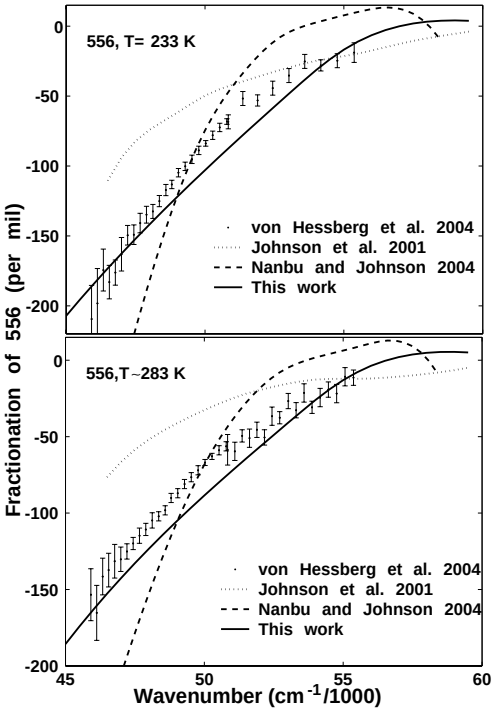

Figure 6.3: Fractionation of 556 at 233 K and 283 K

tionation as a function of the wavenumber, perhaps reflected in the measurements in the form of error bars in fractionation. In the calculations, by neglecting the weak structure, we smooth over the fluctuations and so obtain the mean line for comparison with the mean line for the experiments. In application to atmospheric systems the breadth of the light source averages over fine structure. The results of the current calculation are compared in these Figs. 6.2-6.4 with the experimental data of Refs. (13; 19; 20; 37; 38) and the wide range of wavelength measurements of Ref. (14). The results are also compared with the wave packet calculations of Refs. (21; 25), without applying any shift of the peak position to their results. A comparison of the semi-empirical calculations of Ref. (18), using the differences in zero-point energy (ZPE) of all the modes, by Liang et al. (23), using the difference in ZPE of the two stretching modes, with some experimental measurements and also with the results of Ref. (21) has been given in Ref. (23). Only a comparison with the experiments and with the detailed theoretical calculations is given here.

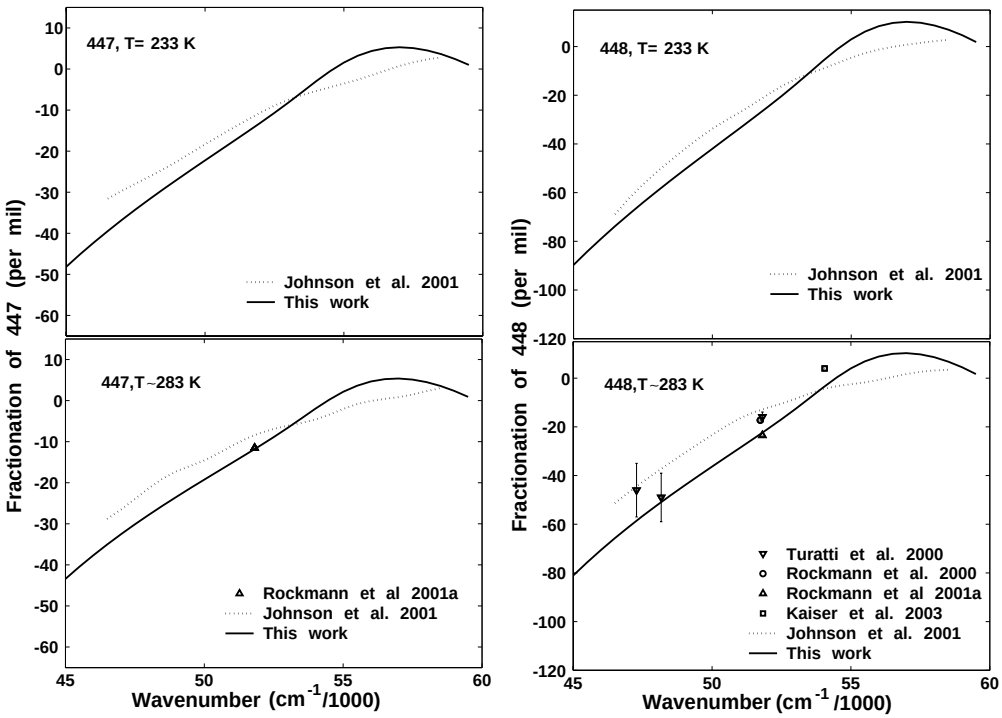

Figure 6.4: Fractionation of 447, 448 at 233 K and 283 K

The sensitivity of the variation of the fractionations of the various isotopomers to changes in wavenumber of the absorption, in both experiment and our calculations, is 556 > 456 > 448 > 447 ∼ 546. The small variation between 546 and 447 relative to that in others reflects the fact that the normal mode frequencies for 546 and 447 differ very little from those of the 446 (Table 6.1). In most cases the present treatment yields improved results compared with the time-dependent treatments in Refs. (21; 25). This improvement can be seen even if appropriate peak shifts were applied to these time-dependent cases, although that was not done in Figs. 6.2-6.4 of this work. The present result and that of Johnson et al. (21) show the maximum deviation for 546 at the longest wavelengths. The freezing of N-N bond was suspected to be the reason, but Nanbu and Johnson's work (25) which included the N-N bond changes, as seen in Figs. 6.2-6.4, yielded poorer results in this region. In another vein, zeroth order correction to our fractionation calculations, made by matching the measured and calculated absorption frequencies at a given intensity of the absorption

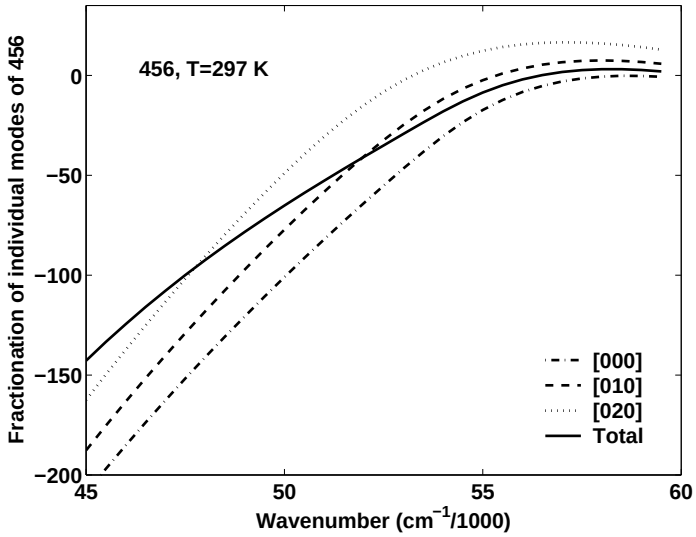

Figure 6.5: Contribution of various bending modes of 456 to the sum

cross-section is given in Appendix E. The correction is seen there to be small but to be closer to experimental value.

The absorption spectrum has contributions from the ground, first and the second bending vibrations, the higher 'hot band' contributions occuring at higher temperatures. The transition dipole-moment increases with the bending angle, and at the same time the vibrationally excited bending states in which high bending angles are possible have a lower thermal population. The contribution from different vibration modes is shown for 456 in Fig. 6.5. At room temperature, the total fraction of the first excited bending state, including the different initial state wavefunctions describing the degeneracy, is 10%, and that of the second excited state is less than 1%. However, at wavelengths longer than 200 nm, the excited bending modes contribute significantly to the fractionation, as seen from the 'total' differing from the ground state alone fractionation by more than 30 per mil. It should be noted that the 'total', indicated in the Fig. 6.5, is not the sum of the fractionations due to individual modes, but it is the fractionation calculated after summing the individual mode contributions to the absorption cross section of 456 and dividing by that of 446. At some wavenumbers, the 'total' fractionation could be more positive than it is in each of the indi-

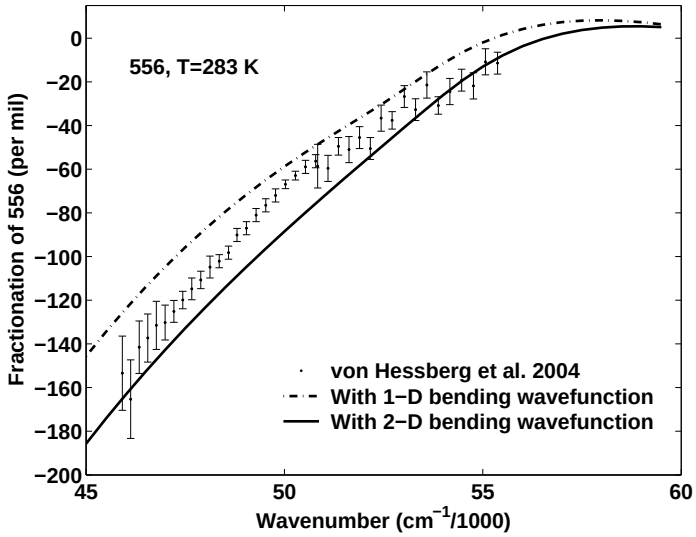

Figure 6.6: Fractionation of 556 at 283 K using 1-D and 2-D bending wavefunctions

vidual modes, because at a given temperature, the thermal population of the excited states in 456 is slightly more than that of 446 because of the different vibrational frequencies of the isotopomers, leading to a slightly higher photolysis cross-section of 456.

The laboratory fractionation studies of 447 and 448 (12) were performed at 185 nm and this choice of wavelength resulted in near-zero fractionations of both 447 and 448. A later analysis (39) showed that for these values of measured fractionations the scatter was too large for a suitable fractionation line to be drawn, presumably because of the high noise in the near-zero fractionations (39). So, no comparison with this data set was made.

Before the results of Daud et al. (26) were published, our calculations were based on the potential energy and dipole moment surfaces of Brown et al. (10). The results obtained with that are comparable to the ones reported in this chapter, with the absorption cross section about 1.15 times the current value and the fractionations within a maximum of 20 per mil of the results reported here.

To estimate the error in using 1-D instead of 2-D bending wavefunctions, the total absorption cross-section was calculated by summing the absorption cross-section for each initial

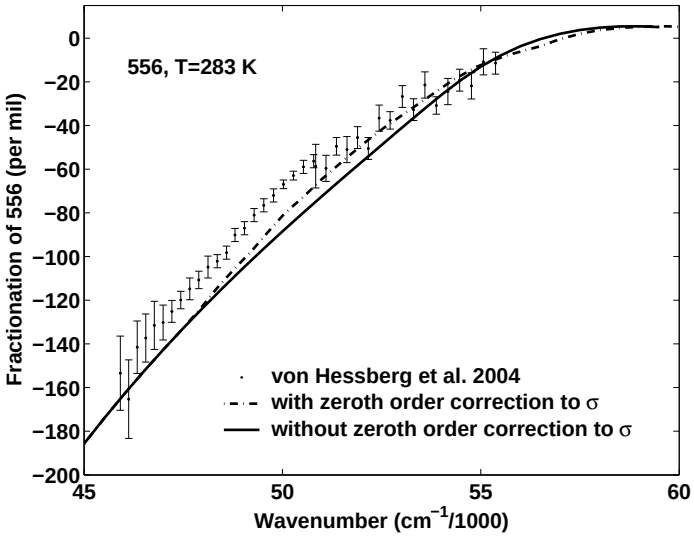

Figure 6.7: Fractionation of 556 at 283 K with and without the zeroth order correction to the absorption cross section described in Appendix E

vibrational energy using 1-D harmonic oscillator wavefunctions, weighted by a degeneracy factor. The resulting cross-section has the same shape as that obtained using 2-D bending wavefunctions. The peak intensity is about 2 times smaller and the peak position occurs at about 800 cm^{-1} higher than before. The fractionations calculated with the 1-D wavefunctions, after accounting for the appropriate peak shift, are approximately 20-25% different from those calculated with the 2-D bending wavefunctions. The difference between the two results for the case of 556 is illustrated in Fig. 8. This difference is qualitatively the same for all the other isotopomers. After considering the shift in the absorption cross-section that would be needed for Johnson et al. (21), the 1-D wavefunction results at around 47500 cm^{-1} account for about 70% of the difference between the calculations of Johnson et al (21) and the measurements.

B. Broadband calculations and atmospheric relevance

In the above discussion, the results of our calculations were compared with the wavelength dependent fractionation measurements. In the atmosphere, there is a flux of photons over a wide range of wavelengths, and the resultant fractionation occurs because of the simultane-

ous fractionation at all those wavelengths. Here we make a comparison with the broadband (185-225 nm) photolysis results of Ref. (40). Using an antimony (Sb) lamp at room temperature, Rockmann et al. (40) obtained fractionations of -34.2±0.8, -54±1.6 and -21.9±1.1 for ϵ^{448}, ϵ^{456} and ϵ^{546} respectively. When a 207 nm filter was used on the lamp, there was no noticeable change in their experimental results. However, the fractionation constants compared with and without the filter differed by about 2 to 4 per mil in the later experiments of Kaiser (39). The wavelength dependent fractionations that we obtained, averaged using the relative overlap of the N_2O absorption and Sb emission spectrum (Plate 4, Ref. (40)) as the weighting factor, gives (ϵ^{447}, ϵ^{448}, ϵ^{456}, ϵ^{546}, ϵ^{556}) as (-19.2, -36.1, -68.0, -21.1, -88.4) and (-22.9, -43.1, -82.1, -25.2, -106.1) at 297 K and 233 K. With the 207 nm filter our results are (-23.7, -44.7, -82.3, -25.3, -106.4) and (-28.1, -52.8, -98.6, -30.1, -127.0) at 297 K and 233 K. The ratio of $\epsilon^{447}/\epsilon^{448}$ from our calculations in all the above cases is between 0.530 and 0.532. In a detailed analysis of the atmospheric relevance the results of the current calculation can be incorporated into a model which contains the transport of N_2O in the atmosphere (41; 42), in addition to these photolysis results.

A significant overlap of the N_2O absorption spectrum with the actinic fluxes in stratosphere exists in the wavenumber range 45,000 to 53,500 cm^{-1} (Plate 4, Ref. (40)). For the wavenumbers in this range, using the detailed calculations in the present chapter, the slope of the three-isotopic plot of $ln(1+\epsilon^{447})$ at each wavenumber, vs. $ln(1+\epsilon^{448})$ at the same wavenumber, is calculated to be 0.525.

A perturbation theoretical expression for the slope of the three-isotope plot in the case of photolytic fractionation, obtained analytically with no computation, is given in (44). The result obtained to first order in mass-effects is the same as that obtained in Ref. (43) for chemical equilibria (44). The slope by perturbation analysis for $ln(1+\epsilon^{447})$ vs. $ln(1+\epsilon^{448})$ plot is $(1/m_{O^{16}} - 1/m_{O^{17}})/(1/m_{O^{16}} - 1/m_{O^{18}}) = 0.529$.

In virtue of the close agreement between the slope 0.525 obtained by detailed calculations

and the slope obtained with no computation 0.529, we suggest that the slope for mass-dependent photolytic fractionation is 0.525. In another form of presenting the fractionation, a ϵ^{447} vs. ϵ^{448} plot, the slope with our detailed calculations is 0.530. A slope of 0.515 was obtained from an assortment of non-photolytic thermal data [Cliff and Thiemens, 1997]. We suggest that a slope of ϵ^{447} vs. ϵ^{448} plot differing from 0.530 for photolysis be considered an anomalous fractionation. However, a small deviation from this slope is not as striking as the mass-independent fractionation found in O_3 formation (45) governed by the symmetry effects (46).

The question of the contribution of photolytic fractionation to 'anomalous' atmospheric observations (47) has been previously discussed (41; 49). The result of the present chapter, in conjunction with a transport model, can be used to see what fraction of the enrichment of 447 in the stratosphere can be accounted for by photodissociation.

V. Conclusions

In absorption cross sections of N_2O isotopomers calculated using a computationally simple time-independent multidimensional reflection principle, the cross-section obtained for 446 is in good agreement with the broad envelope of the experimental cross section, with a shift in peak position. The fractionation of heavy isotopomers obtained in this relatively simple calculation as a function of the wavelength, after introducing this peak shift in all isotopomers correctly accounts for the observed fractionation of 448, 456, 546 and 556. The method does require potential energy and dipole moment surfaces obtained from *ab initio* calculations. Once the potential energy surfaces are obtained the calculation is not computationally intensive. Specific quantities of atmospheric relevance can be calculated by incorporating the results of the present chapter into a transport model.

VI. Appendix A: Approximate expression for the absorption cross-section

Eq. (6.4) gives a time-independent expression for the absorption cross-section as:

$$\sigma_{i\nu}(\omega) = \frac{\pi}{\hbar\epsilon_0 c}\sum_{\nu'}\omega\ \delta(\omega_{f\nu',i\nu}-\omega)\ |\langle\Psi_{\nu'}|\mathbf{e}.\boldsymbol{\mu}_{fi}|\Psi_{\nu}\rangle|^2 \tag{4}$$

This equation can be converted into a time-dependent form (50) using the identity:

$$\delta(\omega-\omega_{f\nu',i\nu}) = \frac{1}{2\pi}\int_{-\infty}^{\infty} e^{i(\omega-\omega_{f\nu',i\nu})}dt \tag{6.10}$$

in Eq. (6.4). Using another identity

$$e^{-iH_2t/\hbar} = \sum_{\nu'}|\Psi_{f\nu'}\rangle e^{-iE_{f\nu'}t/\hbar}\langle\Psi_{f\nu'}| \tag{6.11}$$

where H_2 is the Hamiltonian of the excited state and $E_{f\nu'}$ the energy of the final vibronic state $(f\nu')$. $\sigma_{i\nu}$ can be rewritten as (50):

$$\begin{aligned}\sigma_{i\nu} &= \frac{\pi\omega}{\hbar\epsilon_0 c}\frac{1}{2\pi}\int_{-\infty}^{\infty}\left(\langle\Psi_\nu|\ \mathbf{e}.\boldsymbol{\mu}_{fi}^{\dagger}\ e^{-iH_ft/\hbar}\ \mathbf{e}.\boldsymbol{\mu}_{fi}\ |\Psi_\nu\rangle\right)e^{i(\omega+E_{i\nu}/\hbar)t}\ dt \\ &= \frac{\pi\omega}{\hbar\epsilon_0 c}\frac{1}{2\pi}\int_{-\infty}^{\infty}(\langle y(0)|y(t)\rangle)\ e^{i(\omega+E_{i\nu}/\hbar)t}\ dt\end{aligned} \tag{6.12}$$

where $|y(t)\rangle = e^{-iH_ft/\hbar}|y(0)\rangle = e^{-iH_ft/\hbar}\mathbf{e}.\boldsymbol{\mu}_{fi}\ |\Psi_\nu\rangle$. In this form it is seen that $\sigma_{i\nu}$ is proportional to the Fourier transform of the autocorrelation function $\langle y(0)|y(t)\rangle$.

The time-dependent approach involves finding the time-evolution of the autocorrelation function under the Hamiltonian H_f and then its Fourier transform. To obtain a simpler form in the time-independent approach, an approximation is made, shown to be valid to first order in time t (29), that at short times of evolution the operator H_f can be replaced by $\langle T\rangle_{i\nu}^{(\mu)} + V_f$, where V_f is the potential energy operator of the excited state. T is the kinetic energy operator, which is the same in ground and excited electronic states and

$\langle T\rangle_{i\nu}^{(\mu)} = \langle\Psi_{i\nu}|\mathbf{e}.\boldsymbol{\mu}_{fi}^{\dagger} T \mathbf{e}.\boldsymbol{\mu}_{fi}|\Psi_{i\nu}\rangle / \langle\Psi_{i\nu}|\mathbf{e}.\boldsymbol{\mu}_{fi}^{\dagger}\mathbf{e}.\boldsymbol{\mu}_{fi}|\Psi_{i\nu}\rangle$. The averaged kinetic energy $\langle T\rangle_{i\nu} = \langle\Psi_{i\nu}|T|\Psi_{i\nu}\rangle / \langle\Psi_{i\nu}|\Psi_{i\nu}\rangle$ of the vibrational state ν in the *ground* electronic state i, equal to $\frac{1}{2}E_{i\nu}$ for a harmonic approximation to the potential energy (29) we found by calculation that it differs from $\langle T\rangle_{i\nu}^{(\mu)}$ by only about 10 cm^{-1}. This spectral shift is negligible. So in the present chapter $\langle T\rangle_{i\nu}^{(\mu)}$ is approximated by $\frac{1}{2}E_{i\nu}$.

Physically, time-dependent picture means that because of the excitation, the wavepacket from the ground electronic state is promoted to the excited electronic surface instantaneously and the dynamics of the autocorrelation is considered as the wave packet evolves under excited state Hamiltonian. Since $\sigma_{i\nu}$ is given by the Fourier transform of the autocorrelation function in Eq. (12), the present short-time approximation for the time evolution has as a consequence that one can only obtain the broad features of the absorption cross-section (the envelope) rather than its fine structure. The method is well suited to the analysis of direct or nearly-direct dissocation problems, where the lifetime of the wavepacket is small in the excited electronic state and the superimposed structure is not dominant over the broad background of the absorption. Using the identity in Eq. (6.10), the absorption cross-section is converted back into the time-independent form using the short-time approximation given in Ref. (29):

$$\begin{aligned}\sigma_{i\nu} &= \frac{\pi\omega}{\hbar\epsilon_0 c}\langle\Psi_\nu|\ \mathbf{e}.\boldsymbol{\mu}_{fi}^{\dagger}\ \ \delta\left(\omega - (V_f + \langle T\rangle_{i\nu} - E_{i\nu})/\hbar\right)\ \ \mathbf{e}.\boldsymbol{\mu}_{fi}\ |\Psi_\nu\rangle \\ &= \frac{\pi\omega}{\hbar\epsilon_0 c}\int |\Psi_\nu(\mathbf{Q})|^2 \left|\mathbf{e}.\boldsymbol{\mu}_{fi}(\mathbf{R})\right|^2 \delta\left(\omega - (V_f - \frac{1}{2}E_{i\nu})/\hbar\right) d\mathbf{R} \end{aligned} \tag{6.13}$$

where the second line in the equation above is a coordinate representation of the first line. The dipole moment function $\boldsymbol{\mu}_{fi}(\mathbf{R})$ is obtained by *ab initio* calculations. Averaging over all possible directions, $\mathbf{e}$, of the electric field, we get the absorption cross section by replacing $|\mathbf{e}.\boldsymbol{\mu}_{fi}|^2$ with $\frac{1}{3}|\mu_{fi}|^2$, μ_{fi} being the magnitude of the vector $\boldsymbol{\mu}_{fi}$.

$$\sigma_{i\nu} = \frac{\pi\omega}{3\hbar\epsilon_0 c}\int |\Psi_\nu(\mathbf{R})|^2 \left|\mu_{fi}(\mathbf{R})\right|^2 \delta\left(\omega - (V_f - \frac{1}{2}E_{i\nu})/\hbar\right) d\mathbf{R} \tag{6.14}$$

VII. Appendix B: Normal mode calculation

The procedure for finding the normal modes of vibration and the normal coordintes in terms of the internal coordinates is described in Califano (51) and Steele (52). The inertia matrix G^{-1}, which has the details of the masses and moments of inertia of the molecule, and the force constant matrix F are used for this transformation. We denote the deviations of the internal coordinates from the equilibrium values (r_{NN}^{eq}, r_{NO}^{eq}, θ^{eq}) by (r_{NN}, r_{NO}, θ). The inertia matrix G for the linear molecule N_2O is defined by Califano (51) ($G_{\theta\theta}$, not discussed by Califano, is given by Ferigle et al. (53)).

$$G = \begin{pmatrix} \mu_1 + \mu_2 & \mu_2 & 0 \\ \mu_2 & \mu_2 + \mu_3 & 0 \\ 0 & 0 & \frac{\mu_1}{(r_{NN}^{eq})^2} + \frac{\mu_3}{(r_{NO}^{eq})^2} + \mu_2\left(\frac{1}{(r_{NN}^{eq})} + \frac{1}{(r_{NO}^{eq})}\right)^2 \end{pmatrix} \tag{6.15}$$

where $\mu_i = 1/m_i$, m_i being the mass of the atom in the i^{th} position ($N^{(1)}$-$N^{(2)}$-$O^{(3)}$).

The potential and kinetic energy expressions in the matrix form are: $2V = R^T F R$ and $2T = P^T G P$, where R is a column matrix whose rows R_1, R_2 and R_3 are r_{NN}, r_{NO} and θ, and P is the momentum matrix conjugate to R. Using the Hamilton's equation, we have $\dot{R} = \partial T/\partial P = GP$. Using this relation and the symmetry of G (namely that its transpose, G^T, equals itself, G), $2T = \dot{R}^T \left(G^{-1}\right)^T G G^{-1} \dot{R} = \dot{R}^T G^{-1} \dot{R}$. The normal coordinates Q are transformed in terms of the internal coordinates R. Using a linear transformation L from Q to R, $R = LX$ the expressions for the kinetic and potential energies can be rewritten as: $2V = Q^T L^T F L Q$ and $2T = \dot{Q}^T L^T G^{-1} L \dot{Q}$. To reduce these into the standard forms for normal coordinates, we use the conditions that:

i. $L^T G^{-1} L$ and $L^T F L$ are diagonal. This transformation can be achieved by forming L from the eigenvectors of the GF matrix. Then, L simultaneoulsy diagonalizes F and G^{-1}.

ii. Comparison with the standard form of normal coordinate kinetic energy gives $L^T G^{-1} L = I$ and removes the arbitrary scaling factors in the eigenvectors that form L,

thus making the transformation $R = LQ$ unique.

The natural frequencies for the normal modes are calculated using $\frac{1}{2}\dot{Q}^T L^T G^{-1} L\dot{Q} - L^T F L = 0$ i.e., $W - L^T F L = 0$, where W is a diagonal matrix with elements $W_{i,i} = \omega_i^2$. In conformity with the standard notation, we choose the order of ω_i's such that ω_2 corresponds to the bending vibration and ω_1 and ω_3 to the stretching vibrations. The ω_i's are related to the ν_i's in Table 1 as $\omega_i = 2\pi\,\nu_i$ The data required for the calculation of G matrix are: atomic masses of isotopes in amu $\rightarrow$ ^{14}N - 14.0; ^{15}N - 15.0; ^{16}O - 16.0; ^{18}O - 18.0; equilibrium bondlengths $\rightarrow$ $r_{NN}^{eq} = 1.1273$ A; $r_{NO}^{eq} = 1.1851$ A.

VIII. Appendix C: Calculation of α and β

In the ground vibrational state, the amplitude of the wavefunction is given in terms of the normal coordinates as: $|\Psi|^2 \propto exp\left(-\Sigma\omega_i Q_i^2/\hbar\right)$, where Q_i are the elements of the normal coordinate matrix Q, defined in the previous section. Converting these normal coordinates into internal displacement coordinates, R_i and leaving the normalization factor that includes the Jacobian of the transformation, we have:

$$\begin{aligned}
|\Psi|^2 &\propto exp\left(-\Sigma\omega_i\left(L_{ij}^{-1}R_j\right)^2/\hbar\right) \\
&= exp\left(-A_1 r_{NN}^2 - A_2 r_{NO}^2 - 2A_3 r_{NN} r_{NO} - A_4\theta^2\right) \\
&\propto exp\left(-A_1\left(r_{NN} + A_3/A_1 r_{NO}\right)^2 - \left(A_1A_2 - A_3^2\right) r_{NO}^2/A_1 - A_4\theta^2\right) \qquad (6.16)
\end{aligned}$$

where L_{ij}^{-1} are the elements of the inverse of the matrix L defined in the previous section, R_j are the internal displacement coordinates r_{NN}, r_{NO} and θ. The coefficients A_is were obtained in terms of ω, L_{ij}^{-1} and $\hbar$, by the rearrangement of the internal coordinate terms in Eq. (6.15): $A_1 = 1/\hbar\left(\omega_1(L_{11}^{-1})^2 + \omega_3(L_{31}^{-1})^2\right)$, $A_2 = 1/\hbar\left(\omega_1(L_{13}^{-1})^2 + \omega_3(L_{33}^{-1})^2\right)$, $A_3 = 1/\hbar\left(\omega_1(L_{11}^{-1}L_{13}^{-1}) + \omega_3(L_{31}^{-1}L_{33}^{-1})\right)$ and $A_4 = 1/\hbar\left(\omega_2(L_{22}^{-1})^2\right)$.

Defining $(r_{NN} + A_3/A_1 r_{NO})$ and r_{NN} as the two independent coordinates, the former is

seen to be irrelevant for the absorption analysis since the potentials and dipole moments are independent of that coordinate. In the expression for the absorption cross section, the term corresponding to this coordinate would thus on integration, yield unity. Comparing the coefficient of θ^2 with that for the ground-state wavefunction in Table A in Appendix D, we obtain the parameter $\beta^2 = A_4$. Similarly, α^2 is $(A_1A_2 - A_3^2)/A_1$.

In this chapter, we use the force constant data F for N_2O available from Csaszar [1994] and obtained by their fit to the experimental data on vibration frequencies. These force constants in the units of aJ/A^2 are: $F_{r_{\rm NN}r_{\rm NN}}$ - 18.251; $F_{r_{\rm NO}r_{\rm NO}}$ - 11.960; $F_{r_{\rm NN}r_{\rm NO}}$ - 1.028; $F_{\theta\theta}$ - 0.666; $F_{r_{\rm NN}\theta}$ - 0; $F_{r_{\rm NO}\theta}$ - 0.

The values of (α^2, β^2) thus obtained, in units of $(10^4/\mathrm{nm}^2, /\mathrm{rad}^2)$ are (3.7847, 55.9644), (3.8457, 56.1997), (3.9023, 56.4105), (3.8418, 57.2736), (3.7881, 56.2995) and (3.8450, 57.6329) for 466, 447, 448, 456, 546 and 556 isotopomers.

IX. Appendix D: Wavefunctions

The first three degenerate bending vibrational wavefunctions are given here in Table A.

n=0	m = 0	$\frac{\beta}{\sqrt{\pi}} e^{-\beta^2\theta^2/2}$
n=1	m = 1	$\frac{\beta}{\sqrt{\pi}}\, \beta\theta\, e^{-\beta^2\theta^2/2} e^{i\phi}$
	m = -1	$\frac{\beta}{\sqrt{\pi}}\, \beta\theta\, e^{-\beta^2\theta^2/2} e^{-i\phi}$
n=2	m = 2	$\frac{\beta}{\sqrt{2\pi}} (\beta\theta)^2 e^{-\beta^2\theta^2/2} e^{2i\phi}$
	m = 0	$\frac{\beta}{\sqrt{\pi}} \left((\beta\theta)^2 - 1 \right) e^{-\beta^2\theta^2/2}$
	m = -2	$\frac{\beta}{\sqrt{2\pi}} (\beta\theta)^2 e^{-\beta^2\theta^2/2} e^{2i\phi}$

Table A: Table of wavefunctions for doubly degenerate bending vibration

X. Appendix E: Zeroth order correction to the calculations

In Fig. 6.1, we see that the absorption cross-section calculated in this work, based on vibronic transitions alone, is slightly narrower than the measured absorption cross-section. There can be a broadening in this absorption cross-section if we also include the contribution of the transitions between the rotational states, say J to $J+1$, with thermal populations that depend upon the energies of the states, $E_J = BJ(J+1)$ and $E_{J+1} = B(J+1)(J+2)$. Here, B is the rotational constant. For such a case, corresponding to a total absorption frequency, the vibronic transition will happen at a frequency less by the energy difference $\Delta E = E_{J+1} - E_J = 2B(J+1)$. The total absorption cross-section would be obtained as the sum of the vibronic cross-sections, shifted by the rotational excitation and weighted by the thermal probability of being in the rotational state J. With the total cross-section given by the convolution of the thermal probability distribution as a function of the ΔE and the vibronic cross-section, if we approximate both of these by Gaussian distributions with variances s_{vib}^2 and s_{rot}^2, the variance of the total absorption cross-section will be $s_{vib}^2 + s_{rot}^2$. Since in the case of N_2O, $s_{vib} \sim 2750$ cm^{-1} and $s_{rot} \sim 10$ cm^{-1}, the effect of the inclusion of the rotation on the width of the total absorption cross-section is negligible. Including the other branches $\Delta J = 0, -1$ also has a negligible effect on the width.

It is assumed that the difference between the measured and the calculated cross-sections was due to the potential energy surfaces as one of at least two possibilities, a zeroth order correction to our calculation of fractionation calculations can be made as follows. To implement this correction, after rescaling the height and shifting the peak of the calculated cross-section, corresponding to an intensity in the calculated cross-section, the actual absorption wavenumber (ω_{meas}), which is slightly higher or lower than the calculated one (ω_{calc}) is noted. Then the fractionations calculated as a function of ω_{calc} are plotted as functions of ω_{meas} instead. This new plot is illustrated for the case of 556 isotopomer in

Fig. 6.9. The difference in the fractionation obtained by such a correction is small, but noticeable in the scale of the plots. This correction would be applicable to calculations at temperatures $\sim$ 283 K or 233 K, for which we know the absorption cross-section (14; 35)

Bibliography

[1] Y. L. Yung, Y. L., W. C. Wang, and A. A. Lacis, *Geophys. Res. Lett., 3*, 619 (1976)

[2] C. M. Stevens, D. Walling, A. Venters, L. E. Ross, A. Engelkem, and L. Krout, *Earth Planet. Sci. Lett., 16*, 147 (1972)

[3] C. A. M. Brenninkmeijer, C. Janssen, J. Kaiser, T. Rockmann, T. S. Rhee, and S. S. Assonov, *Chem. Rev., 103*, 5125 (2003)

[4] K. -R. Kim, and H. Craig, *Science, 262*, 1855 (1993)

[5] S. W. A. Naqvi, T. Yoshinari, D. A. Jayakumar, M. A. Altabet, P. V. Narvekar, A. H. Devol, J. A. Brandes and L. A. Codispoti, *Nature, 394 (6692)*, 462 (1998)

[6] K. F. Preston, and R. F. Barr, *J. Chem. Phys., 54*, 3347 (1971)

[7] R. Atkinson, D. L. Baulch, R. A. Cox, R. F. Hampson Jr., J. A. Kerr, M. J. Rossi and J. Troe, *J. Phys. Chem. Ref. Data, 26,* 521 (1997)

[8] S. Nishida, K. Takahashi, Y. Matsumi, N. Taniguchi, and S. Hayashida, *J. Phys. Chem. A, 108*, 2451 (2004)

[9] K. Minschwaner, R. J. Salawitch, and M. B. McElroy, *J. Geophys. Res., 98,* 10543 (1993)

[10] A. Brown, P. Jimeno, and G. G. Balint-Kurti, *J. Phys. Chem. A, 103*, 11089 (1999)

[11] G. S. Selwyn, and H. S. Johnston, *J. Chem. Phys, 74*, 3791 (1981)

[12] J. C. Johnston, S. S. Cliff, and M. H. Thiemens, *J. Geophys. Res., 100*, 16801 (1995)

[13] H. Zhang, P. O. Wennberg, V. H. Wu, and G. A. Blake, *Geophys. Res. Lett., 27*, 2481 (2000)

[14] P. von Hessberg, J. Kaiser, M. B. Enghoff, C. A. McLinden, S. I. Sorensen, T. Rockmann, and M. S. Johnson, *Atmos. Chem. and Phys., 4*, 1237 (2004)

[15] T. Rahn, and M. Wahlen, *Science, 278*, 1776 (1997)

[16] S. Y. Park, E. L. Atlas and K. A. Boering, *J. Geophys. Res., 109,* D01305 (2004)

[17] S. S. Prasad, *J. Geophys. Res., 102,* 21527 (1997)

[18] Y. L. Yung, and C. E. Miller, *Science, 278*, 1778 (1997)

[19] F. Turatti, D. W. T. Griffith, S. R. Wilson, M. B. Esler, T. Rahn, H. Zhang and G. A. Blake, *Geophys. Res. Lett., 27*, 2489 (2000)

[20] J. Kaiser, T. Rockmann, C. A. M. Brenninkmeijer, and P. J. Crutzen, *Atmos. Chem. Phys., 3*, 303 (2003)

[21] M. S. Johnson, G. D. Billing, A. Gruodis, and M. H. M. Janssen, *J. Phys. Chem. A, 105*, 8672 (2001)

[22] G. A. Blake, M. C. Liang, C. G. Morgan, and Y. L. Yung, *Geophys. Res. Lett., 30*, 1656 (2003)

[23] M. C. Liang, G. A. Blake, and Y. L. Yung, *J. Geophys. Res., 109*, D10308 (2004)

[24] T. F. Hanisco, and A. C. Kummel, *J. Phys. Chem., 97*, 7242 (1993)

[25] S. Nanbu, and M. S. Johnson, *J. Phys. Chem. A, 108*, 8905 (2004)

[26] M. N. Daud, G. G. Balint-Kurti and A. Brown, *J. Chem. Phys., 122,* 054305 (2005) [ftp://ftp.aip.org/epaps/journ_chem_phys/E-JCPSA6-122-303502/]

[27] R. Schinke, *Photodissociation dynamics*, Cambridge Univ. Press, New York, NY, 1993.

[28] E. J. Heller, *J. Chem. Phys. 68*, 2066 (1978)

[29] S. Y. Lee, R. C. Brown, and E. J. Heller, *J. Phys. Chem., 87*, 2045 (1983)

[30] S. Y. Lee, *J. Chem. Phys., 76,* 3064 (1982)

[31] J. G. Winans, and E. C. G. Stueckelberg, *Proc. Natl. Acad. Sci. U.S.A., 14*, 867 (1928)

[32] G. Herzberg, *Molecular spectra and molecular structure 1. Spectra of diatomic molecules*, pp. 391-394, Van Nostrand, Princeton, 1950.

[33] C. Cohen-Tannoudji, B. Diu and F. Laloe, *Quantum mechanics, Vol. I*, Wiley, New York (1977)

[34] D. G. Hopper, *J. Chem. Phys., 80*, 4290 (1984)

[35] K. Yoshino, D. E. Freeman and W. H. Parkinson, *Planet. Space Sci., 32*, 1219 (1984)

[36] M. K. Prakash, J. D. Weibel, and R. A. Marcus, *J. Geophys. Res. Atmos., 110*, D21315 (2005)

[37] T. Rockmann, C. A. M. Brenninkmeijer, M. Wollenhaupt, J. N. Crowley, and P. J. Crutzen, *Geophys. Res. Lett., 27,* 1399 (2000)

[38] T. Rockmann, J. Kaiser, J. N. Crowley, C. A. M. Brenninkmeijer, and P. J. Crutzen, *Geophys. Res. Lett., 28,* 503 (2001a)

[39] J. Kaiser, *Stable isotope investigations of atmospheric nitrous oxide*, Ph.D Thesis, Johannes Gutenberg-Univ., Mainz, Germany (2002)

[40] T. Rockmann, J. Kaiser, C. A. M. Brenninkmeijer, J. N. Crowley, R. Borchers, W. A. Brand, and P. J. Crutzen, *J. Geophys. Res., 106,* 10,403 (2001b)

[41] C. A. M. McLinden, J. Prather, and M. S. Johnson, *J. Geophys. Res., 108*, 4233 (2003)

[42] C. G. Morgan, M. Allen, M. C. Liang, R. L. Shia, G. A. Blake, Y. L. Yung, *J. Geophys. Res., 109*, D04305 (2004)

[43] J. Bigeleisen, and M. G. Mayer, *J. Chem. Phys., 15,* 261 (1947)

[44] M. K. Prakash, and R. A. Marcus, *to be submitted to Geophys. Res. Lett.,* (2005)

[45] M. H. Thiemens, and J. E. Heidenreich, *Science, 219,* 1073 (1983)

[46] Y. Q. Gao, and R. A. Marcus, *J. Chem. Phys., 116,* 137 (2002)

[47] S. S. Cliff, and M. H. Thiemens, *Science, 278,* 1774 (1997)

[48] S. S. Cliff, C. A. M. Brenninkmeijer, and M. H. Thiemens, *J. Geophys. Res., 104*, 16171 (1999)

[49] J. Kaiser, T. Rockmann, C. A. M. Brenninkmeijer, *J. Geophys. Res., 109*, D03306 (2004)

[50] G. C. Schatz, and M. A. Ratner, *Quantum mechanics in chemistry*, pp. 201 , Dover, New York, 2002.

[51] S. Califano, *Vibrational states*, John Wiley & Sons, New York (1976)

[52] D. Steele, *Theory of vibrational spectroscopy*, W. B. Saunders Co., Philadelphia (1971)

[53] S. M. Ferigle, and A. G. Meister, *J. Chem. Phys., 19*, 982 (1951)

[54] K. F. Freed, and Y. B. Band., Product energy distributions in the dissociation of polyatomic molecules, in *Excited States*, Vol 3, edited by E. C. Lim, pp. 109-201, Academic Press, New York (1977)

[55] A. G. Csaszar, *J. Phys. Chem., 98*, 8823 (1994)

[56] R. A. Toth, *J. Opt. Soc. Am. B., 3*, 1263 (1986)

[57] C. Amiot, *J. Mol. Spectrosc., 59*, 380 (1976)

[58] K. Jolma, J. Kauppinen, and V. -M. Horneman, *J. Mol. Spectrosc., 101*, 278 (1983)

[59] R. A. Toth, *J. Opt. Soc. Am. B., 4*, 357 (1987)

Chapter 7

Isotopomer fractionation in the UV photolysis of N_2O: comparison of theory and experiment II

Wavelength-dependent fractionation of various isotopomers in the photodissociation of N_2O is studied. The absorption cross sections are calculated by a time-independent reflection principle, similar to the treatment in Chapter 6, but now with the inclusion of the NN stretching coordinate, and both the 2A" and 1A' electronic excited states. The 1A' state is found to have little effect on both the absorption cross section and the fractionation. The improvements include more physical details in the photodissociation of N_2O, while maintaining an advantage of a treatment in Chapter 6 that was not computationally intensive. The present calculated fractionation, without a significant adjustable parameter, gives good agreement with experiments in the absorption cross section in the low-energy region, the important region for the experimentally observed isotopic fractionation.

I. Introduction

The photolytic dissociation of molecules is important in stratospheric and atmospheric chemistry (*e.g.* (1)). N_2O, in particular, is an effective greenhouse gas and a source of singlet oxygen atoms. Isotopomer fractionation measurements help in determining the sources and sinks of atmospheric gases (2; 3). The isotopic fractionation photodissociation

behavior of N_2O has been the subject of many studies (3; 4; 5), including wavelength-dependent measurements (6-11). These studies motivated both empirical (12; 13) and more theoretical (14-16) models to explain the wavelength-dependent fractionation.

Frequently, the process is treated as a two-electronic state process in which the lower electronic state is excited to the upper state by absorption of radiation (*e.g.* (17)). However, for polyatomic molecules, N_2O being an example, there are usually a number of excited electronic states which are accessible even though the excitation to only one of them may be dominant in the wavelength region of interest. It has been convenient in such work to 'broaden' the calculated absorption spectrum as a way of simulating the optical absorption into the other nearby electronic states, as in the treatment of the photolysis N_2O in the work of (18). Analogously, in Chapter 6 such a broadening was included tacitly by using a scaling factor[a] for the potential energy curve of the excited electronic state (16).

In the present paper, we extend the work of Chapter 6 on N_2O by including the effect of the changes in the NN bond length in N_2O, investigating the absorption to an additional electronic state, and using an absorption expression (19) that preserves both the momentum and coordinate parts of Franck-Condon principle. The calculated cross section without any broadening factor gives good agreement with experiment in the energy region of interest for the fractionation measurements (apart from a small shift of the absorption maximum). The fractionation of the various isotopomers is then obtained from these calculated absorption cross sections. We use the results of the vibrational analysis in Chapter 6 to calculate the vibrational wave function in the ground state and then invoke the multi-dimensional reflection principle to calculate the absorption spectrum and the isotopic fractionation factors as a function of wavelength.

[a] The scale used is 1.57. This broadening happened inadvertently in (16) and was not reported therein.

II. Theory

A. Absorption cross section

The theoretical procedure used to obtain absorption cross sections for the N_2O isotopomers is similar to that described previously by (16), but with some additions described below. UV photolysis of N_2O is essentially a direct dissociation, since the shape of the absorption spectrum is a broad envelope with a only weak structure superimposed (see Fig. 7.2). Thereby, the time-dependent expression for the absorption cross section can be rewritten in a time-independent form using the reflection principle in conjunction with the Franck-Condon principle (17; 19). The absorption cross section σ is given as

$$\begin{aligned}
\sigma_{f\nu}(\omega) &= \frac{\pi\omega_i}{\hbar\epsilon_0 c}\frac{1}{2\pi}\int_{\infty}^{-\infty} \mathrm{d}t\langle\Psi_\nu|\vec{e}\cdot\vec{\mu}_{fi}^{\dagger}\mathrm{e}^{-iH_f t/\hbar}\vec{\mu}_{fi}\cdot\vec{e}|\Psi_\nu\rangle\mathrm{e}^{i(\omega-E_i/\hbar)t} \\
&\approx \frac{\pi\omega_i}{3\epsilon_0 c}\int \mathrm{d}\mathbf{Q}\,|\Psi_\nu(\mathbf{Q})|^2\,|\vec{\mu}_{fi}(\mathbf{R})|^2\,\delta\left(\hbar\omega - V_f(\mathbf{R}) + V_i(\mathbf{R})\right) \\
&\approx \frac{\pi\omega_i}{3\epsilon_0 c}\int \mathrm{d}q_1\ldots\mathrm{d}q_{N-1}\,|\Psi_\nu(\mathbf{Q})|^2\,|\vec{\mu}_{fi}(\mathbf{Q})|^2/\Delta S, \qquad (7.1)
\end{aligned}$$

$$\text{where}\quad \Delta S = \left(\partial[V_i(\mathbf{Q}) - V_f(\mathbf{Q})]/\partial q_N\right)_{q_N^\omega}. \qquad (7.2)$$

Here, $\mathbf{R}$ and $\mathbf{Q}$ denote internal and normal coordinates, respectively, as before (16), $\mathbf{R} = (q_1, q_2\cdots q_N)$, $\vec{e}$ is a unit vector, $\vec{\mu}_{fi}(\mathbf{R})$ is the transition dipole moment function for a transition between the ground and the excited electronic states i and f, respectively, $V_f(\mathbf{Q})$ and $V_i(\mathbf{Q})$ denote the potential energy surfaces of the electronic excited and ground states, respectively, and q_N is the repulsive coordinate in the excited state f, along which dissociation happens, while q_N^ω in Eq. (7.2) is the value of q_N where $\hbar\omega$ equals the vertical potential energy difference of the two electronic states:

$$\hbar\omega - V_f(q_1,\cdots,q_{N-1},q_N^\omega) + V_i(q_1,\cdots,q_{N-1},q_N^\omega) = 0, \qquad (7.3)$$

$|\Psi_\nu(\mathbf{Q})|^2$ in Eq. (7.1) is the probability density function of $\mathbf{Q}$ in the initial nuclear vibrational state ν and ground electronic state i. Using the harmonic approximation for the potential energy V_i as a function of the normal coordinates, the probability density function of the vibrational state ν in the ground electronic state can be written as a product of that of each of the normal vibration modes.

In the present calculation of the absorption cross section in Eq. (7.2), the actual potential of the electronic ground state $V_i(\mathbf{Q})$ at coordinate $\mathbf{Q}$ is used (19), instead of the average potential energy $\langle V_i \rangle$ (16; 20). This change corresponds to conserving the momenta in the Franck-Condon principle and enhances the calculated intensity of the absorption cross section on the long wavelength side of absorption maximum. The result obtained with Eq. (7.1) is shown and discussed later in Section IIIA, now without any significant adjustable parameter. [b]

The total absorption cross section is temperature-dependent, due to the dependence of $\sigma_{f\nu}$ on the initial vibrational state ν and thermal excitation of each vibrational state. The total absorption cross section at temperature T is given by

$$\sigma_{total}(T) = \sum_{f,\nu} \sigma_{f\nu} \exp\left(\frac{-E_\nu}{k_B T}\right) / Q_{vib}(T), \tag{7.4}$$

where $Q_{vib}(T)$ is the partition function of the vibrations in the ground electronic state, and E_ν is the vibrational energy of the vibrational state ν. The present calculation for the total absorption cross section of N_2O includes excitation from the ground electronic state to two excited states, 2A" (1Δ) and 1A' ($1\Sigma^-$), and all vibrational states that are significantly populated with energy not more than 1500 cm^{-1} above the zero-point energy. It involves the ground state, the first excited state of NO stretching, and the first and second excited states of the N_2O bending. Since the N_2O is linear in the electronic ground state, this bending vibration is doubly degenerate, as discussed in Ref. (16).

[b] The slope of the excited electronic potential in (16) is enlarged by the broadening scale, which also enhances the intensity of the cross section on the long wavelength side of absorption maximum.

B. Potential energy

The best currently available potential energy and transition dipole moment surfaces appear to be those of (18). However, these surfaces are given in terms of mass-dependent Jacobi coordinates with a fixed NN distance. The present treatment of the potential energy surfaces includes varying the NN distance by expanding it to second-order in terms of a displacement of the equilibrium NN-distance of both electronic ground and excited states. The details of the potential difference used in Eq. (7.2) are given in Appendix A..

C. Fractionation

The expression for the photodissociation rate at energy $\hbar\omega$ in Eq. (7.1) depends upon three factors: the total absorption cross section $\sigma_{total}(\omega)$ in Eq. (7.4), the photon flux, and the quantum yield of the photodissociation. The fractionation $\epsilon(\omega)$ of one isotopomer relative to another due to a direct photodissociation reaction can be defined as the ratio of photodissociation rates. When the upper state is dissociative, the quantum yield equals unity for all the isotopomers. The fractionation then is expressed in terms of the ratio of total absorption cross sections,

$$\epsilon(\omega) = \left[\frac{\sigma'_{total}(\omega)}{\sigma_{total}(\omega)} - 1\right] \times 1000 \,\text{permil} \tag{7.5}$$

III. Results and discussion

A. Absorption Cross Section

In the present treatment the potential difference between the ground and excited states in Eq. (7.2) includes all vibrational modes of N_2O in the calculation. A harmonic approximation is used in the NN-stretching mode, which was fixed in the best currently available potential (18). The N_2 vibration is expected as a spectator and its effect on fractionation is mainly via zero-point energies. Although the stretching mode is expected to cause only a

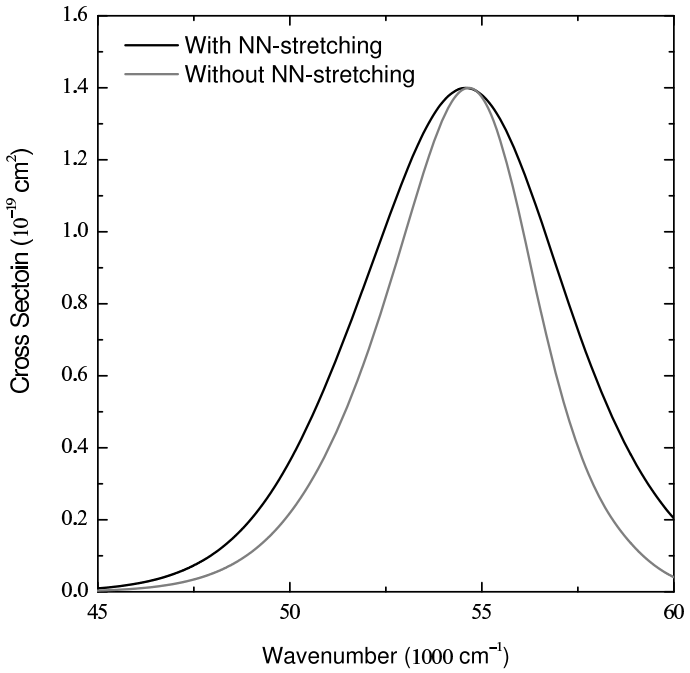

Figure 7.1: The calculated absorption cross section with (black) and without (gray) the NN-stretching mode at 298 K.

small change in the transition dipole moment of the N_2O molecule and to slightly perturb the dissociation reaction in the excited state, it gives a significant broadening effect in the absorption cross section, as shown in Fig. 7.1, since the mode is able to store or release vibrational energy from and to other modes.

The most important spectral region where isotopic fractionation studies of N_2O have been reported is the long wavelength side of the absorption maximum (180 nm to 220 nm). The calculated absorption cross section of 446 is compared with experiments (11; 21) in Fig. 7.2, where the result calculated by our previous formula (16), but without their broadening factor, is also shown. The calculated properties needed to obtain the absorption cross section are provided in Appendix C.. In the comparison with the experimental spectrum, the calculated peak is red shifted by 1100 cm^{-1} and rescaled by a factor of 0.69. The need for the shift arises from a possible small error in the difference between the energy of ground and excited electronic states from the *ab initio* calculations. Such differences are

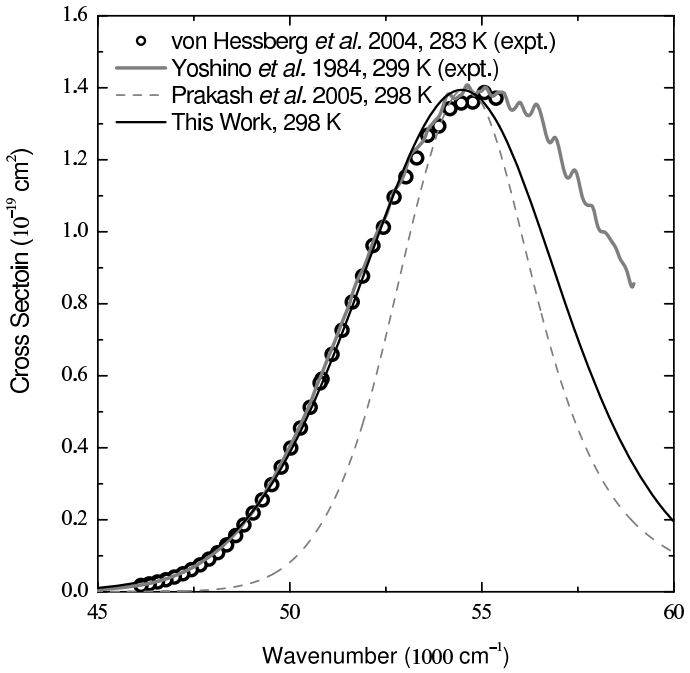

Figure 7.2: Absorption cross section of $^{14}N^{14}N^{16}O$. The black line is the current calculation result. The gray dashed line is the calculation result obtained by our previous formula (16), but without using any broadening factor. Both calculation results are rescaled and shifted to overlap their maximum absorption cross section at $\sim$55000 cm^{-1}

indeed expected. A rescaling in height is also expected since the *ab initio* calculation of the transition dipole moment $\vec{\mu}_{fi}$ is expected to have some error. However, the rescaled factor at the absorption maximum has no effect on the isotopic fractionations since the factor cancels in Eq. (7.5). The total absorption cross sections for other isotopomers are calculated similarly with the same shift in the peak position as that for 446, since the energy difference between potential energy surfaces is independent of isotopic substitution. The red shifted value at the absorption maximum also has a minor red-shifted effect on the isotope fractionations.

The agreement of calculated and measured absorption cross sections in Fig.7.2 is seen to be good on the long wavelength side of absorption maximum, the region of most interest. In the short wavelength side of the absorption spectrum the experimental result has a larger cross section than calculated. A difference is probably due to the presence of higher electronic

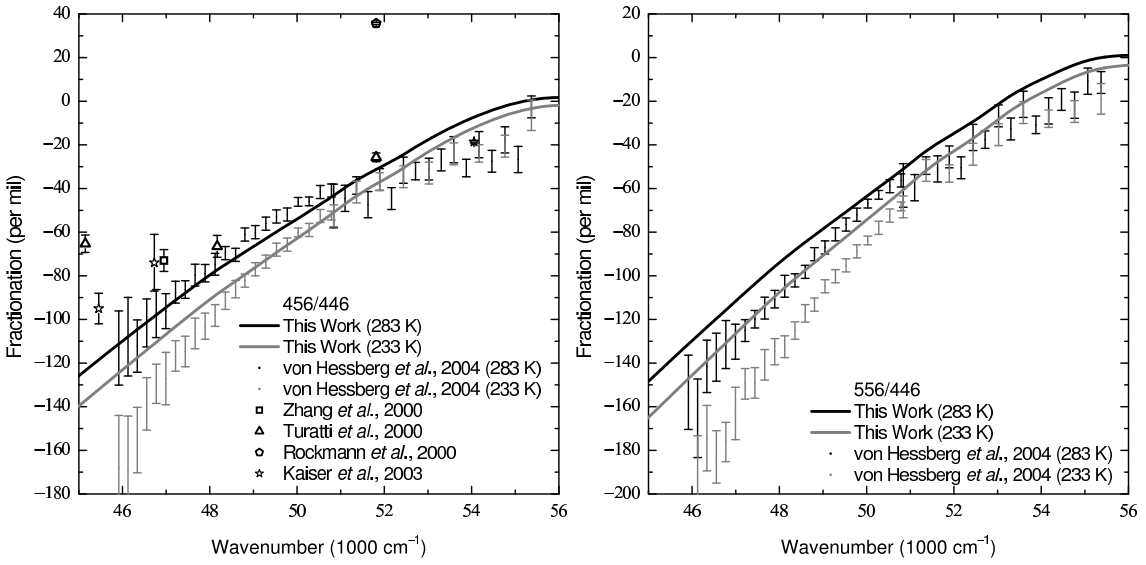

Figure 7.3: Fractionation of 456 and 556 calculated at 233 and 283 K.

excited-states than 2A" and 1A' of N_2O, and perhaps due to the long tail in the cross section that involves the vibrationally excited NN stretching mode in the excited N_2O. Although that mechanism may broaden the absorption cross section at higher energy, it has little effect for the fractionation at the energies of conventional interests since there is less than 2% of products with the vibrationally excited N_2, (22), and (23) both at ∼200 nm, where the fractionations are of interest.

B. Wavelength-dependent fractionation

The calculated wavelength-dependent fractionation of isotopomers 456, 556, and 546 relative to the most abundant isotopomer 446 are shown in Figs. 7.3 and 7.4. The calculated values of 456 and 556 agree well with experimental data (6-11). The values of 546 are not so good. Although the calculated fractionation 546 in Fig. 7.4 is higher than the experimental result obtained by (11) at the long wavelength region, our result is still comparable with other data (6-8,10). Comparison with other *ab initio* values was given in Chapter 6. Since the present calculations neglect the weak structure of the absorption cross section, the calculated fractionation is an averaged curve for comparison with the mean of the experiments.

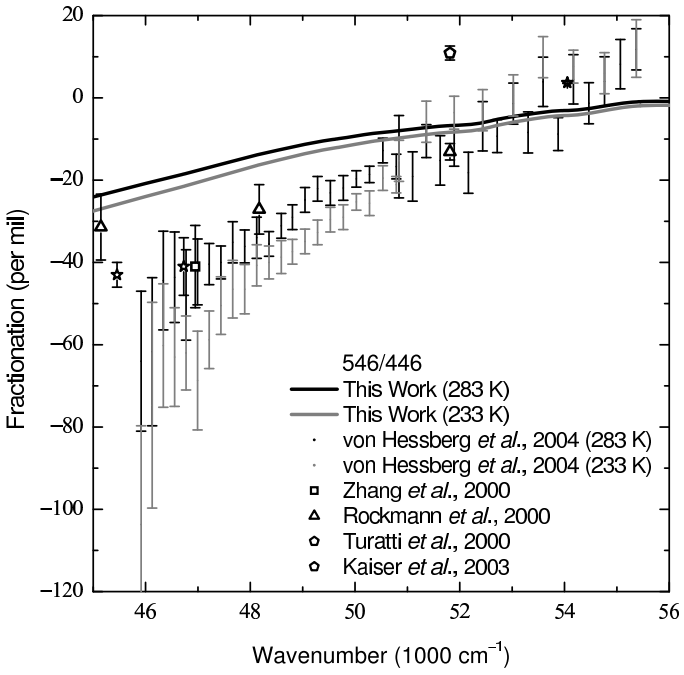

Figure 7.4: Fractionation of 546 calculated at 233 and 283 K.

Compared with the previous paper (16), the current results give a better agreement with experiments and now no *ad hoc* broadening factor is used. This improvement in the results of Chapter 6 is expected since the current treatment includes the effect of the NN stretching and also has a physically more understandable expression, Eq. (7.1-b), for the fractionation.

The calculated fractionations 447 and 448 relative to 446 at 283 K is given in Fig. 7.5. The agreement is very good (7-10). Compared with fractionation of isotopomers, the sensitivity of the calculated fractionation to changes in the wavelength is $556 > 456 > 448 > 447 \sim 546$. This trend is similar to the difference of the vibrational frequency of the bending mode between 446 and the respective isotopomes since the electronic excitation from the ground state to the excited state is forbidden for a linear N_2O. This transition is allowed only when the molecule is bent. In the experiments (6-11) the order is $556 > 456 > 448 \sim 546 > 447$.

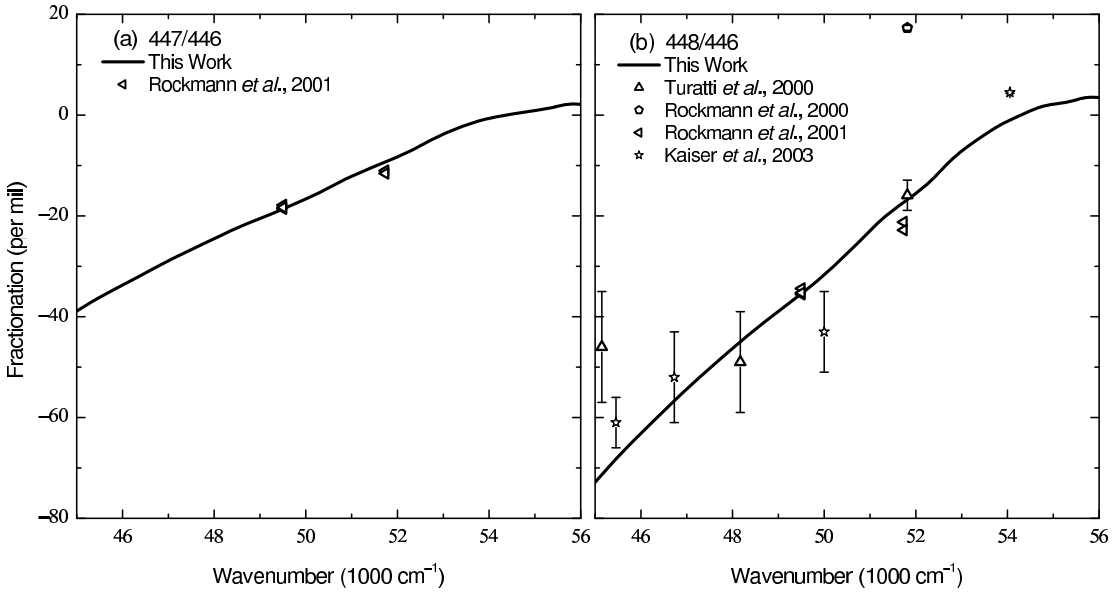

Figure 7.5: Fractionation of 447 (a) and 448 (b). The calculated values are at 283 K.

C. Excited electronic states

There are two potential energy surfaces (2A' and 1A") included in these calculations. The 1A" state has a minor contribution in the calculation of absorption cross section since the peak intensity of the 1A" state is smaller than that of the 2A' state by a factor of ∼100. This difference in intensity is similar to that found in the time-dependent calculation by (18). It also has very minor contribution (<2 per mil) to the fractionation in all isotopomers. Since the effect of the 1A" state is very small, we do not show the results in figures.

IV. Conclusions

The absorption cross section of 446 calculated using a computationally simple time-independent treatment with small adjustments for the position of the peak and its amplitude is in reasonable agreement with the broad envelope of the cross section in experiments. The required computations are similar to that in our previous treatment (16) there are several improvements in the calculations leading to these results, including the effect of NN stretching and

avoiding the need for a broadening parameter. There is a reasonable agreement in the wavelength-dependent fractionations of the isotopomers. The 2A" excited state dominates both the absorption cross section and fractionation in the N_2O photodissociation.

V. Appendix A:

A. Potential energy difference

The potential difference in Eq. (7.2) is expanded as

$$\begin{aligned} V_f(\mathbf{R}) - V_i(\mathbf{R}) &\approx V_f(\mathbf{\Gamma}) + \frac{1}{2}k_{N_2}\left[(r_{NN} - r_\Delta)^2 - r_\Delta^2\right] \\ &\quad -V_i(\mathbf{\Gamma}) - \frac{1}{2}k_{NN,NN}r_{NN}^2 - \frac{1}{2}k_{NO,NO}r_{NO}^2 - k_{NN,NO}r_{NN}r_{NO}, \end{aligned} \tag{7.6}$$

where r_{NN} and r_{NO} are the displacement of the NN and NO distances, respectively, from the equilibrium at the electronic ground state, and r_Δ is the difference in the equilibrium NN distance between N_2 and N_2O. The force constant corresponding to the cross terms of r_{NN} and r_{NO} in the excited state is neglected. In Eq. (7.6), $\mathbf{\Gamma}$ has the same meaning as $\mathbf{R}$, but with $r_{NN} = 0$; The integration in Eq (7.1) is more easily performed in normal coordinates. The relation between internal and normal coordinates satisfies $\mathbf{R}$=$\mathcal{L}\mathbf{Q}$, where $\mathcal{L}$ is a matrix composed of eigenvectors of the $\mathcal{GF}$ matrix (24). The $\mathcal{G}$- and $\mathcal{F}$-matrices of N_2O are given in Appendix B.. The potential difference is rewritten as

$$\begin{aligned} &V_f(\mathbf{R}) - V_i(\mathbf{R}) = V_f(\mathbf{Q}) - V_i(\mathbf{Q}) \\ &\approx V_f(0, L_{2,i}q_i, L_{3,3}q_3) + \frac{1}{2}k_{N_2}\left[(L_{1,i}q_i - r_\Delta)^2 - r_\Delta^2\right] \\ &\quad -V_i(0, L_{2,i}q_i, L_{3,3}q_3) - \frac{1}{2}\omega_1^2\left[q_1^2 - (L_{1,2}^{-1}L_{2,i}q_i)^2\right] - \frac{1}{2}\omega_2^2\left[q_2^2 - (L_{2,2}^{-1}L_{2,i}q_i)^2\right], \end{aligned} \tag{7.7}$$

where $\sum_{i=1}^{2} L_{j,i}q_i$ are abbreviated as $L_{j,i}q_i$, and $L_{i,j}$ and $L_{i,j}^{-1}$ are the (ith, jth) elements of the matrices $\mathcal{L}$ and $\mathcal{L}^{-1}$, respectively.

B. The $\mathcal{G}$- and $\mathcal{F}$-matrices

The $\mathcal{G}$- and $\mathcal{F}$-matrices of N^1N^2O are defined as

$$\mathcal{G} = \begin{pmatrix} \frac{1}{m_{N^1}} + \frac{1}{m_{N^2}} & \frac{-1}{m_{N^2}} & 0 \\ \frac{-1}{m_{N^2}} & \frac{1}{m_{N^2}} + \frac{1}{m_O} & 0 \\ 0 & 0 & \frac{1}{m_{N^1}(r_{NN}^{eq})^2} + \frac{1}{m_{N^2}}\left(\frac{1}{r_{NN}^{eq}} + \frac{1}{r_{NO}^{eq}}\right)^2 + \frac{1}{m_O(r_{NO}^{eq})^2} \end{pmatrix} \quad (7.8)$$

$$\mathcal{F} = \begin{pmatrix} k_{NN,NN} & k_{NN,NO} & 0 \\ k_{NN,NO} & k_{NO,NO} & 0 \\ 0 & 0 & k_{\theta,\theta} \end{pmatrix}. \quad (7.9)$$

The mass of each isotope is available from (25). The equilibrium NN and NO distances for N_2O are 1.1273 and 1.1851 Å, respectively (18). The force constants of the $\mathcal{F}$-matrix are given in Appendix C.. The $\mathcal{L}$-matrix is obtained by solving the eigenvectors of the $\mathcal{GF}$-matrix.

C. Properties of isotopomers

This appendix provides the parameters used for obtaining the absorption cross section of various isotopomers. The mass of each isotope is available from (25). The equilibrium bond length for N_2 is 1.09768 Å.[c] The force constant in the ground state k_{N_2} is 22.948 aJ/Å^2. The force constants for N_2O are: $k_{NN,NN}$=17.655 aJ/Å^2; $k_{NO,NO}$=11.559 aJ/Å^2; $k_{NN,NO}$=1.260 aJ/Å^2; and $k_{\theta,\theta}$ 0.649 aJ/rad^2 (26). The force constants are calculated by fitting the experimental vibrational frequencies of various N_2O isotopomers. The difference between calculated and experimental frequencies, as shown in Table 7.1, are smaller than $\pm$3.7 cm^{-1} in the two stretching modes and $\pm$0.3 cm^{-1} in the bending mode. The force constants used in the present work are slightly different from the experimental values obtained by (27), used in our previous work (16).

[c] http://webbook.nist.gov/cgi/cbook.cgi?Formula=n2&NoIon=on&Units=SI&cDI=on

Table 7.1: The calculated and experimental normal-mode frequencies of various isotopomers in cm^{-1}.

	$\bar{\nu}_1$	$\bar{\nu}_1^{expt.,27}$	$\bar{\nu}_2$	$\bar{\nu}_2^{expt.,28,29}$	$\bar{\nu}_3$	$\bar{\nu}_3^{expt.,30}$
446	2224.424	2223.757	1286.003	1284.903	588.729	588.768
447	2221.012	2220.074	1263.532	1264.704	586.264	586.362
448	2218.085	2216.711	1243.136	1246.885	584.074	584.225
456	2176.677	2177.657	1284.090	1280.354	575.272	575.434
546	2201.880	2201.605	1269.392	1269.892	585.225	585.312
556	2153.347	2154.726	1267.940	1265.334	571.685	571.894

Bibliography

[1] R. P. Wayne, *Chemistry of Atmospheres, 3rd ed.,* Oxford University Press, New York (2000)

[2] C. M. Stevens, D. Walling, A. Venters, L. E. Ross, A. Engelkem, and L. Krout, *Earth Planet. Sci. Lett., 16*, 147 (1972)

[3] C. A. M. Brenninkmeijer, C. Janssen, J. Kaiser, T. Rockmann, T. S. Rhee, and S. S. Assonov, *Chem. Rev., 103*, 5125 (2003)

[4] K. R. Kim, and H. Craig, *Nature, 347*, 58 (1990)

[5] S. W. A. Naqvi, T. Yoshinari, D. A. Jayakumar, M. A. Altabet, P. V. Narvekar, A. H. Devol, J. A. Brandes and L. A. Codispoti, *Nature, 394*, 462 (1998)

[6] H. Zhang, P. O. Wennberg, V. H. Wu, and G. A. Blake, *Geophys. Res. Lett., 27*, 2481 (2000)

[7] F. Turatti, D. W. T. Griffith, S. R. Wilson, M. B. Esler, T. Rahn, H. Zhang and G. A. Blake, *Geophys. Res. Lett., 27*, 2489 (2000)

[8] T. Rockmann, C. A. M. Brenninkmeijer, M. Wollenhaupt, J. N. Crowley, and P. J. Crutzen, *Geophys. Res. Lett., 27,* 1399 (2000)

[9] T. Rockmann, J. Kaiser, J. N. Crowley, C. A. M. Brenninkmeijer, and P. J. Crutzen, *Geophys. Res. Lett., 28,* 503 (2001a)

[10] J. Kaiser, T. Rockmann, C. A. M. Brenninkmeijer, and P. J. Crutzen, *Atmos. Chem. Phys., 3*, 303 (2003)

[11] P. von Hessberg, J. Kaiser, M. B. Enghoff, C. A. McLinden, S. I. Sorensen, T. Rockmann, and M. S. Johnson, *Atmos. Chem. and Phys., 4*, 1237 (2004)

[12] G. A. Blake, M. C. Liang, C. G. Morgan, and Y. L. Yung, *Geophys. Res. Lett., 30*, 1656 (2003)

[13] M. C. Liang, G. A. Blake, and Y. L. Yung, *J. Geophys. Res., 109*, D10308 (2004)

[14] M. S. Johnson, G. D. Billing, A. Gruodis, and M. H. M. Janssen, *J. Phys. Chem. A, 105*, 8672 (2001)

[15] S. Nanbu, and M. S. Johnson, *J. Phys. Chem. A, 108*, 8905 (2004)

[16] M. K. Prakash, J. D. Weibel, and R. A. Marcus, *J. Geophys. Res. - Atmos., 110*, 315 (2005)

[17] R. Schinke, *Photodissociation dynamics*, Cambridge Univ. Press, New York (1993).

[18] M. N. Daud, G. G. Balint-Kurti and A. Brown, *J. Chem. Phys., 122,* Art. No. 054305 (2005) [ftp://ftp.aip.org/epaps/journ_chem_phys/E-JCPSA6-122-303502/]

[19] E. J. Heller, *J. Chem. Phys. 68*, 2066 (1978)

[20] S. -Y. Lee, R. C. Brown, and E. J. Heller, *J. Chem. Phys., 87*, 2045 (1983)

[21] K. Yoshino, D. E. Freeman and W. H. Parkinson, *Planet. Space Sci., 32*, 1219 (1984)

[22] T. F. Hanisco, and A. C. Kummel, *J. Phys. Chem., 97*, 7242 (1993)

[23] D. W. Neyer, A. J. R. Heck, and D. W. Chandler, *J. Chem. Phys., 110*, 3411 (1999)

[24] E. B. Wilson, J. C. Decius, and P. C. Cross, *Molecular Vibrations: The Theory of infrared and Raman Vibrational Spectra*, McGraw-Hill, New York (1955)

[25] Lide, D. R. (Ed.), *CRC Handbook of Chemistry and Physics, 84th ed.*, CRC Press, Boca Raton, FL (2004)

[26] A. G. Csaszar, *J. Phys. Chem., 98*, 8823 (1994)

[27] J. L. Teffo, and A. Chedlin, *J. Mol. Spectrosc., 135*, 389 (1989)

[28] R. A. Toth, *J. Opt. Soc. Am. B., 3*, 1263 (1986)

[29] C. Amiot, *J. Mol. Spectrosc., 59*, 380 (1976)

[30] K. Jolma, J. Kauppinen, and V. -M. Horneman, *J. Mol. Spectrosc., 101*, 278 (1983)

[31] R. A. Toth, *J. Opt. Soc. Am. B., 4*, 357 (1987)

Chapter 8

Three-isotope plot of fractionation in photolysis: a perturbation theoretical expression

The slope of the three-isotope plot for the isotopomer fractionation by direct or nearly-direct photodissociation is obtained using a perturbation theoretical analysis. This result, correct to first order in the mass difference, is the same as that for equilibrium chemical exchange reactions, a similarity unexpected a priori. *Comparison is made with computational results for N_2O photodissociation. This theoretical slope for mass-dependent photolytic fractionation can be used to analyze the data for isotopic anomalies in spin-allowed photodissociation reactions. Earlier work on chemical equilibria is extended by avoiding a high-temperature approximation.*

I. Introduction

Isotopomer fractionation for chemical equilibrium systems is described in the classic papers by Bigeleisen and Mayer (1) and Urey (2). When the isotopic effect for the chemical systems in equilibrium or otherwise follows the conventionally described effect, it is termed as mass-dependent. The slope of 3-isotope plots (defined below) for the mass-dependent oxygen isotopic fractionation in various thermal processes is about 0.52 (3). Slopes substantially different from the mass-dependent value are usually referred to in the literature

as anomalous mass dependent or mass-independent. In some rare and interesting cases a striking mass-independence with a slope of unity (4; 5) has been found.

Mass-dependent fractionation of isotopomers occurs in various geochemical processes (6). The deviations from such mass-dependent behavior are one source of information on geochemical processes (5; 7). Three ways of presenting the isotopic fractionation information are: (1) give the fractionation ${}^{Q}\delta$, the relative rate of reaction of one isotopomer Q relative to another, (2) construct a three-isotope plot by plotting the δ value of one isotopomer against another, each δ value being relative to the same reference isotopomer or (3) give the enrichment ${}^{Q}\Delta$, which represents the difference of the measured fractionation ${}^{Q}\delta$ of an isotope Q from the expected mass-dependent value calculated from the normal isotope. Unless the fractionation is large, the three-isotope plot shows a linear relation between the fractionation of the two isotopomers relative to the third. The slope of this line depends upon the isotopic masses, and can depend on the fractionation of the geochemical process which induces the observed enrichment. The ${}^{Q}\delta$'s and ${}^{Q}\Delta$'s are widely used in atmospheric chemistry.

Deviations of ${}^{Q}\Delta$ from zero are considered as anomalies (7), and to identify anomalies a mass-dependent value appropriate to the process should be used. We note that kinetic processes can have a mass dependent value different from that for chemical equilibria (8). For example, in collisions with a surface the dependence on mass varies as $1/\sqrt{m}$, where m is the mass of the colliding particle, while in Bigeleisen-Mayer-Urey expression, which contains vibrational partition functions, it varies as $1/m$.

Isotopomer fractionation also occurs in photodissociation reactions, a process important to atmospheric chemistry. The observed enrichment is explained in terms of the enrichments and magnitudes of the various sources of a given gas and the fractionations and magnitudes of the various loss mechanisms. In this way the enrichments in atmospheric samples can be used to study and quantify specific generating processes.

Using the theory of nearly-direct photodissociation discussed in chapters 6 and 7 and also described later in the present chapter, we computed the fractionation factor, as defined in Section II.A., of oxygen isotopes in the photolysis of N_2O at different wavelengths (9). In the present chapter we present these wavelength-dependent fractionation factors as a three-isotope plot. To our surprise the slope of the plot was the same as the mass-dependent value predicted by Bigeleisen-Mayer theory for a purely chemical equilibrium system. This similarity is quite unexpected *a priori* since the two processes are different and the functional dependence of the fractionation factors on the mass can be different for kinetic and chemical equilibrium processes. The present perturbation theoretical work on an expression for the slope of a three-isotope plot for photodissociation was undertaken to both understand this computational result and for applications in atmospheric and laboratory systems.

II. Analysis

A. Photodissociation theory

In the absorption of light in the UV or visible region, leading to electronic transitions in molecules, a transition frequently occurs to a repulsive electronic state of the molecule and a direct photodissociation results. The detailed theory for the calculation of photodissociation cross-sections is available (10; 11) The molecule undergoes a direct dissociation when the lifetime of the molecule in the excited electronic state is less than or comparable to a vibrational period of the molecule, and an indirect dissociation when it is much longer. Long lifetimes in the excited state lead to the well known prominent structure in the absorption cross-section (10) and hence the presence of a more diffuse structure can be considered as a nearly direct-dissociation problem. (12)

The absorption cross-sections for direct and nearly-direct photodissociations can be obtained by a simple analysis using the multidimensional reflection principle(11; 13). We use a form of the reflection principle (10) for the absorption cross-section σ at a frequency ω which is

more accurate than an earlier(11; 13) version of the principle. There are several expressions in the literature (10; 13) and one of the expressions we found (9) to represent the absorption cross-section σ data best for a spin-allowed transition is given by (10):

$$\sigma_{i\nu}(\omega) = \frac{\pi\omega}{3\hbar\epsilon_0 c} \int |\Psi_\nu(\mathbf{Q})|^2 \ |\mu_{fi}(\mathbf{R})|^2 \ \delta\left(\omega - (V_f(\mathbf{R}) - \frac{1}{2}E_{i\nu})/\hbar\right) \ d\mathbf{Q} \tag{8.1}$$

where $\mathbf{R}$ denotes internal coordinates and $\mathbf{Q}$ the normal coordinates. $\mu_{fi}(\mathbf{R})$ is the transition dipole moment function for a transition between the ground and the excited electronic states i and f respectively, $V_f(\mathbf{R})$ the potential energy surface of the excited electronic state, and $E_{i\nu}$ the energy of the initial nuclear vibrational state, ν. $|\Psi_\nu(\mathbf{Q})|^2 \, d\mathbf{Q}$ is the probability density of the initial nuclear vibrational state ν in the ground electronic state i. For the latter we use as a zeroth order approximation the harmonic oscillator wavefunctions corresponding to the normal coordinates $\mathbf{Q}$.

The difference in the absorption cross-sections of various isotopomers leads to a fractionation of the isotopomers during photodissociation. The rate of photodissociation for each isotopomer is given as $J(\omega) = \sigma_{total}(\omega)I(\omega)\phi(\omega)$, where $I(\omega)$ is the intensity of the incident light at frequency ω. $I(\omega)$ is independent of the molecule; $\phi(\omega)$ is the quantum yield of the reaction at that ω and is usually unity for direct or nearly-direct photodissociation and σ_{total} is the total absorption cross-section obtained by adding the contributions from all vibrational states in the ground electronic state, weighted by their thermal populations. The fractionation factor is dependent upon the ratio of the rates of photodissociation of two isotopomers, say A and A' as:

$$\epsilon^{(A',A)} = \frac{J^{(A')}(\omega)}{J^{(A)}(\omega)} - 1 = \frac{\sigma^{(A')}(\omega)}{\sigma^{(A')}(\omega)} - 1 \tag{8.2}$$

As expected from Eq. (8.1) the fractionation factor arises mainly from isotopic differences in the wings of the wavefunction, and so is least at the absorption maximum. Indeed, using N_2O as an example, Yung and Miller (14) found zero fractionation near the absorption

maximum of 185 nm.

B. Slope of the three-isotope plot

In the present note we derive a perturbation theoretical expression for the slope of the three-isotope plot of $\epsilon^{(A'',A)}(\omega)$ vs. $\epsilon^{(A',A)}(\omega)$, for three isotopomers A, A' and A''. Our derivation of the perturbation theoretical expression is as follows: in evaluating the integral in Eq. (8.1), the $\mathbf{Q}$'s are transformed into mass-independent internal coordinates $\mathbf{R}$, because the fact that $V_i(\mathbf{R})$, $V_f(\mathbf{R})$ and $\mu_{fi}(\mathbf{R})$ are independent of isotopic substitutions simplifies the analysis. The mass effects occur in the vibrational frequencies, the normal coordinates $\mathbf{Q}$ in the ground electronic state vibrational wavefunctions and in the energies $E_{i\nu}$. The method used to relate $\mathbf{Q}$ in the $|\Psi(\mathbf{Q})|^2 d\mathbf{Q}$ to internal coordinates $\mathbf{R}$ depends functionally on the G matrix (9; 15) and the latter depends on masses in the functional form of reciprocal masses, $1/m_i$. Similarly the vibrational frequency and hence the energy $E_{i\nu}$ depend in a rather complicated way on G and hence on $1/m_i$'s. In summary, the expression for the absorption cross-section is a function of reciprocal masses $1/m_i$, i.e., $\sigma_{total} = \sigma_{total}(\omega, 1/m_1, 1/m_2, ..)$. To find the first-order isotopic perturbation in σ_{total}, a Taylor series expansion of σ_{total} is used to the first-order. The perturbation treatment for the entire expression of the cross-section when the mass m_i is isotopically substituted involves a differentiation of the expression for the cross-section with respect to $1/m_i$ and multiplied by the first-order difference $\Delta(1/m_i) = 1/m_i^{(A')} - 1/m_i^{(A)}$ in the two isotopes, i.e.,,

$$1 + \epsilon^{(A',A)}(\omega) = \sigma^{(A')}/\sigma^{(A)} \approx \left(1 + \sum_i \frac{\partial \sigma^{(A)}}{\partial(1/m_i)} \Delta(1/m_i)\right) \tag{8.3}$$

where the subscript *total* is omitted and where the sum is over all the masses that are isotopically substituted. The factor $\partial\sigma^{(A)}/\partial(1/m_i)$ that is common to both the abscissa and the ordinate has no effect on the slope of the three-isotope plot. Thus, the slope β of

the $\epsilon^{(A'',A)}(\omega)$ vs. $\epsilon^{(A',A)}(\omega)$ plot based on the above perturbation method is obtained as:

$$\beta = (1/m_i^{(A'')} - 1/m_i^{(A)})/(1/m_i^{(A')} - 1/m_i^{(A)}) \tag{8.4a}$$

and

$$\epsilon^{(A'',A)} = \beta\ \epsilon^{(A',A)} \tag{8.4b}$$

Thus, in this perturbation treatment of the three-isotope plot, it is the form ($1/m$ in the above case) in which the masses appear in the function, rather than the function itself that is important.

Like the isotopic fractionation in chemical equilibrium the present isotopic fractionation in the photolysis is a quantum effect: if the probability distribution in the coordinates $|\Psi_\nu(\mathbf{R})|^2$ were replaced by a thermally equilibrated classical Boltzmann probability distribution that is proportional to $exp(-V_i(\mathbf{R})/k_BT)$, the result for σ_{total} in the reflection principle approximation would be:

$$\sigma_{total}(\omega) \;=\; \frac{\pi\omega^2}{3\epsilon_0 c k_B T}\ \frac{\int e^{-V_i(\mathbf{R})/k_BT}\ |\mu_{fi}(\mathbf{R})|^2\ \delta(\omega - \omega_{fi}(\mathbf{R})\ d\mathbf{R}}{\int e^{-V_i(\mathbf{R})/k_BT}\ d\mathbf{R}} \tag{8.5}$$

where $\omega_{fi}(\mathbf{R}) = (V_f(\mathbf{R}) - V_i(\mathbf{R}))/\hbar$, $V_i(\mathbf{R})$ is the potential energy function in the ground electronic state whose averaged value $\frac{1}{2}E_{i\nu}$ appears in the quantum case as given in Eq. (1) of Ref. (10). For a comparison with this classical equation, the quantum mechanical one in Eq. (1) should have an extra factor of $(1 - e^{-\hbar\omega/k_BT})$ to include emission in the net absorption (16). In the classical limit, $\hbar \to 0$, the coefficient with this added factor reduces to that in Eq. (8.5) (17). $V_i(\mathbf{R})$, $V_f(\mathbf{R})$ is dependent upon the electronic nature of the molecule alone and is unaffected by isotopic substitution, as is the σ_{total} with the classical distribution. In the classical Franck-Condon approximation, since the momenta cancel in the expression for the absorption, the thermal distribution of the momenta at a

given temperature does not affect the absorption.

C. Three-isotope plot for high conversions

When the photodissociation reaction proceeds to a high conversion to products, the result in Eq. (8.4a) can still be applied to obtain the relative amounts of different isotopomers remaining undissociated after time t: Treating photodissociation as a first-order rate process, the concentration $Q^A(t)$ of isotopomer A remaining at time t decays because of the photodissociation at ω as $Q^A(t) = Q^A(0)\ exp\big(-J^A(\omega)t\big)$. The relative amount of isotopomer A' remaining at time t can be described by a function $\delta^{A',A}(\omega)$ defined by $1 + \delta^{A',A}(\omega) = \Big((Q^{A'}(t)/Q^{A'}(0))/(Q^A(t)/Q^A(0))\Big) = exp\Big(-(J^{A'} - J^A)t\Big)$. Thereby, $ln(1+\delta^{A',A}(\omega)) = -(J^{A'} - J^A)t$. The relative amount of isotopomer A' surviving, considering the dissociation for the given range of frequencies ω of the light source, can be obtained by weighting the contribution from each ω by $I(\omega)\sigma^{(A)}(\omega)$:

$$\langle ln(1+\delta^{A',A})\rangle = \frac{\int I(\omega)\ \sigma^{(A)}(\omega)\ ln(1+\delta^{A',A}(\omega))\ d\omega}{\int I(\omega)\ \sigma^{(A)}(\omega) d\omega} = -\frac{\int I(\omega)\ \sigma^{(A)}(\omega)\ (J^{A''} - J^A)\ t\ d\omega}{\int I(\omega)\ \sigma^{(A)}(\omega) d\omega} \tag{8.6}$$

A photodissociation reaction with broadband absorption and high conversions thus yields a ratio of the relative amounts of isotopomers A', A'' remaining at time t as:

$$\begin{aligned} S &= \frac{\langle (Q^{A''}(t)/Q^{A''}(0))/(Q^A(t)/Q^A(0))\rangle}{\langle (Q^{A'}(t)/Q^{A'}(0))/(Q^A(t)/Q^A(0))\rangle} \\ &= \frac{\langle ln(1+\delta^{A'',A})\rangle}{\langle ln(1+\delta^{A',A})\rangle} = \frac{\int I(\omega)\ \sigma^{(A)}(\omega)\ (J^{A''} - J^A)\ t\ d\omega}{\int I(\omega)\ \sigma^{(A)}(\omega)\ (J^{A'} - J^A)\ t\ d\omega} = \frac{\int I(\omega)\ \sigma^{(A)}(\omega)\ \epsilon^{(A'',A)} d\omega}{\int I(\omega)\ \ \sigma^{(A)}(\omega)\ \epsilon^{(A',A)} d\omega} \end{aligned} \tag{8.7}$$

This S is the slope of a plot of $\langle ln(1+\delta^{A'',A})\rangle$ vs.$\langle ln(1+\delta^{A',A})\rangle$ where the points are taken from different conversions (different reaction times). The value of S from Eq. (8.7) is seen to be independent of t. Using Eq. (8.4b), $S = \beta$. That is, the slope of the plot based on different conversions of reactants is equal to the slope of the plot obtained using the values from different frequencies as the points on the plot.

D. General comments

A merit of three-isotope plots is that the slope obtained in the plot is dependent on the isotopic masses and the process that leads to the mass-dependent fractionation, without emphasizing many details of the process. For example, in the case of photodissociation the three-isotope plot only highlights the functional dependence of the absorption cross section σ on the reciprocal masses, $1/m_i$. Even though the potential energy and dipole moment surfaces are needed for the exact calculation of the absorption cross section, the three-isotope plot becomes independent of these quantities to a good approximation.

Sometimes, at negligible conversions, the rates of reaction of the three isotopomers are plotted as $ln(\sigma^{A''}/\sigma^{A})$ vs. $ln(\sigma^{A'}/\sigma^{A})$ for various frequencies (18). However, it should be noted that this logarithmic form obtained from different frequencies and used for small conversions is different from the logarithmic form obtained from different times and high conversions discussed in Section II. C. We have given arguments (Eq. (8.7)) showing that for small conversions the slope α of the linear plot, rather than the corresponding log-log plot, is equal to the slope S of the log-log plot at high conversions. The equality is not based on perturbation theory.

The analysis thus far is applicable when the photodissociation process is spin-allowed and the factors governing the rate of the photodissociation in different isotopomers are the mass-dependent frequencies and the normal coordinates. Photodissociation may also involve spin-forbidden processes, such as singlet-triplet transitions that become more allowed with a small probability due to, for example, a spin-orbit coupling perturbation in the Hamiltonian or an electron spin-nuclear spin coupling (hyperfine coupling). The rates of such reactions for isotopes of odd atomic masses with a non-zero nuclear spin and even atomic masses with a zero nuclear spin are different (19; 20). In such spin-forbidden photodissociation reactions, the isotopic fractionation depends on spin as well as mass. Thus, there can then be unusually high isotopic fractionations (19; 20). Also, in a three-isotope plot a slope

of opposite sign compared to that for the regular mass-dependent processes also becomes possible. The result in the present chapter is not applicable to such spin-forbidden cases. However, the fractionation of the two spin-zero isotopomers can be calculated using the present method.

E. Perturbation method applied to other processes

The final result for photodissociation, Eq. (8.4a), is the same as that found for equilibrium chemical exchange reactions to first-order. (1; 21) Bigeleisen and Mayer pointed out that in a chemical separation of isotopes, the fractionation is a quantum effect (1). The ratio of classical partition functions is unity, apart from any symmetry factors. Treating the rotational and translational partition functions classically and the vibrational partition function quantum mechanically, they obtained (22) a ratio of partition functions:

$$\frac{s}{s'}f = \Pi_i \, \frac{u_i}{u_i'} \, \frac{e^{-u_i/2}/(1-e^{-u_i})}{e^{-u_i'/2}/(1-e^{-u_i'})} = \frac{F(u_i)}{F(u_i')} \tag{8.8a}$$

$$\approx 1 + \sum_i \frac{\Delta(u_i^2)}{24} \tag{8.8b}$$

where s, s' are the symmetry numbers for the isotopomers, $F(u_i) = \Pi_i u_i e^{-u_i/2}/(1-e^{-u_i})$, $u_i = \hbar\omega_i/k_BT$ where ω_i is the frequency of the i^{th} vibrational mode, and u_i' is defined similarly for the other isotopomer. The approximation in Eq. (8.8b) is valid for small u_i or at high temperatures. Their analysis then uses the invariance of trace of the characteristic matrix to find the ratios of partition functions in terms of the isotopic masses. Alternatively, following exactly the method we have used in deriving Eq. (8.4a), we see from Eq. (8.8a) that the partition function depends upon the normal mode frequencies u_i and these u_i are the eigenvalues of the characteristic matrix which depends on masses in the form $1/m_i$, i.e., $u_i = u_i(1/m_1, 1/m_2, ..)$ and so $F(1/m_1, 1/m_2, .., 1/m_i, ..)/F(1/m_1, 1/m_2, .., 1/m_i', ..) \approx 1 + (\partial F/\partial(1/m_i))\,\Delta(1/m_i)$. Thus we recover the $1/m - 1/m'$ rule for the chemical equilibrium reaction fractionation. In deriving this result, we have avoided the high temperature approximation, used in Bigeleisen and Mayer. So, to first-order in $\Delta(1/m)$, our result is

independent of temperature.

When a different type of mass-dependent process is involved the functional dependence on m can differ, as noted earlier in the introduction. For example if the ratio of condensation rates of a molecule AB onto a surface were proportional to $1/\sqrt{m_{AB}}$, where m_{AB} is the mass of the molecule, then the slope of a three isotope fractionation plot would be $(1/\sqrt{m_{A'B}} - 1/\sqrt{m_{AB}})/(1/\sqrt{m_{A''B}} - 1/\sqrt{m_{AB}})$ to first order in mass differences. This value differs somewhat from the value given in Eq. (8.4a), because of the difference in the nature of isotopic mass-dependence of the rate process.

III. Numerical and analytical example: N_2O photolysis

Nitrous oxide (N_2O) is of considerable atmospheric interest since it is an efficient greenhouse gas, and we select it as an example. In the stratosphere, the photodissociation reaction $N_2O + \hbar\omega \rightarrow N_2(^1\Sigma^+) + O(^1D)$ is the most prominent mechanism for the removal of 446 (abbreviation for $^{14}N^{14}N^{16}O$) and its isotopomers 447, 448, 456 and 546. (23) The principal range of absorption 175nm-215nm corresponds to a singlet-singlet transition.

In Ref. 9 (Chapter 6) detailed computations for the wavelength-dependent absorption cross-sections of the isotopomers and hence the fractionation factors were presented using the multidimensional reflection principle and the *ab initio* potential energy surfaces and transition dipole moment function obtained from Ref. 24. To find $|\Psi_\nu(\mathbf{Q})|^2\, d\mathbf{Q}$ we first determined the normal mode coordinates and frequencies with the procedure (15) summarized in Appendices B and C of Ref. 9, using the inertia matrix G^{-1} and the force constant matrix F as defined in Ref. 15 and then finding the eigenvectors of the GF matrix. The element $G_{\theta\theta}$ corresponding to the inertia for the bending vibration, not defined in Ref. 15, was obtained from Ref. 25. We expressed the harmonic oscillator wavefunction in terms of the mass-dependent normal mode coordinates $\mathbf{Q}$ and vibrational frequencies and $\mathbf{Q}$ was then transformed to $\mathbf{R}$ with the appropriate transformation matrix that depends on isotopic

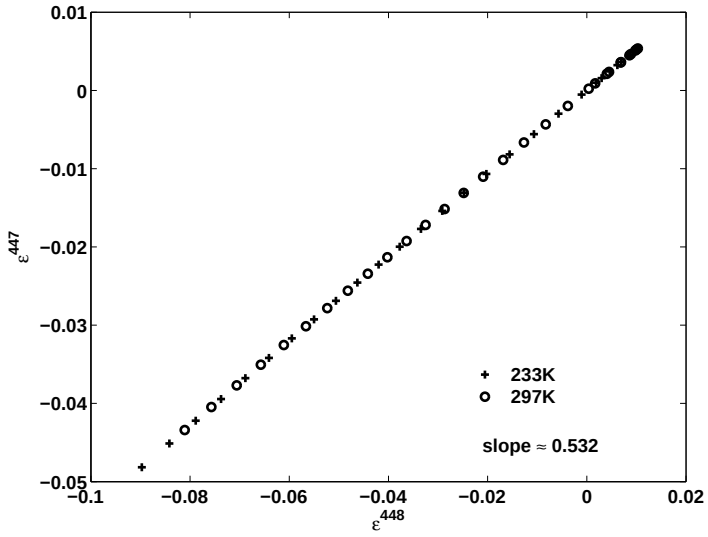

Figure 8.1: Three isotope plot of oxygen isotopes of N_2O

substitution (9; 15). The force constants obtained from Ref. 26 were used to form the force constant matrix F. Using the results from those detailed calculations the fractionation factors ϵ^{447} and ϵ^{448} were obtained as functions of wavelength. In the wavelength range over which calculations were made, these fractionation factors were found to be approximately in the ranges (-0.1, 0.01) and (-0.05, 0.005), respectively, with the zero of fractionation near the absorption maximum, 185 nm. In Ref. 9 calculations were also made for the other isotopomers of N_2O: 456, 546 and 556 and comparison with the extensive experimental data on fractionation was given. Oddly, experimental data on the 447 spectral absorption seems to have been not published, even though 447 is commonly used in atmospheric analysis.

The emphasis of the current work is on the relation between $\epsilon^{447}(\omega)$ and $\epsilon^{448}(\omega)$ plotted using results for the different frequencies. A plot of ϵ^{448} vs. ϵ^{447} is given in Fig. 8.1, each point obtained from Ref. 9 by evaluating both the fractionation factors 447 and 448 at the same wavelength, using the results from the different wavelengths. This linear plot gives a slope of approximately 0.532 with a zero intercept in the temperature range $233 - 300$ K. The slope for the fractionation by photolysis, is close to the perturbation

slope $(1/m_{O^{16}} - 1/m_{O^{17}})/(1/m_{O^{16}} - 1/m_{O^{18}}) = 0.529$ for the mass-dependent fractionation, obtained in the present perturbation analysis. They are not precisely the same, since one is 0.532 and the other is 0.529, because the terms of higher order in $\Delta(1/m)$ that are present in the computational result are absent in the perturbation treatment.

Using the computational results, we found that the slope of the linear plot $\epsilon^{448}(\omega)$ vs.$\epsilon^{447}(\omega)$ was 0.5325 at 233 K and 0.5338 at 297 K, while for $ln(\sigma^{448}(\omega)/\sigma^{446}(\omega))$ vs.$ln(\sigma^{447}(\omega)/\sigma^{446}(\omega))$ plot the slopes were 0.5248 and 0.5250, respectively, indicating that both plots are relatively unaffected by temperature, although the log-log plot is slightly less affected. The present results for $233 - 300$ K show that the slope is nearly the same over this temperature range. At even lower temperatures the contribution to absorption comes significantly from the ground vibrational state of the molecule alone and so the coefficients of the powers of $\Delta(1/m)$ will depend weakly on temperature. So we expect that the slopes do not change much at lower temperatures, even though one is far from the high temperature regime.

Because of the close comparison between mass-dependent values obtained using computed fractionation factors and the theoretical analysis with no computation, the importance of the perturbation theoretical result for the N_2O test case becomes apparent. The small variation of the absorption cross-section with the mass, as indicated by the fractionation factors less than 0.1, justifies the use of perturbation expansion in σ to the first order.

From data on N_2O fractionation in unspecified processes different from photodissociation, a slope of 0.515 was obtained (27) for a three-isotope plot of ϵ^{448} vs. ϵ^{447}. In their later experiments, Cliff et al., (28) observed an excess of O^{17} when the samples from lower stratosphere were analyzed using this slope of 0.515. This observation called for an accurate estimate of the three-isotope plot slope obtained by photolysis. An assumed slope of 0.515 for photolysis required additional N_2O sources/sinks to explain the observation. Kaiser et al., (18) used a slope of about 0.520 obtained from the broadband photolysis experiments by Rockmann et al. (29). The measured value of 447 fractionation factor is not published in

Ref. 29, and with slopes between 0.50 and 0.53 are possible with the published data on 448 (30). More refined experiments (31) do not give the measured value of 447 fractionation factor nor the slope of the three-isotope plot. Other theoretical estimates for this slope 0.525 and 0.517 from Refs. 32 and 33 using detailed quantum mechanical wavepacket propagation on the potential energy surface, also could not help resolve the debate about the interpretation of the O^{17} excess in atmospheric samples (28). The slope 0.532 we obtained in a linear plot of fractionation factors from the detailed computation, and supported by the almost similar perturbation theory result, should, we believe, be used as the mass-dependent slope standard for the N_2O photodissociation. We also believe that this slope of 0.532 should be included in a chemical transport model similar to that of McLinden et al. (34) to see what fraction of the current discrepancy in the atmospheric measurements of Ref. 28 can be accounted for solely by photodissociation. A decision could then be made whether a search for additional sources/sinks of N_2O is needed.

IV. Conclusions

Using a perturbation theoretical analysis an expression is obtained for the slope of three-isotope plots in photolytic fractionation. The result obtained here is expected to be a good approximation to analyze the mass-dependent effects in the photolytic process when the fractionation factors are small, justifying a first-order perturbation in the absorption cross-section. For N_2O, the result obtained by the present analysis is a close match with that of detailed computational calculations (9) of photodissociation fractionation. The comparison of the linear and log-log plots is discussed in the context of small and large conversions. This perturbation method given here for photodissociation reactions can be extended to some other kinetic processes once the functional form in which the masses appear in the equation for fractionation is known.

Bibliography

[1] J. Bigeleisen and M. G. Mayer, *J. Chem. Phys., 15*, 261 (1947)

[2] H. C. Urey, *J. Chem. Soc.,* 562 (1947)

[3] Y. Matsuhisa, J. R. Goldsmith, and R. N. Clayton, *Geochim. Cosmochim. Acta., 42*, 173 (1978)

[4] R. N. Clayton, L. Grossman, and T. K. Mayeda, *Science, 182*, 485 (1973)

[5] M. H. Thiemens and J. E. Heidenreich, *Science, 219*, 1073 (1983)

[6] C. A. M. Brenninkmeijer, C. Janssen, J. Kaiser, T. Rockmann, T. S. Rhee, and S. S. Assonov, *Chem. Rev., 103*, 5125 (2003), *and references cited therein.*

[7] R. E. Weston, *Chem. Rev., 99*, 2115 (1999), *and references cited therein.*

[8] E. D. Young, A. Galy, and H. Nagahara, *Geochim. Cosmochim. Acta, 66*, 1095 (2002)

[9] M. K. Prakash, J. D. Weibel, and R. A. Marcus, *J. Geophys. Res.-Atmos., 110*, D21315 (2005)

[10] S. Y. Lee, R. C. Brown, and E. J. Heller, *J. Phys. Chem., 87*, 2045 (1983)

[11] R. Schinke, *Photodissociation Dynamics* Cambridge Univ. Press, New York (1993)

[12] A comparison of the absorption cross-sections associated with direct, nearly-direct and indirect photodissociation is given in Fig. 1.6 of Ref. 11.

[13] E. J. Heller, *J. Chem. Phys., 68*, 2066 (1978)

[14] Y. L. Yung, and C. E. Miller, *Science, 278*, 1778 (1997)

[15] S. Califano, *Vibrational States* John Wiley & Sons, New York (1976)

[16] D. A. McQuarrie, *Statistical Mechanics*, University Science Books, Sausalito, CA (2000)

[17] P. H. Berens and K. R. Wilson, *J. Chem. Phys., 74*, 4872 (1981)

[18] J. Kaiser, T. Rockmann, and C. A. M. Brenninkmeijer, *J. Geophys. Res., 109*, D03305 (2004)

[19] E. M. Galimov, *Geokhimiya,* 274 (1979) [*Translated in Geochem. Internatl.* 155 (1979)]

[20] S. E. Bhattacharya, J. Savarino, and M. H. Thiemens, *Geophys. Res. Lett., 27*, 1459 (2000)

[21] J. Bigeleisen, *J. Chem. Phys., 23,* 2264 (1955)

[22] The partition function given in Eqs. (8.8a), (8.8b) is from Eqs. (10), (11b) in Ref. 1.

[23] K. Minschwaner, R. J. Salawitch, and M. B. McElroy, *J. Geophys. Res., 98*, 10543 (1993)

[24] M. N. Daud, G. G. Balint-Kurti, and A. Brown, *J. Chem. Phys., 122*, 054305 (2005). [Potential energy and dipole moment surfaces are available at ftp://ftp.aip.org/epaps/journ_chem_phys/E-JCPSA6-122-303502/]

[25] S. M. Ferigle and A. G. Meister, *J. Chem. Phys., 19*, 982 (1951)

[26] A. G. Csaszar, *J. Phys. Chem., 98*, 8823 (1994)

[27] S. S. Cliff and M. H. Thiemens, *Science, 278*, 1774 (1997)

[28] S. S. Cliff, C. A. M. Brenninkmeijer, and M. H. Thiemens, *J. Geophys. Res., 104*, 16171 (1999)

[29] T. Rockmann, J. Kaiser, C. A. M. Brenninkmeijer, J. N. Crowley, R. Borchers, W. A. Brand, and P. J. Crutzen, *J. Geophys. Res. - Atmos., 106*, 10403 (2001)

[30] The measured data on 447 was not published in Ref. 29 and 448 fractionation factors relative to 446 was 34.2 ± 0.8. If the 0.520 was calculated using the mean value 34.2 per mil given for 448 in Ref. 29, then with the error bar of ± 0.8 per mil, the slope can have any value between 0.50-0.53.

[31] J. Kaiser, *Stable isotope investigations of atmospheric nitrous oxide*, Ph.D Thesis, Johannes Gutenberg-Univ., Mainz, Germany (2002)

[32] M. S. Johnson, G. D. Billing, A. Gruodis, and M. H. M. Janssen, *J. Phys. Chem. A, 105*, 8672 (2001)

[33] S. Nanbu, and M. S. Johnson, *J. Phys. Chem. A, 108*, 8905 (2004)

[34] C. A. McLinden, M. J. Prather, and M. S. Johnson, *J. Geophys. Res.-Atmos., 108*, 4233 (2003)

Chapter 9

Conclusions

In the present thesis, theoretical studies related to three different kinds of experiments have been conducted. In relation to the single molecule enzyme experimental observations on the fluctuations of catalysis rate, spectral diffusion and fluorescence lifetime, a formulation based on fluctuations in the electrostatic interaction energy at a local site in the enzyme was developed. The autocorrelation functions of these three observables were related to that of the fluctuations in electrostatic interaction energy. The autocorrelation functions in the experiments decay on the time scales of milliseconds, and real-time trajectories of the enzyme cannot be obtained by computer simulations. To estimate the fluctuations in electrostatic interactions on these time scales, a formulation based on dielectric measurements of enzymes is developed. The autocorrelation function of the catalysis rates and fluorescence lifetime are compared with the experimental data using dielectric dispersion of proteins.

To understand the single molecule unfolding experiments that were used to verify a nonequilibrium fluctuation theorem (Crooks' theorem), the subtleties in the derivation of the theorem are studied. We note that the experimental system does not satisfy the condition in the theorem that the external parameter of the system should be varied in a steady way. It was also shown that in the limit of a quasi-static variation of the external parameter, Crooks' theorem can be recovered for this system. The experimental unfolding and refolding work distribution data are then analyzed using a phenomenological model for distortion of the

free-energy surface under applied forces. Based on the analysis, a few conditions that need to be checked before extracting ΔG from the experiments are noted.

To model the experimental data on the absorption cross-section of N_2O, two different calculations using two variants of the multidimensional reflection principle are performed. The calculated absorption cross sections are compared with the experiments. In the first calculation, an empirical broadening was used to match the experimental data, and in the second calculation the cross section was fit to the data on the lower energy side of the absorption peak where the isotopic fractionation data is available. Using these adjustments for the absorption cross sections, the wavelength-dependent fractionations of N_2O isotopologues by photodissociation are calculated and compared with the experiments. The calculated fractionation of the isotopologue $^{14}N^{14}N^{17}O$ by both these methods showed a simple linear relation to that of $^{14}N^{14}N^{18}O$. A perturbation theoretical method was used to explain this relationship.